Fall 2021

Recent Advances in Catalytic Ethylene Epoxidation: Synthesis, Characterization, and Evaluation

Benjamin Thomas Egelske

Recent Advances in Catalytic Ethylene Epoxidation: Synthesis, Characterization, and Evaluation

By

Benjamin Thomas Egelske

Bachelor of Science
University of Minnesota Duluth, 2014

Submitted in Partial Fulfillment of the Requirements

For the Degree of Doctor of Philosophy in

Chemical Engineering

College of Engineering and Computing

University of South Carolina

2021

Accepted by:

John R. Regalbuto, Major Professor

John R. Monnier, Major Professor

Donna A. Chen, Committee Member

Mark J. Uline, Committee Member

Melissa A. Moss, Committee Member

Tracy L. Weldon, Interim Vice Provost and Dean of the Graduate School

DEDICATION

To my mother, Maxine L. Schwantes.

I owe my success to your patience, love, and good judgment.

I miss you Mom, but I know you are proud.

ACKNOWLEDGMENTS

From my mother I learned the joy of good conversation.

From my stepfather, whom I call Dad, perspective.

From my advisor Dr. John Monnier, wisdom to merge fundamentals with application.

From my advisor Dr. John Regalbuto, that family comes first.

From my advisor Dr. Donna Chen, to search the scientific theory.

From my advisor Dr. Mark Uline, high standards in ChE.

From my favorite authors, J. R. Rostrup-Neilson and Herman Pines, to avoid unreasonable claims.

From Dr. Wen Xiong, sanity to continue when things get tough. A true friend.

From Dr. Greg Tate, to go beyond basic understanding.

From Dr. John Tengco, catalyst synthesis and a love for Friday lunch.

From Dr. Weijian Diao, epoxidation chemistry and an appreciation for BBQ.

From Masud Rahman, that one extra C-C bond will make a substantial difference.

From Dr. Jayson Keels, synthesis, characterization, and evaluation.

From Dr. Soumitra Ghoshroy and Jibin Zhao, microscopy in all forms.

From Dr. Stavros Karakalos, The virtues and vice of X-ray photoelectron spectroscopy.

From Dr. Mehdi Zare and Dr. Mozhdeh Parizad, to surround yourself with positivity.

From Leandro “Andy” DeCastro, the benefit of insightful discussion.

From Chuck Holland, the advantage of a fully stocked toolbox.

From Kiré Pavlovski, to read for fun, knowledge, and informed discussion.

From Chester Dzieciolkiewicz and Dr. Ralph White, sustained hard work is rewarding.

From my automation mentors Tyler Anderson and Mason Bautista, professionalism.

From my climbing partners Nick Peterson and Michael Madden, an everlasting love for the outdoors.

From my co-workers Connor McDonough and Jacob Stiles, the patience to mentor.

From Carol Stork, gas chromatography from A to Z.

From my industrial partners not mentioned by name, an experienced perspective of data analysis and catalyst development.

From my many academic colleges not recognized by name, a love of the field. Thank you all.

ABSTRACT

First synthesized in 1859 by French chemist Charles-Adolphe Wurtz, ethylene oxide (EO) is produced from the direct epoxidation of ethylene and molecular oxygen over a low surface area α-Al_2O_3 supported silver (Ag) catalyst [1-6]. With a production capacity over 35 Mt/year, EO is the largest chemical by volume synthesized from a heterogeneously catalyzed process and is used in the production of ethylene glycol, ethoxylates, and ethanolamines [6, 7]. State-of-the-art catalyst formulations now contain high loadings of Ag, typically 12-30wt%, required to recover activity in the presence of promoter elements which increase EO selectivity from ~75% for unsupported Ag to 80% for Cs-Ag/α-Al_2O_3 and 82% for Cs-Re-Ag/α-Al_2O_3 but reduce the number Ag-O sites available for olefin epoxidation. In addition to Cs and Re, current generation high selectivity catalysts also contain co-promoter high valent transition metal oxy anions and Group I light elements such as Li and K [8, 9] that when combined with ppm levels of a halide moderator, typically chloroethane (EtCl) or vinyl chloride (VCL), added during operation, EO initial selectivity can reach 92% at 1.5 – 2.5 mole% EO in the product [10].

In Chapter 1 the structure sensitivity of Ag for EO formation is studied using a novel synthesis technique, electroless deposition (ED), to vary particle size distributions for a series of Ag catalysts supported on an α-Al_2O_3 used for industrial epoxidation reactions. In this work, catalytic evaluation is combined with ex-situ microcopy and

hydrogen titration collected before and after reaction to show that particles <100 nm in diameter are susceptible to sintering and carbon foulant and that selectivity not TOF is significantly improved with large particles. Furthermore, prescreening of the alumina indicates the absence of acid catalyzed isomerization of EO suggesting that the observed structure sensitive performance is intrinsic to direct epoxidation on the Ag surface and not dependent on background combustion from the support. In Chapter 2, the hydrogen titration of unpromoted Ag is expanded to include combinations of Cs, Re, Mo, S, and W which complicate the quantification of Ag active sites [11] but are critical for state-of-the-art material compositions [2, 10, 12]. In this section the question is proposed, can one extract meaningful information from the pulsed titration of promoted Ag/α-Al_2O_3 samples? Finally, in Chapter 3, the exothermicity of selective and nonselective epoxidation is studied though the application of a microfibrous mesh comprised of Ni, Cu, or stainless steel (SS), and packed with Cs promoted Ag/α-Al_2O_3 in a configuration known as a microfiborous entrapped catalyst (MFEC). In this section it is shown that heat transfer rates can be controlled using MFEC technology providing an isothermal intrabed temperature profile that is resistant to process upset. Consequently, improvements to several key performance indicators (KPI) are discussed.

TABLE OF CONTENTS

DECICATION…….. iii

ACKNOWLEDGEMENTS…….. iv

ABSTRACT…….. vi

LIST OF TABLES…… x

LIST OF FIGURES……... xi

CHAPTER 1 THE STRUCUTRE SENSITIVITY OF Ag/α-Al_2O_3 CATALYSTS FOR ETHYLENE EPOXIDATION…..……..…….. 1

1.1 ABSTRACT…… 2

1.2 INTRODUCTION……... 3

1.3 EXPERIMENTAL METHODS…….. 13

1.4 RESULTS AND DISCUSSION……. 18

1.5 CONCLUSION……... 39

CHAPTER 2 HYDROGEN TITRATION OF Ag/α-Al_2O_3 OLEFIN EPOXIDATION CATALYSTS CONTAINING PROMOTERS AND CO-PROMOTERS…….…… 42

2.1 ABSTRACT…… 43

2.2 INTRODUCTION……... 44

2.3 EXPERIMENTAL METHODS…….. 48

2.4 RESULTS AND DISSCUSSION……... 50

2.5 CONCLUSION……... 59

CHAPTER 3 MICROFIBER ENTRAPPED CATALYSTS FOR HEAT REMOVAL IN EXOTHERMIC ETHYLENE EPOXIDATION……..…… 61

3.1 ABSTRACT…… 61

3.2 INTRODUCTION……... 62

3.3 EXPERIMENTAL METHODS…….. 70

3.4 RESULTS AND DISSCUSSION……... 74

REFERENCES…….. 87

APENDIX A CHAPTER 1 SUPPLEMENTAL INFORMATION……...…….……..... 99

LIST OF TABLES

Table 1.1 Literature reported Ag particle size and preparation parameters for catalysts supported on α-Al_2O_3…… 11

Table 1.2 Catalysts prepared by ED of Ag on 0.1wt% Ag/SA5562…….. 26

Table 1.3 Summary of turnover number for EO formation calculated from the quantity of active sites from H_2 titration and particle size distributions from SEM.…….……... 34

Table 3.1 Operating parameters for a typical 100 kton EO reactor…… 65

Table 3.2 Economic analysis for conventional EO technology containing a fraction of tubes in exothermic runaway with MFEC technology containing no ignited tubes…….……. 66

Table 3.3 Reactor parameters for MFEC evaluation compared with a similar pilot operation for EpB…….……... 85

LIST OF FIGURES

Figure 1.1 SEM image for 12wt% Ag supported on SA5562 α-Al_2O_3…..……..... 5

Figure 1.2 Partile size distribution generated from 17500 particles for a 13.4wt% Ag/α-Al_2O_3 catalyst…… 5

Figure 1.3 Pore size distribution for st Gobain SA5562 α-Al_2O_3 determined by Hg intrusion…… 13

Figure 1.4 EO isomerization as a function of reactor temperature……. 19

Figure 1.5 Major and minor pathways for ring opening by molecular and support bound oxygen……. 20

Figure 1.6 Nitrate decomposition by reduction of 12% Ag/SA5562……. 21

Figure 1.7 Configuration for a percolating bed electroless deposition bath with continuous recycle…….. 23

Figure 1.8 Thermal stability of ED bath and kinetic deposition profiles……... 24

Figure 1.9 Pulsed H_2 uptake for the hydrogen titration of oxygen precovered Ag at 170 ºC……. 25

Figure 1.10 SEM (top), STEM (middle), and histogram (bottom) from fresh 0.1Ag/SA5562 following reduction at 200 ºC……. 28

Figure 1.11 SEM images for "Fresh" samples treated in flowing 50% H_2 balance He at 200 ºC and "Spent" samples treated under reaction conditions at 210 ºC…….…….. 29

Figure 1.12 Temperature programed oxidation of fresh and spent 0.1wt% Ag catalyst prepared from $AgNO_3$…… 31

Figure 1.13 Foulant factors calculated from fresh and spent H_2 Titration results as a function of Ag particle sizes……. 32

Figure 1.14 Activity and selectivity results for 1.5wt% Ag/SA5562 evaluated with a feed composition of 25% C_2H_4, 8%O_2, balance CH_4…… 33

Figure 1.15 Turn over frequency for EO formation……... 35

Figure 1.16 Oxygen and ethylene reaction orders for select catalysts……... 36

Figure 1.17 Activity-Selectivity plot for select samples…… 37

Figure 1.18 EO formation vs selectivity for unpromoted 12wt% Ag/SA5562 and the same catalysts promoted with Cs, Re, and co-promoters……..…… 39

Figure 2.1 Thermal desorption of ethylenediamine in flowing Ar for two 12wt% Ag/SA5562 samples prpaired from $Ag_2C_2O_4$……..... 50

Figure 2.2 Hydrogen uptake for three separate experiments containing 2.0g of ground 841-400 μm 12wt% Ag/SA5562 particles……..... 52

Figure 2.3 Temperature programed reduction and pulsed hydrogen titration at 170 ºC for, 3% Cs/SA5562, 3%Re/SA5562 and 4%Mo/SA5562……...…… 53

Figure 2.4 Hydrogen uptake plotted against μmol promoter loading on 12wt%Ag/SA5562 samples prepared by co-imp of $Ag_2C_2O_4$ and promoter salts…….…….. 55

Figure 2.5 H_2 uptake for two samples containing an equal umol loading of Cs, Re, Mo, & S but 12wt % Ag and 24wt % Ag…… 56

Figure 2.6 Temperature programed titration for promoted Ag samples following oxygen precoverage at 170 ºC…….. 58

Figure 3.1 Reaction network and heats of reaction for selective and non-selective oxidation of ethylene on Ag…….. 62

Figure 3.2 Schematic for a single tube reactor denoting heat transfer……...……. 64

Figure 3.3 A comparison of performance for 12wt% Ag/α-Al_2O_3 and Cs-Re promoted 12wt%Ag/α-Al_2O_3 catalysts as a function of CO_2 in the feed stream……..……... 68

Figure 3.4 Schematic for the MFEC loaded with catalyst media..……. 69

Figure 3.5 Bed temperature deviation from jacket setpoint…….…….. 72

Figure 3.6 Reactor assembly used in catalytic evaluation…….……. 73

Figure 3.7 Material screening for C_2H_4 combustion compared with a 350ppm Cs, 12wt% Ag/SA5562 catalyst…… 75

Figure 3.8 Catalyst bed profile for a ½" OD Nickel MFEC and traditional bed diluted with SA5562 α-Al_2O_3 following startup at 225 ºC……. 76

Figure 3.9 Bed profiles following low temperature startup…….…….. 78

Figure 3.10 Selectivity as a function of catalyst work rate…..……... 79

Figure 3.11 Combustion of EO as a function of nominal reactor temperature for the Ni MFEC without catalyst…….. 81

Figure 3.12 Rate of energy generation as a function of catalyst selectivity for a 100kton/year EO reactor…….……. 82

Figure 3.13 Schematic for the 1" OD reactor loaded with diluted catalyst bed or MFEC media…….. 83

Figure 3.14: Catalyst temperature in the 1"OD reactor as a function of vertical position…… 84

Figure A. 1 Particle size distributions and active site concentrations derived from SEM…….. 98

CHAPTER 1

THE STRUCTURE SENSITIVITY OF Ag/α-Al_2O_3 CATALYSTS FOR ETHYLENE EPOXDATION

1.1 ABSTRACT

Catalysts have been prepared on a low surface area α-Al_2O_3 support used commercially for previous generation olefin epoxidation catalysts. Prescreening of the low surface area alumina (0.73 m^2/g) indicated the absence of acid catalyzed isomerization of EO at evaluation temperature of 210 ºC. A 0.1 wt% Ag base material synthesized by incipient wetness impregnation of $AgNO_3$ was used as a base material for electroless deposition of additional Ag to increase particle sizes by controlled reduction of Ag^+ directly onto the preexisting Ag surface to form weight loadings of Ag between 0.3 and 5.0 wt% metal. A 12wt% Ag/α-Al_2O_3 was also prepared from $Ag_2C_2O_4$ precursors to compare performance of the ED samples with catalysts more typical of industrial formulations. Characterization by SEM, STEM, and hydrogen titration of oxygen precovered Ag characterized before and after catalytic evaluation indicated that microscopy is required to accurately represent distributions of Ag particle sizes, but titration gives the best representation of active sites since it directly counts the number of Ag surface sites. Larger particles >100 nm are resistant to both Ag sintering and carbon foulant; TOF values were relatively insensitive to particle size with only a 2.25 X difference between the best and worst performing samples. Selectivity, which is not a function of TOF, shows the most significant structure sensitivity effect where particle sizes follow the trend 67nm ≈ 92nm (58% EO) < 157nm (67% EO) < 211-542nm (73% EO). The lower EO selectivities were also correlated with increased fouling for the smaller Ag sizes, suggesting that more strongly bound EO precursor(s) leads to combustion and CO_2/H_2O formation.

1.2 INTRODUCTION

Ethylene Oxide (EO) is currently a 35M metric ton/year chemical that is expected to continue to grow at a 5 – 7% annual growth rate for the foreseeable future [13]. This is a remarkably healthy growth rate, particularly for a mature chemical like EO. Several billion lbs of additional capacity have recently been added in the Texas and Louisiana gulf coast due to the supply of cheap ethylene from cracking of natural gas [14]. It is the largest volume product prepared by a heterogeneously-catalyzed oxidation process [6] and accounts for almost 50% of the volume of all oxidation products. Modern high performances catalysts no longer resemble the unpromoted Ag catalyst disclosed by Lefort in 1933 [1]. Catalyst developments to improve selectivity to EO have gone through several phases as detailed in a Shell company magazine [10]. The Cs-promoted, Ag catalyst boosted selectivity to the 80% level and then was replaced based on the work of Lauritzen [15, 16] that described the addition of $Re^{+7}$and other high valent salts including Mo^{+6}, W^{+6}, S^{+6} (as the primary promoters) existing as high valent oxyanions. EO selectivities are now as high as 90 – 92% for initial time online periods. Because the active Ag surface is loaded with multiple promoters to boost selectivity, the Ag surface site concentrations are often too low for acceptable space time yields, forcing Ag weight loadings to be increased to 30 – 40 wt% on non-acidic, fused α-Al_2O_3 supports. These supports typically have surface areas < $1 m^2/g$, so the resulting Ag particle sizes are very large and exist in a wide size distribution of surface and various surface morphologies. The scanning electron micrograph (SEM) in Figure 1.1 illustrates the variety of Ag particle sizes for “only” 12 wt% Ag supported on older generation fused α-Al_2O_3 rings with a surface area of 0.73 m^2/g, determined in our laboratory using Kr BET surface area

analysis. The Ag is shown as white particles on the dark gray α-Al_2O_3 surface. Note the wide distribution of Ag particle sizes and the presence of different morphologies including triangles, spheres, and faceted cuboctahedrons (Ag is an fcc metal). Even at 20K magnification, the α-Al_2O_3 surface appears rather featureless and not likely to anchor Ag particles as well as higher surface area and more interactive supports. However, to achieve the low acidity required to maintain the epoxide ring structure, low surface area is a basic requirement of all catalyst supports used for ethylene epoxidation.

One of the obvious questions that has not been clearly resolved is whether ethylene epoxidation is a structure-sensitive reaction; that is, does the rate of reaction per Ag site, more commonly known as the turnover frequency (TOF), change with the Ag particle size. It is not possible to answer this question if Ag particle sizes exist over a wide range as in Figure 1.1, since reaction rates are the sum of all particle sizes. Likewise, it is critical to have an accurate way to measure active Ag surface site concentrations. Monnier showed in earlier work [17] that a comparison of four typical techniques to measure active Pt surface site concentrations of a PEM fuel cell, specifically selective chemisorption, electrochemical surface area (ESA), x-ray line broadening, and electron microscopy, by far the two preferred methods were selective chemisorption and ESA because they actually measured, or counted, either H_2 molecules or electrons, respectively. X-ray line broadening worked only until XRD peaks became too narrow and insensitive to reflect further changes in the sizes of small crystallites. Of course, the problem with electron microscopic methods is the small number of particles actually measured and whether they represent the entire surface.

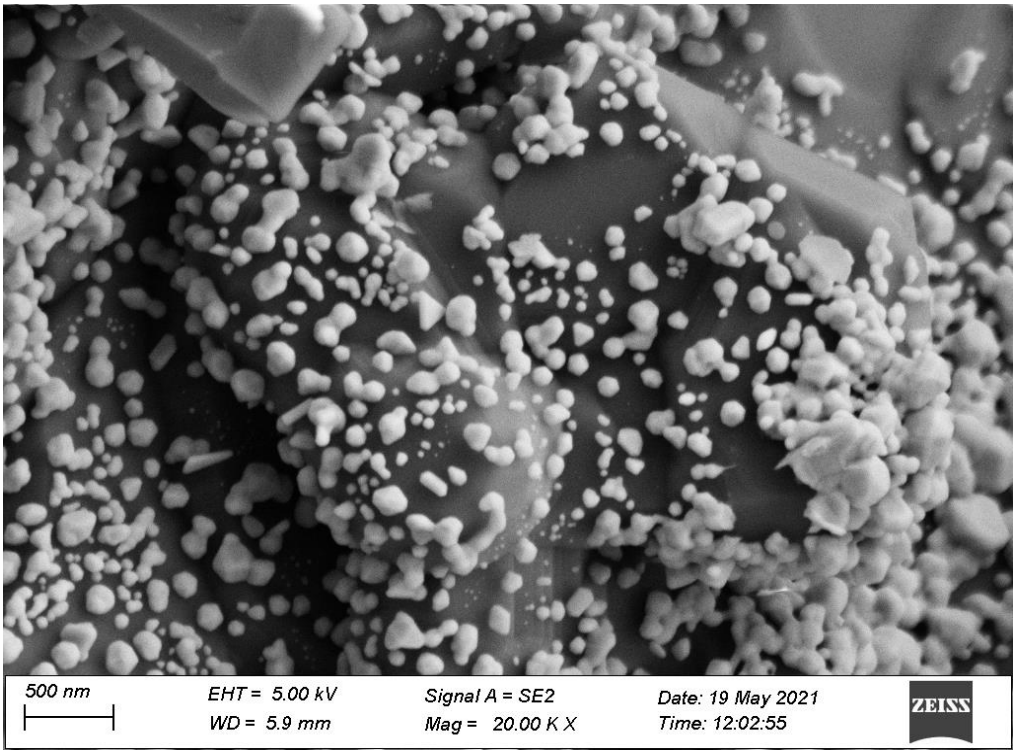

Figure 1.1: SEM image for 12wt% Ag supported on SA5562 α-Al_2O_3. This sample was prepared from silver oxalate according to reference [8]. Note the wide distribution in particle size and the presence of different morphologies including triangles, spheres, and faceted cuboctahedrons.

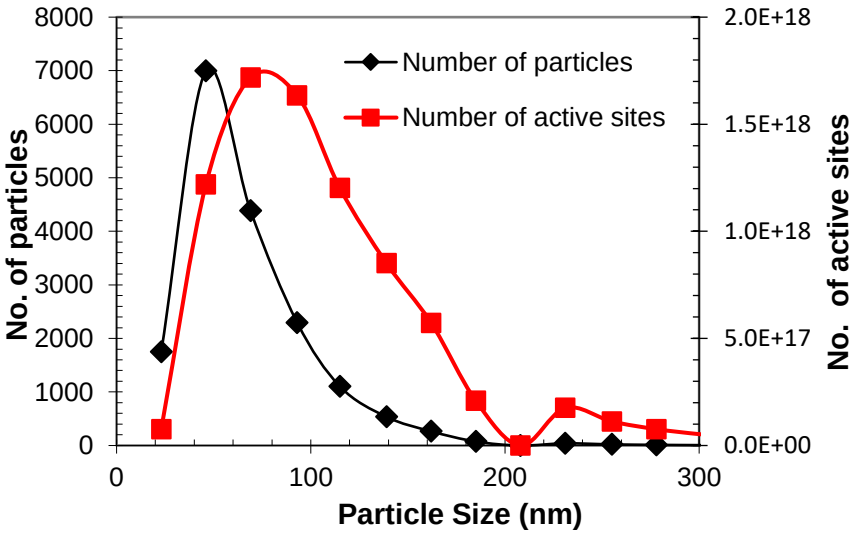

Figure 1.2: Particle size distribution generated from 17500 particles for a 13.4wt% Ag/α-Al_2O_3 catalyst. The difficulty of conventional approaches based on SEM data is that site concentrations as a function of particle size may not track well with the quantity of particles for a given size range.

Regardless, structure-sensitivity on α-Al_2O_3 supports has been investigated by a number of groups whose particle size determinations are shown in Table 1.1. Ag particle sizes were determined by both chemisorption and particle counting of microcopy images. In some cases, the numbers of particles countered were < 200, and in all cases less than 500. It was also not stated whether the observed size distributions were assumed to be representative of the entire sample and whether the distribution was assumed for the full Ag weight loading to determine the Ag site concentrations for spherical or hemispherical (same result) particles. In earlier work, Monnier [18] used SEM measurements and automated particle counting software to count many more particles (17500 particles) to determine a well-defined distribution of particle sizes. This result is shown in Figure 2 and is simply intended to demonstrate the benefits/necessity of adequate particle counting to determine active sites. The size distribution in Figure 1.2 was applied to the entire 13.4% Ag loading to calculate the Ag site concentration for each particle size. The results indicated there were 4.0×10^{13} Ag particles/g-catalyst with 8.1×10^{18} Ag surface sites, and a corresponding Ag particle size of 0.110 μm with a dispersion of 0.011. Even here, the average Ag particle size was estimated to be ~ 0.050 μm using the standard method of particle size estimation using electron microscopy, while if the total number of Ag surface sites calculated from the projected value of 8.7 A^2 for a Ag surface atom [19], Ag particle sizes between 70 – 100 μ account for the majority of the Ag sites.

For instances where chemisorption has been reported, the data are typically based on dissociative O_2 adsorption and use 1 Ag to ½ O_2 stoichiometry. Both O_2 chemisorption and H_2 titration of O precovered Ag sites have been used by Vannice but results were shown to be more consistent with H_2 titration [20] where the only species capable of

undergoing reaction with H_2 to form H_2O was monoatomic oxygen bound to the Ag surface [21]. While there are possibly and likely more than metallic Ag sites capable of adsorbing atomic oxygen, particularly for current generation, heavily promoted Ag catalysts containing Cs, Re, Mo, W, S after a high temperature reduction treatment, only Ag-O species are likely to be reactive for H_2 titration at 170 ºC. The high valencies of Re and its co-promoters and the very low ionization potential of Cs_2O (or CsOH) make it difficult for reduction by H_2 at temperatures such as 170 ºC. This work will be discussed in more detail in a soon to be published paper [22]. Furthermore, the 1 : 1 H_2 to Ag-O stoichiometry doubles the sensitivity of detection improving sample-to-sample repeatability specifically for systems with low Ag site concentrations such as EO catalysts with large particle sizes.

Many have examined the EO reaction for structure sensitivity but problems exist not only for sensitive and accurate methods of measuring Ag active sites, but also the preparation of catalysts with narrow particle size distribution. The listing of some of the more recent studies is shown in Table 1.1. Verykios [23] prepared Ag particle sizes between 35 and 170 nm using four different α-Al_2O_3 supports with surface areas ranging from 0.2 to 3.0 m^2/g. Samples were characterized by selective oxygen chemisorption at 200 ºC and evaluated between 180 and 240 ºC at 220 psig in an oxygen-rich feed. For one series, EO selectivities decreased as Ag particles increased from 120 to 170 nm diameter; however, with a different α-Al_2O_3, selectivity increased as particles grew from 50 to 130 nm [23]. In later work Verykios, Pitchai, and Lee re-examined Ag particle size effects for a wide range of oxide supports and found that most of the oxides strongly contributed to the rate of combustion with only SiO_2 and α-Al_2O_3 having significant selectivity for EO

formation [24]. Contrary to the prior work where a minimum in EO formation rate was identified at 70nm [23], the α-Al_2O_3 supported samples in this study exhibited a maximum rate of formation between 40 and 80nm [24]. Danilyuk et al later noted the difficulty of obtaining tight particle size distributions on low surface area α-Al_2O_3. Even using a higher surface area of 7 m^2/g for alumina prepared in their laboratory which should help in narrowing particle size distributions, Ag particles between 19 and 140nm were formed by incipient wetness. Ag particle sizes were determined by TEM imaging of approximately 100 particles and compared with oxygen chemisorption whose experimental parameters were referenced in earlier work [25]. Evaluation for a C_2H_4-lean feed containing 2% C_2H_4, 7% O_2, balance N_2 at 230 ºC and 14.7 psia pressure gave a linear increase in the rate of EO formation with increasing Ag particle size over the range 19 to 140 nm; selectivity values were not discussed. In 2017 de Jongh examined the effect of gas compositions on precursor decomposition for Ag particle sizes during preparation of 15wt% Ag samples supported on 8.0 m^2/g α-Al_2O_3 [26]. Particle size measurements were determined using a combination of TEM and SEM for 100 - 170 particles per sample. These results were supplemented with UV/Vis spectra to examine the Ag plasmon peak positions in the 300-750nm range to infer Ag particle diameters assuming spherical geometry. Catalyst evaluation was conducted in a C_2H_4-rich feed and the authors concluded that at constant C_2H_4 conversions of ~2.8%, the EO selectivity was independent of particle size. However, in the analysis it was assumed that selectivity was dependent only on the competitive rates of epoxidation versus C_2H_4 combustion and that the rate of sequential EO combustion was zero and independent of the temperature used to reach 2.8% C_2H_4 conversion. Recently, Hoof et al studied a series samples supported

on 1.04 m^2/g α-Al_2O_3 with loadings between 1.7 and 14.0 weight % Ag. Particle sizes between 20 and 185 nm were determined from Scanning Transmission Electron microscopy (STEM) for 200 – 485 particles per sample [27]. For an oxygen-rich feed (10% O_2, 5% C_2H_4, balance He at 225 ºC and 290 psig) it was concluded that O_2 dissociation does not occur on the external Ag surface and instead only proceeds at defect sites to form subsurface monatomic oxygen which is the responsible species for selective epoxidation. The authors noted a theoretical maximum of EO selectivity of 75% for particles < 100 nm and 80% for Ag particles > 100 nm as C_2H_4 conversion approached 0%. In summary, there have been no agreements in activity or selectivity trends, likely because of the methods used to measure Ag particle sizes, methods of catalyst preparation, and the variety of supports that were used.

Thus, in this communication, we prepare a series of supported Ag catalysts using our method of electroless deposition (ED) [28] to deposit Ag on pre-existing Ag nuclei prepared by dry impregnation of 0.1 wt% Ag/α-Al_2O_3 to give better control of resulting Ag particles. We also use an authentic older generation low surface area α-Al_2O_3 ring that has been used as a commercial EO catalyst support that was ground and sieved to 841 – 400 μm (20/40 mesh) before Ag was deposited. Interestingly, this process is much like development of silver halide photographic films where Ag particles of 2 – 6 atoms (called latent images) produced by the photoreduction of AgCl during light exposure were reduced further (by unexposed AgCl particles adjacent to the latent image) during film development by a formaldehyde-containing developer solution to form a negative film [29]. In this study we also use formaldehyde as the reducing agent in the ED bath and

$AgNO_3$ as the reducible Ag salt. The principal difference here is we begin with ultra-small Ag particles prepared by dry impregnation.

Ag particles have been analyzed by H_2 titration of oxygen-precovered Ag surface sites at 170 ºC using the method developed by Vannice [21] to measure Ag surface site concentrations and compared to SEM micrographs which determine Ag particle size distributions and only infer Ag active site concentrations. The catalysts have been evaluated using an automated reactor system operating at authentic reaction conditions similar to those used industrially. By knowing the number of active surface Ag sites and accurately measuring reaction rates and EO selectivities, it should be possible to determine with substantial accuracy whether ethylene epoxidation is structure sensitive and if EO selectivity has an optimum Ag size range. Finally, the TOF's in this manuscript are reported for site concentrations determined before and after 150 hours or more of reaction time to measure steady state activities and to determine sintering characteristics of different Ag particle sizes on the α-Al_2O_3 support.

Table 1.1: Literature reported Ag particle size and preparation parameters for epoxidation catalysts supported on α-Al_2O_3.

Ref	Ag Precursor	α-Al_2O_3 Support	Synthesis	SA (m^2/g)	Ag (wt %)	Max Synthesis Temperature (^oC)	Fresh SizeChemi (nm)	Fresh $Size_{TEM}$ (nm)	n
[23]	$AgNO_3$	MAG-99	Note E	0.2	1	200	36	-	-
				0.2	1	400	43	-	-
				0.2	1	480	47	-	-
				0.2	1	600	53	-	-
				0.2	1	750	59	-	-
		Norton SA-5202		0.63	13.92	200	120	-	-
				0.63	13.92	400	141	-	-
				0.63	13.92	500	166	-	-
		Carborundum SAH7-99-Series		0.97	5.6	200	55	-	-
				0.97	5.6	400	70	-	-
				0.97	5.6	500	78	-	-
				0.97	5.6	600	100	-	-
				0.97	5.6	700	121	-	-
		Prepared by Authors		3.03	6.43	200	31	-	-
				3.03	6.43	410	43	-	-
				3.03	6.43	510	75	-	-
				3.03	6.43	700	108	-	-
				3.03	6.43	850	123	-	-
[24]	$AgNO_3$	Source Not Specified	Note D	0.5	0.5	200	13	10	100-200
				0.5	1	200	26	20	100-200
				0.5	2	200	41	35	100-200
				0.5	5	200	80	78	100-200
				0.5	10	200	100	88	100-200
[30]	Ag Amine in Ethanolamine	Prepared by Authors	Note A	7	0.4	240	13	16 ± 9	100
				7	0.6	240	-	20	-
				7	1.5	240	-	24.3	-
				7	2.4	240	20	18.4	-
				7	2.7	240	30	30.6	-
				7	3.7	240	25	40	-
				7	5.2	240	-	56	-

				7	6.5	240	56	45	-
				7	13.8	240	126	100 ± 32	100
[26]	$Ag_2C_2O_4$	BASF AL4196E	Note C, H_2	8	15	215	-	28 ± 19	170
			Note C, N_2	8	15	215	-	62 ± 21	105
			Note C, O_2	8	15	215	-	76 ± 37	104
[27]	$Ag_2C_2O_4$	Saint-Gobain NorPro SA 5102	Note B He / O_2 (100/0)	1.04	1.3	400	-	19 ± 9	200
				1.04	1.7	275	-	23 ± 11	400
				1.04	4.5	275	-	41 ± 16	400
			Note B He / O_2 (90/10)	1.04	1.7	275	-	48 ± 19	400
				1.04	4	275	-	57 ± 21	400
				1.04	8.7	275	-	99 ± 32	400
				1.04	8.2	275	-	106 ± 47	199
				1.04	10	275	-	127 ± 47	349
			Note B He / O_2 (90/10)	1.04	7.8	500	-	167 ± 58	291
				1.04	14.4	275	-	183 ± 89	484

A. Incipient Wetness -> Contact Drying (25 ºC) -> Vacuum Reduction (90 ºC) -> Water Wash -> Dry in Static Air (100 ºC) -> Calcination (240 ºC, 2 hours) [30].
B. Incipient Wetness -> Vacuum Drying (25 ºC, 1 hour) -> Calcination in He/O_2 (275, 400, or 500 ºC, 10 ºC/min, 4 hours) [27].
C. Incipient Wetness -> Drying in Static Air (60 ºC, 24 hours) -> Heating in H_2, O_2, or N_2 (215 ºC, 5ºC/min, 2 hours) [26].
D. Incipient Wetness -> Atmospheric Drying (70 ºC) -> H_2 Reduction (200 ºC, 6 hours) [24].
E. Incipient Wetness -> Atmospheric Drying (50 ºC) -> Water Wash -> Atmospheric Drying (50 ºC) -> H_2 Reduction (200 ºC, 60 hours) -> N_2 Sintering (6-70 hours) [23].
F. Prepared by impregnation of Ag oxalate and fast calcined in high velocity air at 260 ºC [8].
G. The fresh notation indicates that the sample was reduced or calcined but was not exposed to epoxidation conditions.

1.3 EXPERIMENTAL METHODS

1.3.1 Synthesis

The 0.1 wt% Ag base catalyst was prepared by wet impregnation of $AgNO_3$ (Alpha Aesar) dissolved in deionized water on fused α-Al_2O_3 rings, provided by St. Gobain (denoted as SA5562.) Figure 1.3 shows Hg intrusion data, illustrating a bimodal macro-pore distribution at 1 and 30 μm in diameter. For supports such as these, internal diffusion limitations are largely nonexistent.

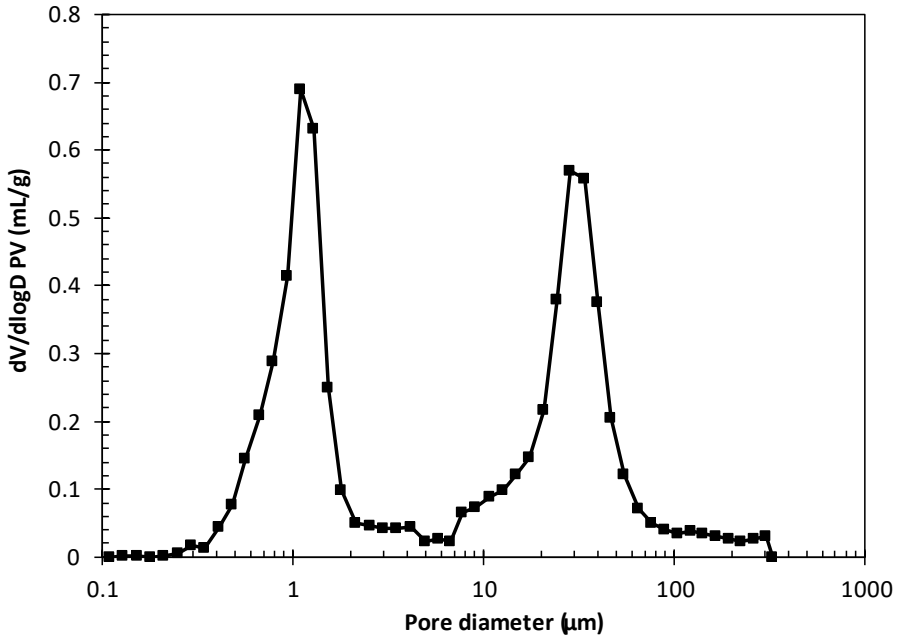

Figure 1.3: Pore size distribution for St Gobain SA5562 a-Al_2O_3 determined by Hg intrusion.

After impregnation of 0.1 wt% $AgNO_3$ on 20/40 mesh SA5562, the sample was transferred to a 400ml round bottom flask and tumble dried at 10 in of Hg pressure at 70 ºC until free tumbling of the precursor was observed. Samples were transferred to a vacuum oven (VWR Model 1410) at 20 in Hg pressure and heated to 110 ºC, for 12 hours prior to reduction in 125 SCCM of 50% H_2 with balance He at 200 ºC (ramp rate

5ºC/min) for 4 hours in a separate vertical split tube furnace. All temperatures used in this study were maintained at ≤ 200 ºC to minimize sintering of Ag particles. Comparison samples of 12wt % Ag were prepared by impregnation using $Ag_2C_2O_4$ (silver oxalate) as previously noted [8].

The 0.1% Ag/SA5562 catalyst was used as the base material for all electroless deposition (ED) derived samples. The ED bath was prepared using $AgNO_3$ as the source of Ag^+, formaldehyde (HCHO) as the reducing agent (RA), and NH_4OH as needed to maintain pH 11. The $AgNO_3$ solution and HCHO solutions were added from two different motor-driven syringe pumps at a fixed molar ratio of $[HCHO]/Ag^+ = 2 / 1$. The Ag weight loadings deposited by ED were controlled by controlling the duration of pumping time of RA (6.0×10^{-2} M) and Ag salt (3.2×10^{-1} at pumping speeds of HCHO (11.30ml/h) and $AgNO_3$ (11.45ml/h) into an agitated ED bath at pH 11. The bath solution was then peristaltically pumped to the base of a vertically mounted 15 ml tube and the flowrate adjusted until the 842 – 400 μm (20/40 mesh) particles behaved as a percolating catalyst bed to give good convective mixing of the catalyst particles with the ED components. At the top of the tube, the solution was filtered through a glass frit to remove and maintain the fines in the tubular percolating bed and then recirculated back to the stirred bath as shown in Figure 6. Initial attempts using a magnetic stirrer bar in the ED vessel resulted in attrition of the catalyst particles to produce fines, which changed diffusion characteristics during catalytic reaction. Control experiments indicated the absence of electrostatically adsorbed Ag on the α-Al_2O_3 support and that there was no thermal reduction of the HCHO and Ag^+ solution. Elemental analyses were made using inductively coupled plasma-optical emission spectroscopy (ICP-OES, Perkin Elmer Avio

200) of periodically collected aliquots of liquid samples. All vessels, tubing, and the pump liner were constructed from inert plastic or Teflon and were cleaned with 37% nitric acid, and thoroughly rinsed with DI water, between samples.

Following electroless deposition, all samples were filtered and washed with 1 L/g-catalyst of deionized (DI) H_2O to remove residual ED byproducts and unreacted components. The catalysts were then dried overnight in vacuo at 110 °C and reduced at 200 °C using the same conditions used for the 0.1% Ag/SA5562 base catalyst. Nominal Ag loadings on α-Al_2O_3 that were determined from analysis of periodic aliquots were confirmed to match results after digestion of the catalyst in concentrated 37% nitric acid and ICP analysis.

1.3.2 Characterization

Temperature programed oxidation (TPO) and temperature programed reduction (TPR) experiments were performed using Brooks 5850E mass flow controllers to deliver specific feed compositions to 200 mg samples in a quartz micro-reactor using a high wattage, split-tube furnace (capable of linear heating up to 60 ºC/min) connected to an Inficon Transpector 2 Mass Spectrometer using a modified Varian 951 variable leak valve customized for fast detection [31]. Samples were loaded into a ¼-inch quartz tube supported on a quartz plug, dried in-situ at 120 ºC for 1hr, then cooled to room temperature in flowing (30 SCCM) Ar. For TPO, 10% O_2 with balance Ar was introduced to the system and samples were ramped at 20 ºC/min to 600 ºC while monitoring for CO_2 (m/e = 44) and H_2O (m/e = 18). For TPR, samples were heated to 500 ºC at 20 ºC/min or, alternatively, heated in a separate experiment to 200 ºC at 20 ºC /min,

maintained for 4.5 hours, and then ramped to 260 and 340 ºC to verify the absence of residual nitrates from $AgNO_3$ decomposition (NO^+ at m/e = 30).

A Micromeritics ASAP 2020 was used for Kr BET analysis, and for chemisorption of exposed Ag sites, H_2 titration of oxygen precovered Ag (Ag-O) was performed on a Micromeritics 2920 pulsed chemisorption analyzer using the method of Vannice [21]. Prior to analysis, samples were heated to 200 ºC at 10 ºC/min in flowing 10% O_2 with balance He and held for 10 hours to remove any potential residue from formaldehyde during ED. After this, the samples were reduced for an additional 2 hours at 200 ºC in 10% H_2, balance Ar before cooling to 170 ºC and purging with flowing Ar. Samples were then exposed to 10% O_2, balance He for 30 min to saturate the Ag surface with Ag-O species before conducting the pulsed H_2 titration, also at 170 ºC. Each sample was given two additional sequences of H_2 titration and results are reported as an average; error bars represent the standard deviation between in-situ titration cycles and show good agreement for H_2 uptakes.

Aberration-corrected JEOL 2100 F scanning transmission electron microscopy (STEM) was used to do Z-contrast imaging with a 200 kV field emission gun and a double tilt holder for tilting the sample across a range of angles (± 20°) for obtaining images. Sample preparation involved direct deposit of ground powder on a copper TEM grid with a thin holey carbon coating. Scanning electron microcopy (SEM) was also performed using a Zeiss Gemini 500 equipped with a secondary electron detector (SE2). SEM samples were crushed, applied to carbon backed adhesive tape, and coated with a thin layer of Pd-Au using a Denton Desk II sputter coater with global rotation and tilt. SEM images were collected using an SE2 detector at 5KV beam energy and particle

counting was performed with ImageJ software version 1.8.0 - 172. Great care was taken to ensure that each sample was well represented with >15 images collected at various positions with magnification to give accurate detail at the 200nm scale.

1.3.3 Evaluation

Catalyst evaluations were performed in a parallel flow system consisting of six stainless-steel reactors of 0.25" OD and 0.035" wall thickness that were loaded with 3.0g of 20/40 mesh samples supported on a plug of glass wool. Each reactor tube was press fit into a 1" OD aluminum sheath to improve isothermal performance. Reactors were heated by 1" ID x 15" long BriskHeat heating mantles with no air gaps between the aluminum jacket and the heating mantle. Temperatures were controlled and recorded using a 1/16" thermocouple embedded in the Al sheath. The master reaction feed stream consisted of 25% C_2H_4 (Praxair, EY 2.5-T), 8% O_2 (Praxair, OX 4.3UH-T), balance CH_4 (Praxair, ME3.7UH-T) and was blended using Brooks 5850E mass flow controllers. No ethyl chloride (EtCl) modifier was added to the feeds in this series of experiments to avoid potential issues that might arise from unequal rates and extents of Cl addition for different weight loadings of Ag [32]. The master feed composition was plumbed to a second manifold of mass flow controllers which provided 50 SCCM (GHSV 1000 hr^{-1}) to each reactor at a pressure of 250 psig. Reaction pressures were let down to 1 Bar pressure using Parker Veriflo ABP1 series back pressure regulators maintained at 120°C. All product streams were heated to 120 °C to avoid condensation and were sampled automatically using a six-stream Valco sample valve at 2-hour intervals using an Agilent 7890A gas chromatograph (GC) equipped with two Poraplot-Q columns (30m x 0.32 ID, 19091P-QO4) connected to a TCD for CO_2, EO, and H_2O analyses and a separate FID for

trace amounts of ethylene glycol and acetaldehydes (never observed). Carbon mass balance calculations between the feed and the product streams for CO_2, EO, and C_2H_4 gave carbon balances of 100 ± 0.5%. All reaction order studies were performed at < 10% C_2H_4 conversion and Weisz-Prater calculations indicated the absence of internal mass transfer limitation.

EO isomerization studies were performed in the same reactor system used for catalyst evaluation, except a 2.1% EO balance He mixture (AirGas) was blended with O_2 and CH_4 to give feed concentrations of 0.5%EO, 8% O_2, and balance He + CH_4; 100 SCCM of mixed gas was supplied to each reactor containing 2.0g of sample at atmospheric pressure. One reactor was left empty to determine thermal EO conversion and mass balance of the isomerization reaction; isomerization results were conducted at 220, 245, and 270 ºC.

1.4 RESULTS AND DISCUSSION

1.4.1 Isomerization Activity

Figure 1.4 illustrates the effect of temperature on the isomerization of EO for α-Al_2O_3 (SA5562) and 12wt% Ag/SA5562. At 245 and 270 ºC, EO conversions for SA5562 were 5.1%/m² and 13.5%/m², respectively, with acetaldehyde (HAc) being the only product detected; the amount of isomerization approached 0% conversion at 210 ºC, the temperature used for catalyst evaluations. Thus, we can ignore the consecutive support-catalyzed isomerization of EO in our Ag size effect evaluations. Interestingly, both EO and HAc were thermally stable even at 270 ºC. Neither epoxide ring opening of EO or scission of one of the three reactive α-C-H bonds of HAc occurred, indicating the thermal oxidative stability of both oxygenates at high temperatures. Note that when an

amount of Li^+ corresponding to 0.5 ML (assuming 1.2 x 10^{19} "sites/m^2 surface) was added to neutralize residual acid sites on α-Al_2O_3, acidity was reduced even further to give a largely isomerization-free catalyst support. However, at similar conditions for 12 wt% Ag/α-Al_2O_3, considerably more EO underwent combustion to form CO_2 and H_2O, indicating that consecutive combustion had occurred. At 245 ºC, EO conversion had increased from 5.1% to 20.0% when 12% Ag was present. This does not mean that combustion levels of EO this high occur at typical reaction conditions for promoted catalysts, where in addition to a large number of inorganic promoters [2, 8, 12] and the presence of ppm levels of ethyl chloride (EtCl) in the gas feed [33, 34], there are other gas phase components adsorbed more strongly on the Ag surface. Reported reaction orders [35, 36] for EO formation over Ag catalysts give near zero order for C_2H_4, negative reaction orders for CO_2, and approximately first order for O_2. Thus, the Ag surface is Ag-O starved at typical reaction conditions which would necessarily inhibit EO combustion.

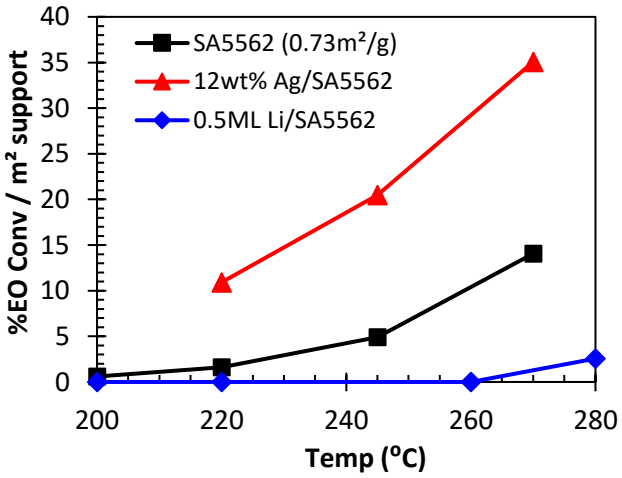

Figure 1.4: EO isomerization as a function of reactor temperature (Feed Composition: 0.5% EO, 8%O_2, Bal CH_4, 14.7 psig). Acetaldehyde was the sole product detected at 270 ºC for Ag free SA5562 α-Al_2O_3.

Sensitivity to oxygen concentration was examined by temporarily removing O_2 from the feed, while maintaining a fixed concentration of 0.5% EO balance inert. At 245 ºC, EO conversion on SA5562 decreased from 5.1 to 2.8%/gcat m²-sup indicating that molecular oxygen may participate as a nucleophile for ring opening of the EO-$Al^{\delta+}$ intermediate, Figure 1.5 [37, 38]. For the 12wt% Ag /SA5562 sample without supplemental oxygen, EO conversion decreased from 20 to 10% and chromatographs collected for 2 consecutive hours showed the formation of HaC, CO_2, and H_2O. Cumulative CO_2 formation was equivalent to 120 ML of monatomic oxygen assuming $2.32x10^{18}$ Ag sites/g-cat determined from hydrogen titration suggesting the presence of an oxygen reservoir with sufficient capacity to sustain combustion. Regardless, the 210 ºC temperature selected for evaluation is insufficient to cause isomerization.

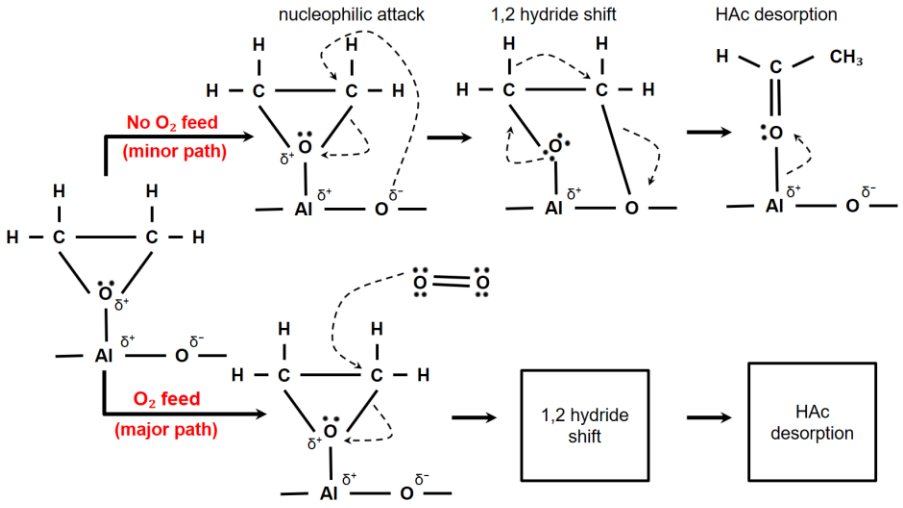

Figure 1.5: Major and minor pathways for ring opening by molecular and support bound oxygen.

1.4.2 Electroless Deposition

Water soluble $AgNO_3$ was selected as the Ag source for base catalysts synthesis of 0.1% Ag/SA5562 due to its clean thermal decomposition as shown in Figure 1.6 (left).

Temperature programed reduction (TPR) was performed on a portion of the 12wt% Ag/SA5562 sample where the catalyst precursor was heated at 20 °C/min in flowing 10% H_2, balance Ar up to 200 °C and NO was monitored at m/e = 30; there was a sharp and symmetrical peak centered at ~240 ºC with a small shoulder at ~ 340 ºC. In order to determine whether reduction would occur at 200 ºC by maintaining that temperature for a longer period of time, the plot in Figure 1.6 (right) was obtained, indicating that complete reduction occurs within a time period of 120 min. No additional NO peak was observed at higher temperatures. Neither was H_2O from reduction of oxides observed for either experiment; only physically adsorbed H_2O appearing as a broad featureless peak between 70 – 150 ºC; thus, H_2O peaks are not shown. More importantly, the TPR experiments confirmed that reduction at 200 ºC was sufficient for reduction, helping to minimize Ag particle sintering from higher temperatures exposures.

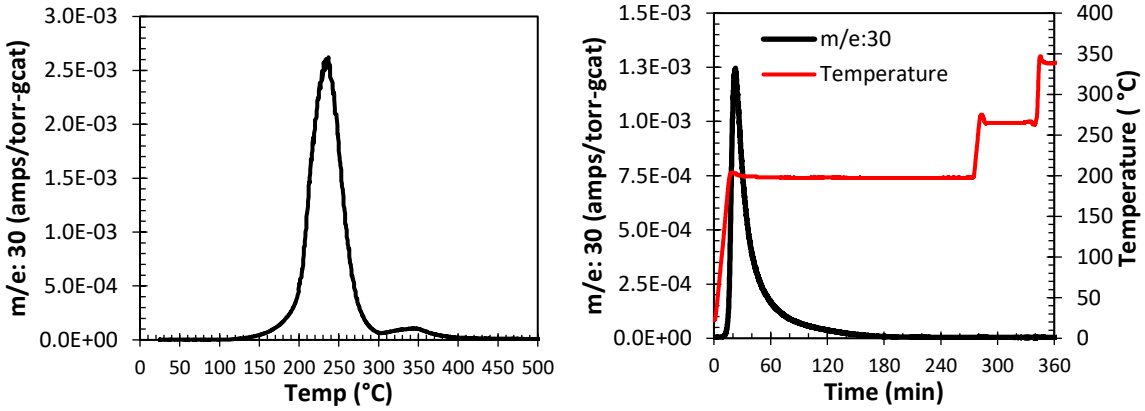

Figure 1.6: Nitrate decomposition by reduction of 12%Ag/SA5562 in 20 sccm of flowing 10% H_2 balance Ar. Experiment 1: The sample was heated from 25 to 500 ºC at 20 ºC/min (Left). Experiment 2: The sample was held at 200 °C for 4hrs then ramped to 265 and 340 °C to check for residual nitrate compounds (Right).

The electroless deposition (ED) bath was developed from prior work for the deposition of Ag [28, 39] on Pt and Pd base catalysts. Formaldehyde was selected as the reducing agent based on results of Djokic [40] and Ohno [41] for ED on Ag surfaces.

Control experiments for thermal instability indicated that reduction of $AgNO_3$ was kinetically slow. Following a period of 128 min where Ag salt and RA were syringe pumped into DI water containing no 0.1 wt Ag catalyst, only 5% of the Ag^+ in solution was reduced to Ag^0 at rather high concentrations of 0.81 umol Ag^+/ml and 102 umol-RA/ml; these data are shown in Figure 1.8. In the presence of a Ag catalyst, the rate of electroless deposition greatly exceeds the rate of thermal instability so the concentrations of Ag^+ and HCHO never reach critical concentrations for thermal reduction to occur [42]. Theoretical Ag weight loadings were confirmed by digestion and ICP analysis of the ED samples following ex-situ reduction in flowing H_2 further indicating that none of the reduced Ag existed as nanoparticles in solution.

Initial ED experiments were performed using a continuous ED bath where catalysts, RA, and salt were added to a beaker and agitated using a stir bar [28]. With this configuration, only 40 % of the 20/40 mesh material was recovered; the remaining 60% was ground to a fine powder. Consequently, a percolating ED bed shown in Figure 1.7 was developed where RA and $AgNO_3$ solutions were syringe pumped into an agitated reservoir containing DI water. A peristaltic pump transferred the ED solution at a rate sufficient to cause percolation and thorough mixing of the catalyst and ED components. Catalyst particles and any fines were maintained in the percolation bed using a glass frit exiting at the top of the tube. Mass recovery of the 20-40 mesh material approached 100% for all samples used in this study.

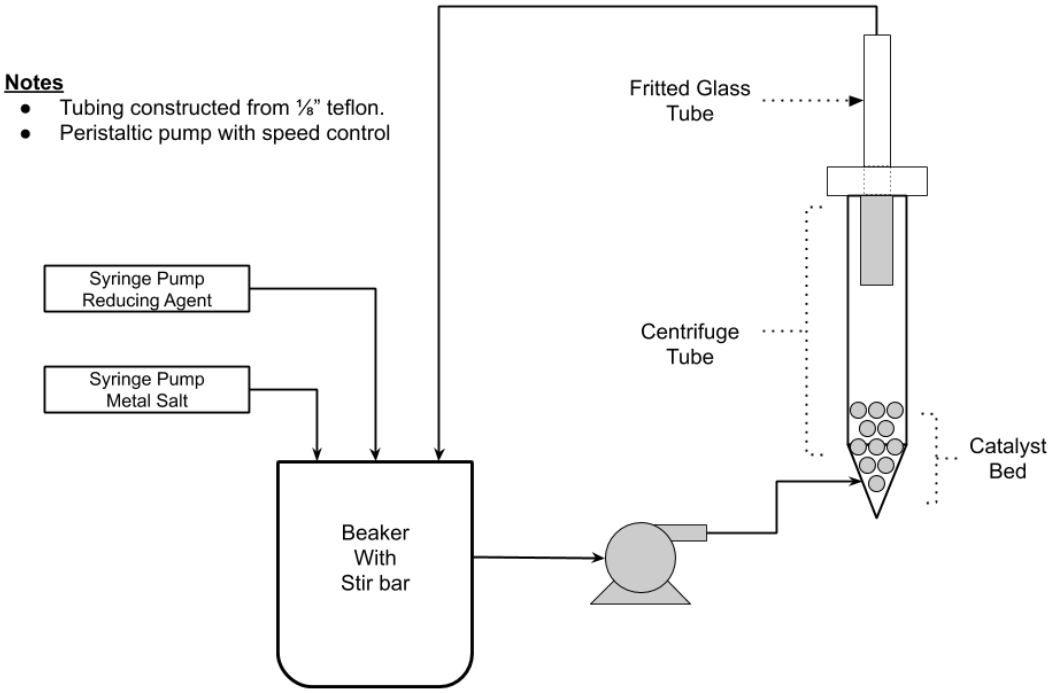

Figure 1.7: Configuration for a percolating bed electroless deposition bath with continuous recycle. All components constructed from metal free materials to prevent deposition on non-desired surfaces.

Figure 1.8 displays the rate of deposition for all catalysts prepared in this study. All higher weight loading samples derived from the common 0.1wt% Ag base catalyst have similar rates of Ag deposition indicating good reproducibility and the absence of experimental artifacts. The sluggish reduction of Ag^{+} over the initial 60 min can be attributed to the kinetics of deposition. Previous work demonstrated Ag ED on Pt to be first order in Pt sites, factional order in HCHO as a RA, and zero order in Ag^{+} concentration [39], indicating that HCHO activation on Pt was the kinetically slow step. Where Pt is an effective catalyst for hydrogen abstraction [43], Ag is relatively weak and will thus require higher HCHO concentrations before electroless deposition becomes favorable. The percolating ED bath demonstrates an effective strategy for controlling particle size with only a minor modification to the ED configurations previously

published [28, 39, 42, 43] and can be adapted to synthesize catalysts on a variety of formed supports suitable for industrial application.

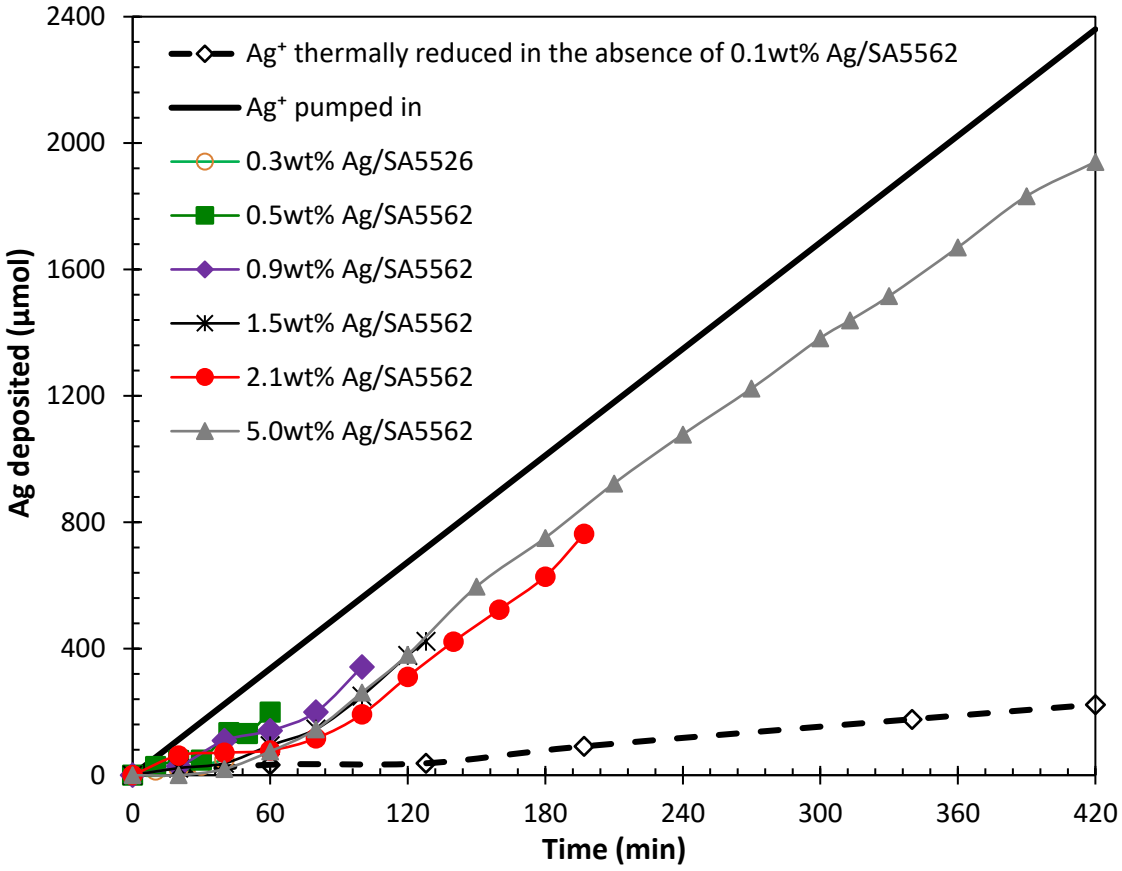

Figure 1.8: Thermal stability of ED bath and kinetic deposition profiles for samples made in this study. No thermal instability was detected before 120min. All ED samples were prepared using a common 0.1wt% Ag/SA5562 base catalyst. Bath conditions: pH 11, HCHO /$AgNO_3$ (2/1), 30 ºC. Ag concentrations were determined by ICP analysis.

1.4.3 Characterization

Catalyst characterization focused on the determination of size and distribution of Ag particles using gas adsorption and microscopy techniques. X-ray diffraction was not performed because particle sizes exceeded the diameters necessary for using FWHM values and the Scherrer equation. Chemisorption using H_2 titration of O-precovered Ag was used to determine the concentration of Ag surface sites to calculate average Ag

particle sizes assuming either spherical or hemispherical geometries. Even more importantly, it determined the actual number of surface Ag sites for calculation of turnover numbers to test for structure sensitivity of EO formation. Typical examples of H_2 uptake plots are shown in Figure 1.9 for 0.1 and 1.5 wt% Ag. Note the significant uptake for Ag loadings as low as 0.1 wt % demonstrating the sensitivity of 1 : 1 H_2 to Ag-O titration stoichiometry.

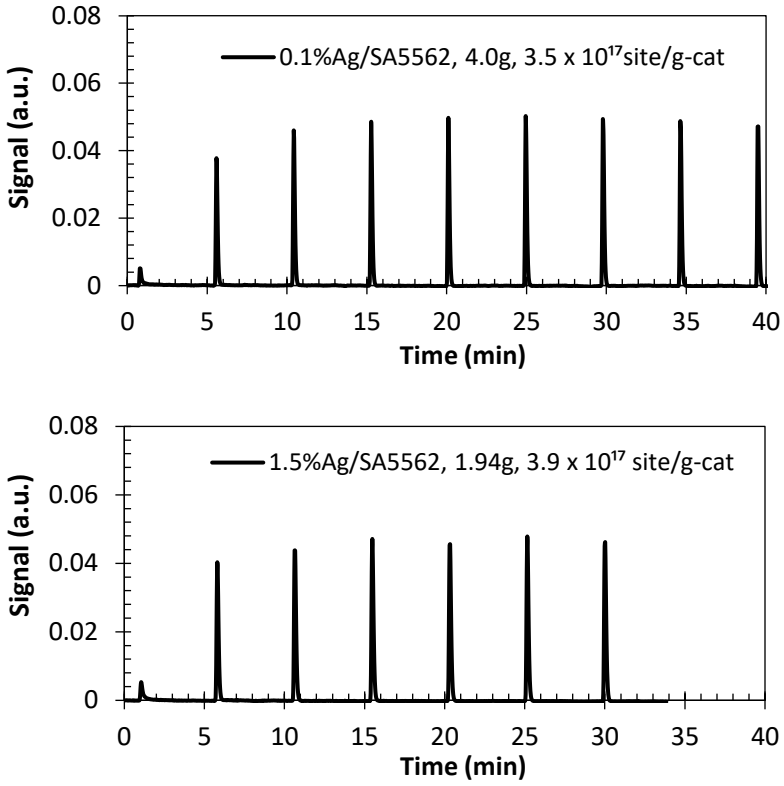

Figure 1.9: Pulsed H_2 uptake for the hydrogen titration of oxygen precovered Ag at 170 ºC for fresh samples of 4.0 g of 0.1% Ag/SA5562 (top) and 1.94 g of 1.5% Ag/SA5562 (bottom).

A summary of particle sizes determined by H_2 titration and SEM are displayed in Table 1.2. Results for fresh samples prepared by electroless deposition and reduced in flowing 20% H_2 balance Ar at 200 ºC for 4 hours indicate an increasing particle size that agrees with the anticipated trend for Ag^+ deposition. 12wt% Ag samples prepared by

incipient wetness of $Ag_2C_2O_4$ show a significantly different average particle size likely related to the oxalate complex [44] or the ethylenediamine solvent which may anchor Ag^+ to the rather featureless α-Al_2O_3 surface [45].

Table 1.2: Catalysts prepared by ED of Ag on 0.1wt% Ag/SA5562.

	Fresh Samples			After Reaction		
Catalyst	**Chemi (nm)**	**SEM[A] (nm)**	**Active Site Max[B] (nm)**	**Chemi (nm)**	**SEM[A] (nm)**	**Active Site Max[B] (nm)**
0.1Ag	19	44 ± 12	20	240	67 ± 19	40
0.3Ag	80	84 ± 30	90	294	112 ± 37	90
0.5Ag	85	90 ± 26	90	119	92 ± 27	70
0.9Ag	148	160 ± 54	150	182	172 ± 63	180
1.5Ag	201	138 ± 46	120	238	157 ± 47	150
2.1Ag	220	211 ± 67	190	290	212 ± 71	210
5.0Ag	292	381 ± 154	370	520	300 ± 112	280
12Ag($Ag_2C_2O_4$)	284	172 ± 60	140	463	160 ± 54	160

A. Results generated from 400 to 1000 particle measurements. Details in Supplemental Figure S2.
B. Particle size shown represents that which contains the maximum number of active sites within the SEM particle size distribution.

SEM particle diameters were measured at the longest particle dimension (for non-spherical geometries) using 400-1000 crystallites and reported in Table 1.2 as the surface average diameter $Ds=\sum n_i d_i^3/\sum n_i d_i^2$ where n_i is the number of particles with diameter d using a 10nm bin spacing and a hemispherical geometry [46]. Active site concentrations were calculated using the full particle size distribution normalized to Ag wt loading; key parameters include the volume of a Ag atom in a low index plane (17.1 $Å^3$) and a projected surface area of 8.7 $Å^2$ for these Ag atoms [19]. This formalism is displayed in Figure 1.10 & 1.11 where histograms based on the quantity of particles are shown as black lines overlayed with a red trace denoting the number of Ag surface sites for the same bin size. Where samples at or below 0.3 wt% Ag have relatively narrow

distributions and the quantity of sites tracks well with the number of particles, particle size begins to broaden as Ag loading increases. When higher weight loading samples are compared using the basis of exposed Ag sites, it is evident that although present, particles below 75nm contribute far fewer surface sites. This feature is most strongly observed in the histogram for fresh 1.5 wt% Ag where a modest, bimodal particle size distribution is centered at 50 and 100 nm but a unimodal site distribution is observed at 120 nm when the size corresponding to the maximum number of active sites is the chosen metric.

SEM-derived particle sizes were in general agreement with those reported from H_2 titration for Ag loadings on fresh samples between 0.3 and 5.0 wt%. The difference in particle sizes comparing chemisorption and SEM for the 0.1 wt% Ag sample in Table 1.2 is likely due to the presence of ultra-small nanoparticles below the limit of detection by SEM but visible by high magnification STEM (Figure 1.10) and also show activity for H_2 titration. In Figure 1.10, additional evidence for the existence of small particles for the 0.1 wt% Ag sample following epoxidation at 210 ºC where small Ag clusters apparently sinter to form larger agglomerations visible in SEM. A similar trend is observed for the 0.5wt% (Figure 1.11) sample where a higher density of particles appears after Ag^+ deposition on previously non-visible Ag sites.

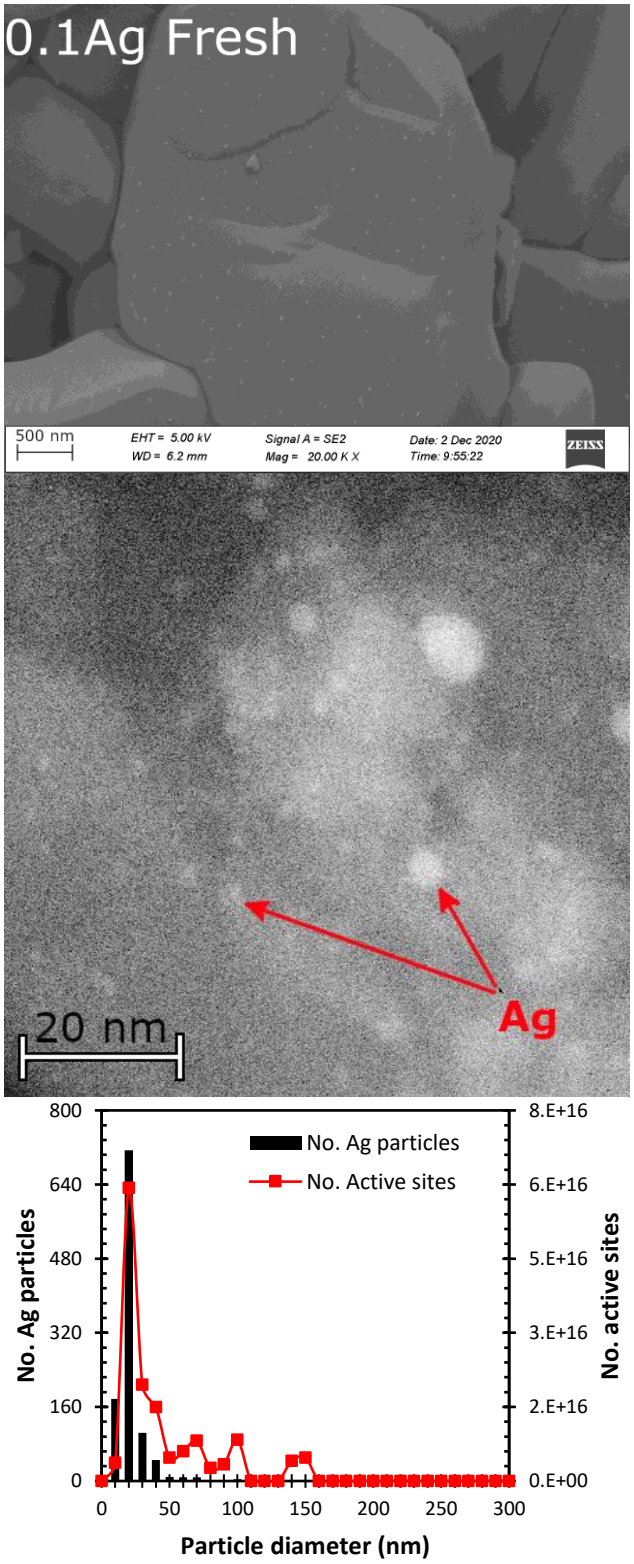

Figure 1.10: SEM (top), STEM (middle), and histogram (bottom) from fresh 0.1Ag/SA5562 following reduction at 200 ºC.

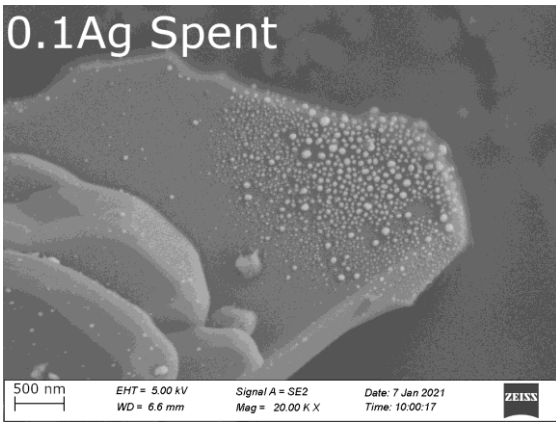
0.1Ag Spent
500 nm
EHT = 5.00 kV
WD = 6.6 mm
Signal A = SE2
Mag = 20.00 K X
Date: 7 Jan 2021
Time: 10:00:17
ZEISS

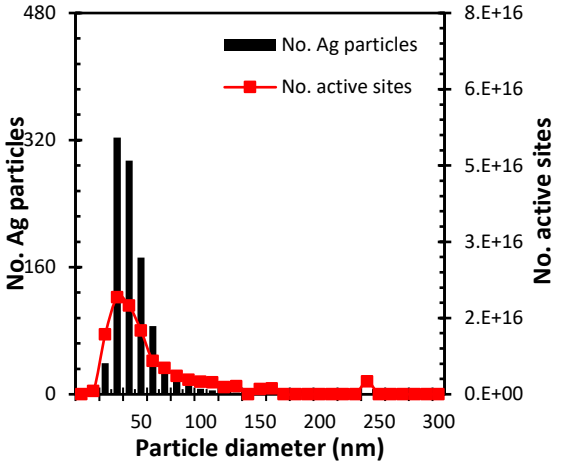
No. Ag particles
No. active sites
No. Ag particles
No. active sites
Particle diameter (nm)
480
320
160
0
8.E+16
6.E+16
5.E+16
3.E+16
2.E+16
0.E+00
50
100
150
200
250
300

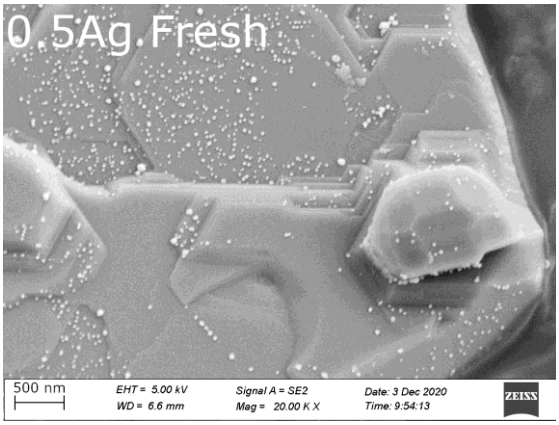
0.5Ag Fresh
500 nm
EHT = 5.00 kV
WD = 6.6 mm
Signal A = SE2
Mag = 20.00 K X
Date: 3 Dec 2020
Time: 9:54:13
ZEISS

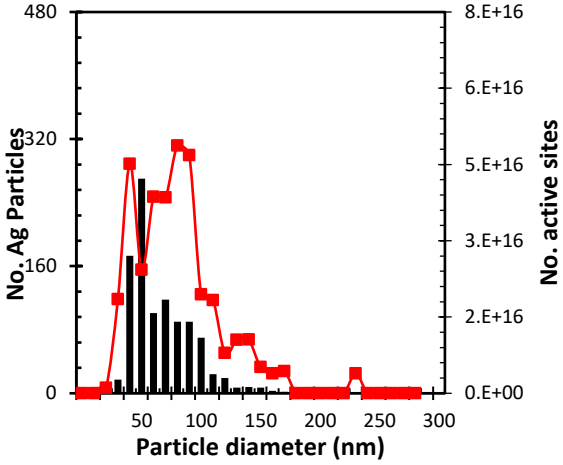
No. Ag Particles
No. active sites
Particle diameter (nm)
480
320
160
0
8.E+16
6.E+16
5.E+16
3.E+16
2.E+16
0.E+00
50
100
150
200
250
300

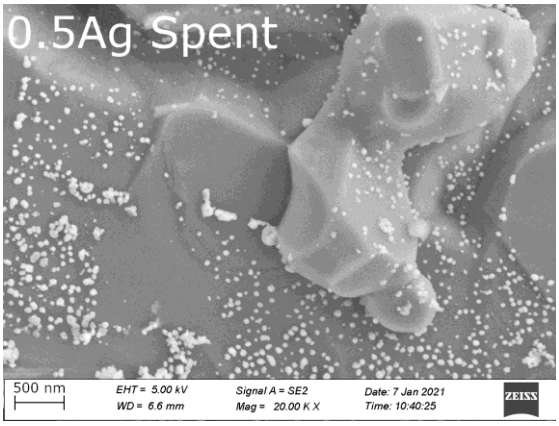
0.5Ag Spent
500 nm
EHT = 5.00 kV
WD = 6.6 mm
Signal A = SE2
Mag = 20.00 K X
Date: 7 Jan 2021
Time: 10:40:25
ZEISS

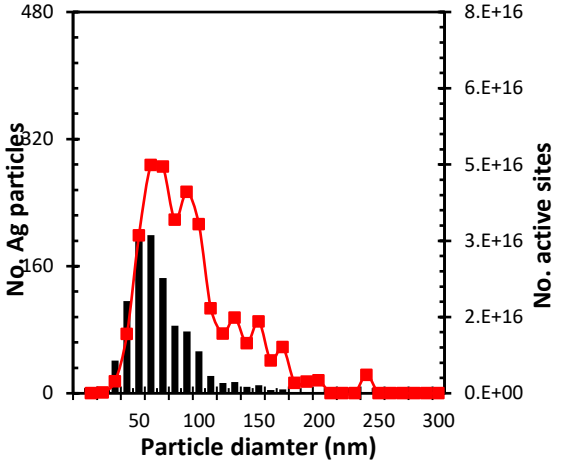
No. Ag particles
No. active sites
Particle diamter (nm)
480
320
160
0
8.E+16
6.E+16
5.E+16
3.E+16
2.E+16
0.E+00
50
100
150
200
250
300

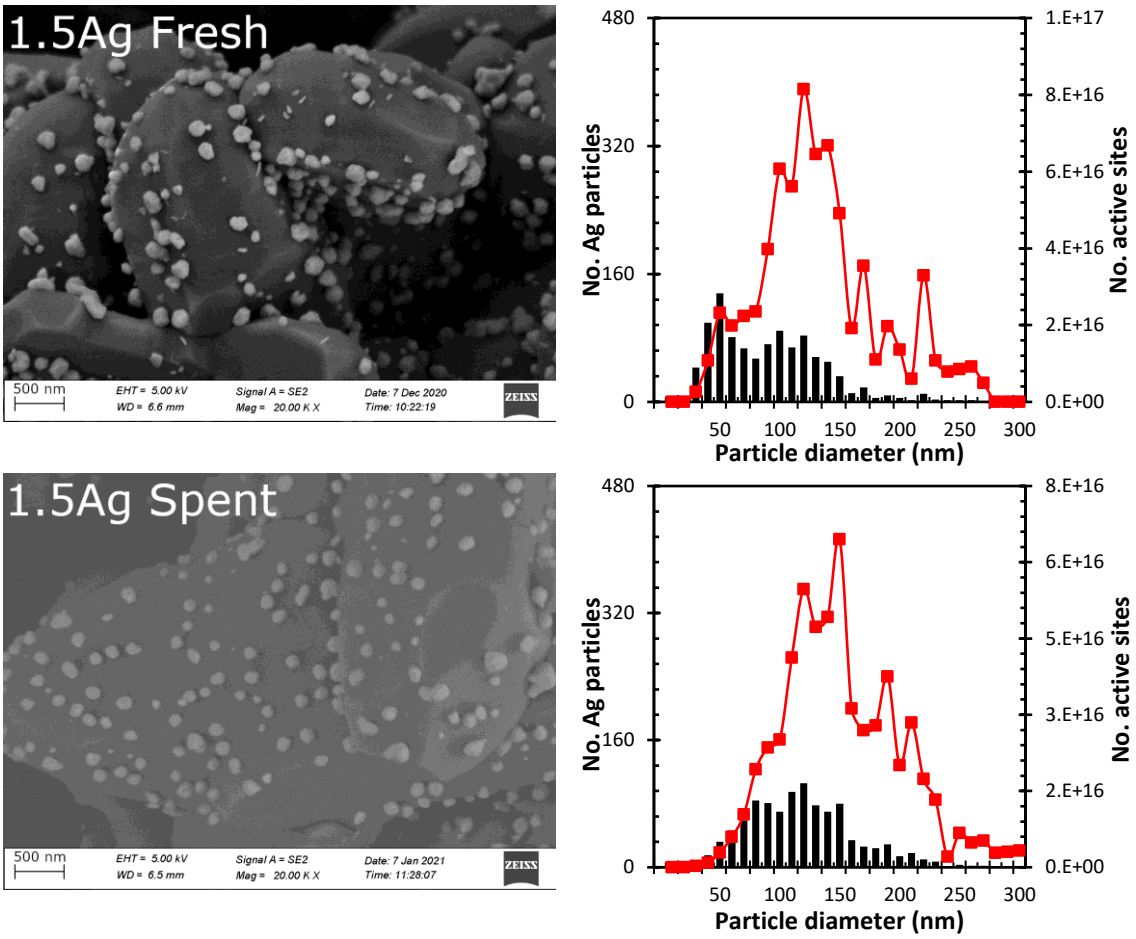

Figure 1.11: SEM images for "Fresh" samples treated in flowing 50% H_2 balance He at 200 °C and "Spent" samples treated under reaction conditions at 210 °C.

Particle size measurements following reaction using H_2 titration indicated growth for all samples, but most notably for the 0.1 wt% Ag sample; the fresh sample was 19 nm and spent increased dramatically to 240 nm in size (Table 1.2). However, SEM analysis showed an apparent growth only from 44 to 67 nm in diameter. Temperature programmed burnoff (TPO) curves in Figure 1.12 for the spent 0.1 % Ag sample suggests the presence of extensive carbon fouling; the peaks centered at 225 and 370 ºC are attributed to carbon in contact with the Ag and alumina surfaces, respectively. TPO analysis of the α-Al_2O_3 support rings indicated the 370 ºC peak may in part be due to residual burnout agents used to generate the macropores during support manufacturing.

However, STEM analysis of the spent 0.1wt% Ag sample also showed accumulation of cloud-like, carbon deposits on the spent material. These findings suggest the high temperature burnoff peak is associated with carbon at the perimeter of the Ag-alumina interface and represents thermal, rather than Ag-catalyzed, burnoff. However, some of the Ag particles are likely encapsulated by the carbon deposits.

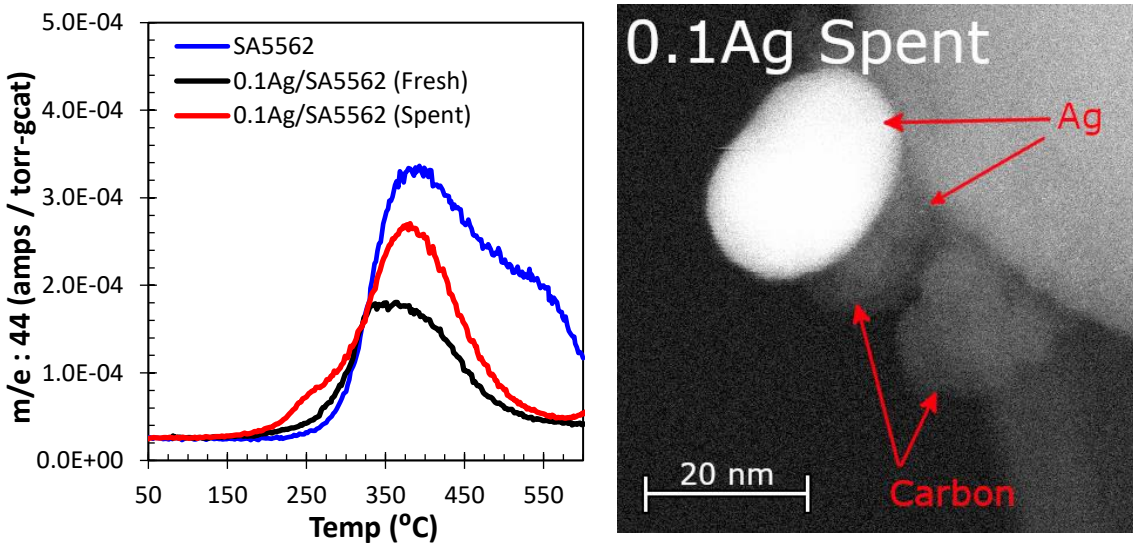

Figure 1.12: Temperature programed oxidation of fresh and spent 0.1wt% Ag catalyst prepared from $AgNO_3$ and factory supplied SA5562 α-Al_2O_3 (left). The large m/e:44 peak presence for the unmodified support suggests residual burn out agent from the manufacturing process. STEM image for 0.1 wt% Ag/SA5562 indicating the deposition of carbon following reaction. All experiments were performed with a ramp rate of 20°C/min and a gas flow rate of 20 SCCM.

A foulant factor (λ) denoting the extent of Ag fouling can be calculated according to Equation 1.1 where the number of hydrogen titration sites is scaled to adjust for sintering across the entire distribution of particles using SEM measurements collected before and after reaction. C_f and C_s denote the number of Ag sites determined by H_2 titration for the fresh and spent samples, respectively, and the second term corrects for particle sintering during reaction; S_S and S_f denote the Ag surface site concentrations determined by SEM before and after reaction, respectively.

$$\lambda = \left(\frac{C_f}{C_s}\right)\left(\frac{S_s}{S_f}\right) \quad (1.1)$$

Foulant factors equal to unity represent a sample that exhibits no sintering and no fouling during reaction. Values > 1 indicate fouling occurs and for < 1, some Ag particles undergo redispersion and fouling is non-existent. The results in Figure 1.13 imply that samples comprised of particles below 100 nm in diameter are subject to increased carbon deposition and sintering as indicated by λ values of 8.1 and 2.5 for the 0.1 and 0.3 wt% samples respectively. Histograms for the spent 2.1 and 5.0 wt% samples in Supplemental Figure S2 suggest a possible redispersion of particles above 200 nm with some Ag particles centered between 50 and 75nm following reaction. Hensen [47] noted a similar behavior for 5 and 10 wt% Ag/α-Al_2O_3 catalysts prepared by incipient wetness of $Ag_2C_2O_4$ for particles >100 nm when vinyl chloride was included in the feed. Even if higher Ag loadings catalysts contain some Ag particles < 50 nm, these particles make little contribution to the total number of accessible sites.

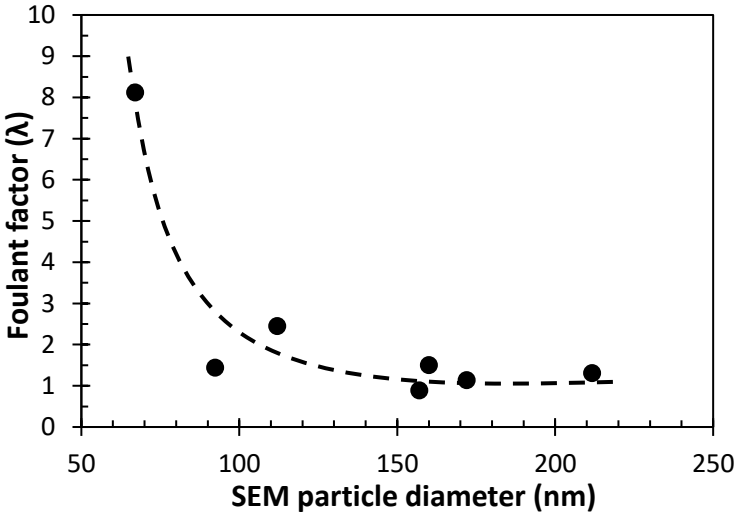

Figure 1.13: Foulant factors calculated from fresh and spent H_2 titration result as a function of Ag particle sizes determine by SEM measurements for used samples.

1.4.4 Evaluation

Ethylene epoxidation rates were measured at 210 ºC using a EO feed containing 25% C_2H_4, 8% O_2, balance CH_4. As stated earlier ppm levels of ethyl chloride feed additive were omitted to avoid potentially different rates of Cl deposition on different sized Ag particles [47]. Turn over frequencies (TOF) are reported at steady state reaction conditions, typically after 65 hours on-line, although some samples took longer to achieve steady state behavior. A representative time on stream (TOS) plot for 1.5wt% Ag is displayed in Figure 1.14 for a reaction period of 300 hrs. Gaps in the data are periods where EO work rates were varied to determine intrinsic selectivity (Figure 1.17) or represent the initial 20-hour startup where catalyst performance is quite transient.

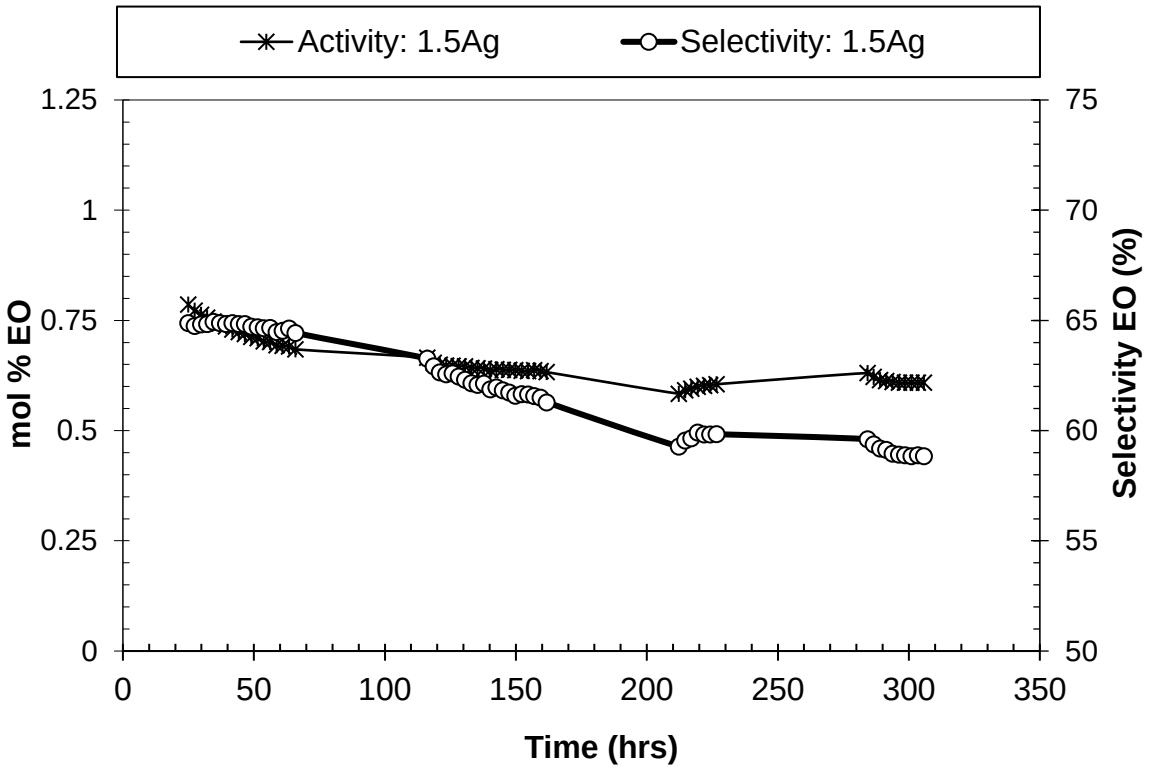

Figure 1.14: Activity and selectivity results for 1.5wt%Ag/SA5562 evaluated with a feed composition of 25% C_2H_4, 8%O_2, balance CH_4.

Similarly, the other catalysts were evaluated and the data used to generate TOF plots, Figure 1.15, and summarized in Table 1.3. Where microscopy accurately captures geometric changes in particle size, it can only infer active site concentrations and thus TOF numbers are in relative agreement for the fresh and spent samples. Conversely, TOF numbers determined by pulsed H_2 titration for the fresh samples were quite different compared to the spent material. We believe that the true active surface is best characterized by pulsed titration using samples collected following reaction after the material has reached pseudo steady state operation since this technique directly measures the number of chemically accessible Ag-O bonds. Interestingly the TOF for 12wt% catalyst on SA5562, denoted as an open marker in Figure 1.15, is 0.12 s^{-1} with an active site concentration of 1.66 X 10^{+18} and is in agreement with all ED derived samples by a factor of 2x. Consequently, there is no significant particle size effect considering TOF multipliers of this magnitude are within the error of characterization or similar space time yields can be obtained by minor adjustments to the reactor parameters such as catalyst loading and gas hourly space velocity (GHSV).

Table 1.3. Summary of turnover number for EO formation calculated from the quantity of active sites from H_2 titration and particle size distributions from SEM.

	TOF, Fresh Samples (s^{-1})		**TOF, Spent Samples (s^{-1})**		**Sites from Spent Chemi (sites / g cat)**
Catalyst	**SEM**	**Chemi**	**SEM**	**Chemi**	
0.1Ag	0.05	0.02	0.07	0.24	2.82 X 10^{+16}
0.3Ag	0.07	0.11	0.10	0.34	5.06 X 10^{+16}
0.5Ag	0.06	0.06	0.06	0.08	2.75 X 10^{+17}
0.9Ag	0.10	0.09	0.10	0.11	3.09 X 10^{+17}
1.5Ag	0.08	0.11	0.09	0.11	4.84 X 10^{+17}
2.1Ag	0.11	0.11	0.11	0.15	4.77 X 10^{+17}
5.0Ag	0.13	0.10	0.10	0.18	6.25 X 10^{+17}
12Ag($Ag_2C_2O_4$)	0.05	0.09	0.04	0.12	1.66 X 10^{+18}

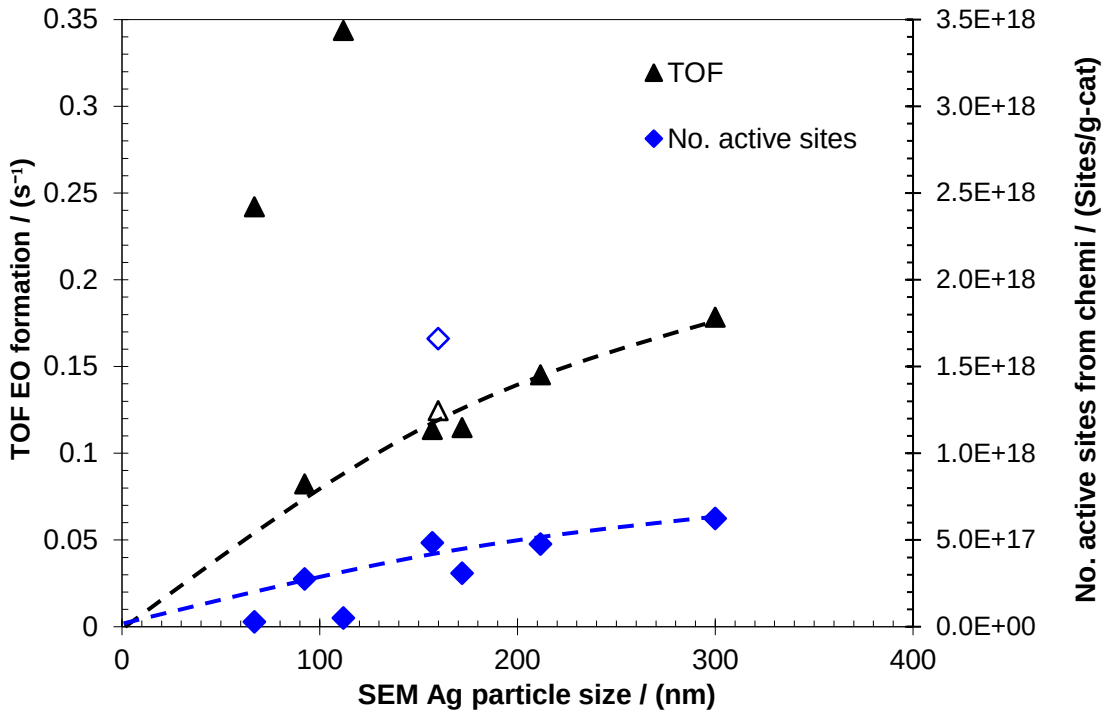

Figure 1.15: Turn over frequency for EO formation. Particle size was determined from SEM imaging of samples following reaction. Active site quantities were determined from H_2 titration of spent samples. Open markers denote the 12wt% Ag control sample prepared from $Ag_2C_2O_4$.

The high activity of the 0.1Ag (0.24 s^{-1}) and 0.3Ag (0.34 s^{-1}) is not likely the result of increased turnover for small particles but an artifact from EO integration at low olefin conversion and division by a small number of active sites in the presence of carbon foulant. Furthermore, small particles were not able to stabilize from sintering despite the mild thermal conditions (210 ºC) used during evaluation. This finding is not unexpected considering the inert, rather featureless, surface of the α-Al_2O_3. It is also worth noting that the reaction order for O_2 was between 0.8 and 0.91 and the reaction order for C_2H_4 was between -0.04 and -0.2 for average particle sizes between 67 and 211 nm determined by SEM following catalytic evaluation, Figure 1.16. These reaction orders are similar to those determined by Jankowiak and Barteau for EO formation under oxygen lean

conditions [35] and suggests there is no change in the rate determining step(s) and that the mechanism is independent of particle size.

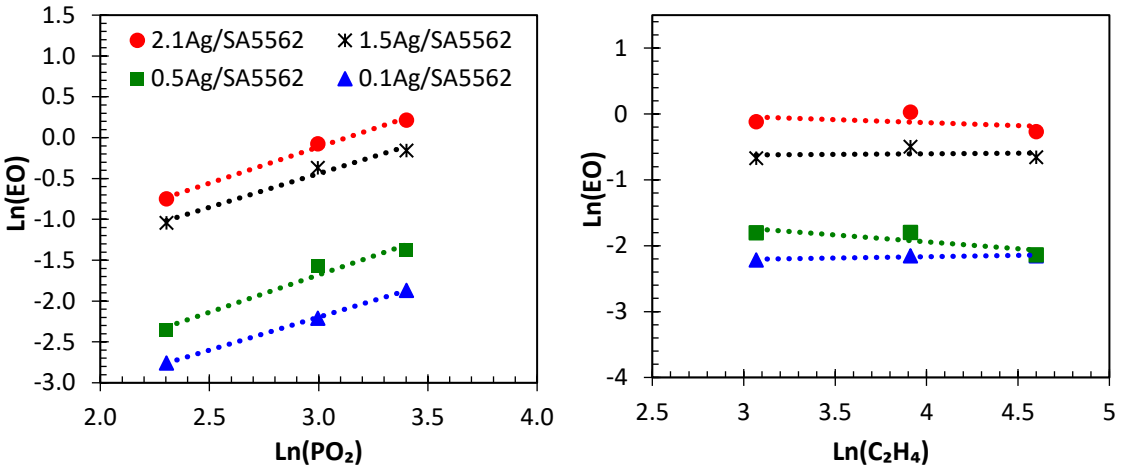

Figure 1.16: Oxygen (left) and ethylene (right) reaction orders for select catalysts representing particles between 19 and 211 nm in size. Oxygen and ethylene reaction orders were determined to be pseudo first and zero order respectively.

Where turnover numbers are relatively similar, a significant particle size effect is that of selectivity for EO formation plotted as a function of catalyst work rate, Figure 1.17. The slope, indicative of sequential EO combustion, for the 1.5, 2.1, 5.0, and 12 wt% Ag samples is identical within experimental error suggesting particles between 157 and 300 nm have no effect on the metal catalyzed combustion of reabsorbed EO. That is as the reaction chemistry is directed towards EO formation, each catalyst sacrifices an equal quantity of selective product and at the mild conditions used, this behavior can be directly attributed to the Ag crystallites independent of background isomerization on the support. A comparison of intrinsic selectivity where the best fit lines intersects the Y axis at 0 mol% EO does indicate a particle size effect following the trend 67nm ≈ 92nm (58% EO) < 157nm (67% EO) < 211-300nm (73% EO). The presence of carbon foulant

concentrated on small particles implies the combustion of a strongly bound species, likely an EO intermediate, is responsible for the observed trend in selectivity. This finding is not unlike that observed for butadiene epoxidation [48] where foulant was determined to originate from adsorbed product, epoxybutene (EpB), by addition of small amounts of EpB to reactor feed.

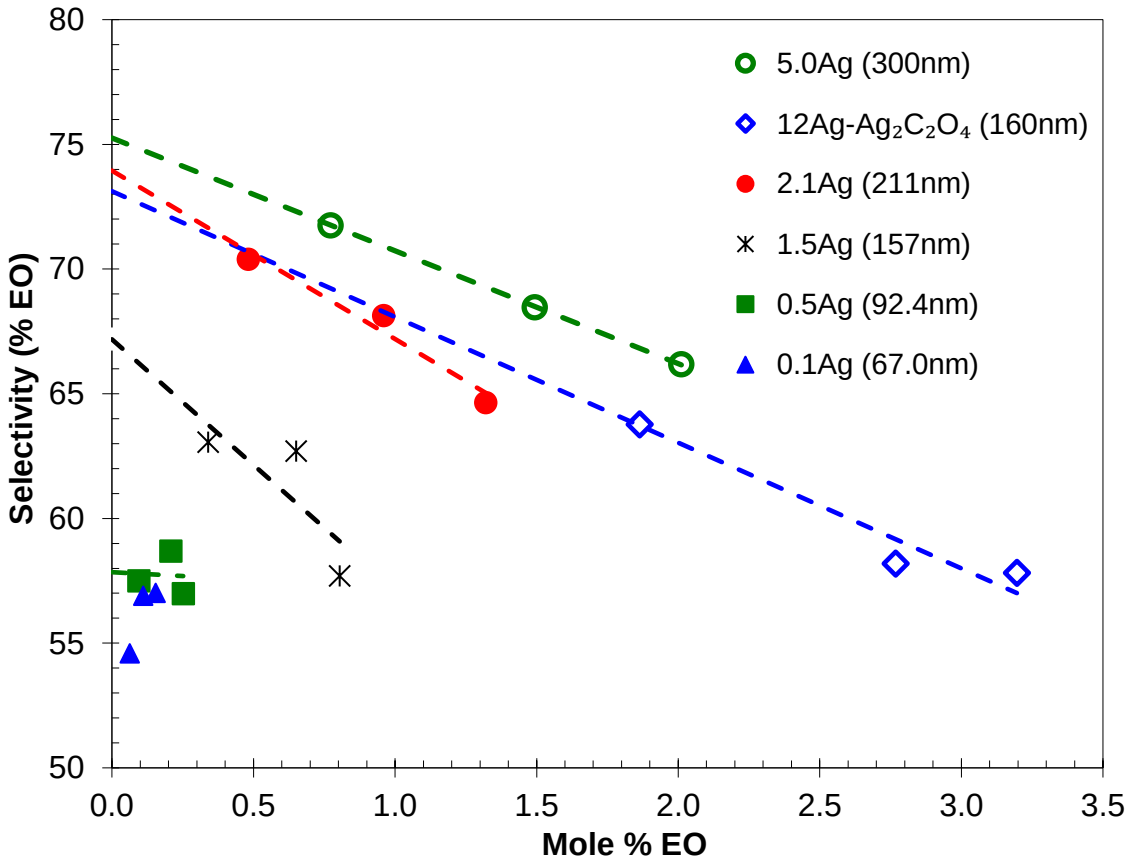

Figure 1.17: Activity-Selectivity plot for select samples. The relative slopes for samples containing > 1.5wt%Ag are in agreement suggesting the same magnitude of consecutive combustion. For particles below 160nm, the intercept is significantly reduced indicating selectivity suffers due to C_2H_4 combustion. Data was collected at 210 ºC where EO isomerization on the support was negligible.

While we have focused on particle size to improve TOF and selectivity the state-of-the art method for adjusting catalyst performance is the addition of promoters and co-promoters. This effect is evident in Figure 1.18 where EO selectivity is plotted as a

function of catalysts work rate for an unpromoted 12wt% Ag/SA5562 and a fully promoted 12wt% Ag/SA5562 containing Cs, Re, Mo, and S. Samples were evaluated in a feed containing 25% C_2H_4, 8%O_2, 2.0ppm ethyl chloride (EtCl), balance CH_4. Work rate was adjusted by varying gas hourly space velocity between 4200 and 13800 hr^{-1}. Suppression of sequential EO combustion is demonstrated by the relative slopes with the fully promoted catalyst having a value of -1.29 and the unpromoted sample having a value of -5.05. In operation using a common 2.0 mol% EO in the product, these slopes translate to a working selectivity of 75 and 90% for the unpromoted and promoted samples respectively. Note that that the addition of a promoter package also increases intrinsic selectivity from 85% to 92% indicating the promoters may aid desorption of EO and EO intermediates [8, 9, 11, 49-51]. Another possible role of the alkali metal promoters is the titration of Lewis acidity on the alumina which reduces the degree of sequential EO combustion via acid catalyzed isomerization [52, 53]. Reactions in the current study were performed at 210 ºC where no isomerization products were detected by GC analysis however, in commercial applications it is common to operate using reactor temperatures above 230 ºC in order to obtain space time yields [2, 10, 12]. These promoters represent a strategy for obtaining catalysts that are both highly active and highly selective under commercially relevant conditions.

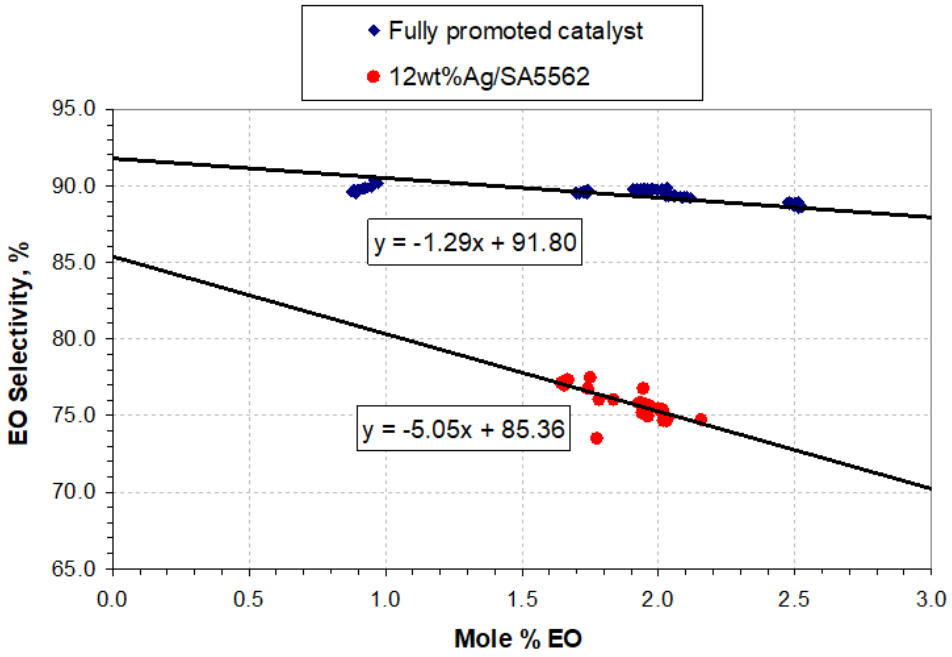

Figure 1.18: EO formation vs selectivity to EO for unpromoted 12wt%Ag/SA5562 and the same catalyst promoted with Cs, Re, and co-promoters. Samples were evaluated in ¼" OD reactors in a 150sccm feed containing 25% C_2H_4, 8% O_2, 2.0ppm EtCl, balance CH_4.

1.5 CONCLUSION

The present study has indicated that the structure sensitivity for ethylene oxide formation is indeed present in α-Al_2O_3 supported Ag catalysts with varying particle size. It is found that not only the method of characterization but whether the particles were measured before or after reaction to be significant factors for determining performance. Where microscopy is sufficient for the determination of geometric particle size it can only infer active site concentrations and not chemical accessibility which is better represented by the hydrogen titration of oxygen precovered Ag. A combination of these methods indicates that particles >100 nm are resistant to both Ag sintering and the formation of carbon foulant. TOF as a function of particle size shows a Langmuir type curve with a relatively minor increase (2.25X) between the highest and lowest

performing samples. Selectivity, which is independent of TOF, shows the greatest sensitivity to particle size in which intrinsic selectively follows the trend 67nm ≈ 92nm (58% EO) < 157nm (67% EO) < 211-542nm (73% EO) at the primary reaction independent of background activity on the support. It is therefore concluded that particle size is a relatively insensitive parameter for improving EO formulations provided particle diameters are in excess of 100nm.

CHAPTER 2

HYDROGEN TITRATION OF Ag/α-Al_2O_3 OLEFIN EPOXIDATION CATALYSTS CONTAINING PROMOTERS AND CO-PROMOTERS

2.1 ABSTRACT

In Chapter 1 we identify structure sensitivity trends on unpromoted Ag noting the significance of active site quantification using hydrogen titration when characterizing samples before and after catalytic evaluation. In Chapter 2 the question is proposed can meaningful information be extracted from the pulsed hydrogen titration of Ag/α-Al_2O_3 catalysts containing one or more common EO promoters. Re, Cs, Mo, S and/or W were co-impregnated with Ag from $Ag_2C_2O_4$ (Ag oxalate). Following a standardized pretreatment to remove residual organic ligand, pulsed hydrogen titration preceded by oxygen dissociation, both performed at 170 °C, showed a sample-to-sample deviation of ± 0.004 cm^3-STP/g-cat for unpromoted Ag/α-Al_2O_3. Control experiments using high loadings of Cs, Re, or Mo on Ag free α-Al_2O_3 showed no indication that the 170 °C titration temperature used in this study caused reduction of the cationic salts or high valent nonmetal promoters. H_2 uptake following oxygen dissociation on promoted Ag samples was found to be a linear function of umol promoter loading and was independent of the promoter element or co-elements indicating coverage of the Ag surface sites. Experiments holding promoter concentration constant while increasing Ag loading resulted in a significant increase in H_2 uptake. Consequently, it is believed that pulsed H_2 titration can be directly correlated with the quantity of Ag-O bonds.

2.2 INTRODUCTION

Following the discovery of Ag catalyzed ethylene epoxidation in 1931 [1], the maximum selectivity towards ethylene oxide (EO) formation was assumed to be limited at 6/7 (85.7 mol% EO) according to the stoichiometry in Equation 2.1.

$$7C_2H_4 + 6O_2 \rightarrow 6C_2H_4O + 2H_2O \quad (2.1)$$

In 1937, the possibility of surpassing this limit was first disclosed by Carter who noted increased EO yield attributed to trace amounts of alkali metal salt contained in a clay carrier. Others later elaborated on this concept with Mc Namee citing a promotional effect from Na and K [54], Sears Jr citing a broad range of promoter elements including various halides of the Group 1 and 2 elements [55], and Sacken who noted a promotional effect from alkali metal sulfates[56]. Specific ranges for mono promoted Cs and co-promoted Cs-Re samples were later noted by scientists at Shell, Nielsen in 1976 [57] and in most notably Lauritzen in 1988 [15]. Today promoter packages contain Cs and Re and may contain W, Li, S, Mo, and other high valent transition metal oxy-anions which enable state-of-the-art catalysts to operate at an initial EO selectivity approaching 92% with meaningful single pass olefin conversion [10]. However, the high concentration of non Ag species in modern EO formulations will require higher operating temperatures and higher Ag loadings to achieve the same space time yield as unpromoted or previous generation high activity catalysts containing lower quantities of Cs-Re [8].

The kinetics of unpromoted Ag/α-Al_2O_3 have been investigated in detail by Jankowiak and Barteau who noted that the temperature dependency for CO_2 formation exceeds selective epoxidation under a wide variety of feed compositions [35]. Where promoters suppress the pathways for both direct and sequential combustion, these

findings demonstrate that increasing temperature as a strategy to recover C_2H_4 turnover will ultimately lead to non-selective products. Consequently, many EO producers have selected to operate in hydrocarbon rich feeds at lower than historic EO work rates (%EO in the product) which favor selective product formation. To design promoted catalysts that are both active and selective requires an understanding of Ag site concentrations best characterized by gas adsorption techniques that directly measure the number of chemically accessible Ag-O bonds.

In 1984 Vannice et al developed the method of hydrogen titration using oxygen precovered Ag whereby hydrogen reacts with Ag bound monatomic oxygen forming H_2O as a product. The procedure used Ag/TiO_2 samples prepared by incipient wetness of $AgNO_3$. The nitrate ligand was removed by hydrogen reduction at 300 ºC followed by O_2 dissociation at 170 ºC to obtain 1 ML oxygen coverage based on the work of Czanderna [58]. Where the prior technique, oxygen chemisorption, followed a ½ to 1 stoichiometry, Equation 2.2, hydrogen titration has the advantage of doubling the sensitivity of detection following a 1 to 1 H_2 to Ag-O ratio, Equation 4 [21]. Prior work from our group has shown this technique to be effective at determining Ag-O site concentrations on Ag/α-Al_2O_3 catalysts containing metal loadings as low as 0.1wt% Ag [59].

$$O_2\ (g) + 2\ Ag\ (s) \rightarrow 2\ AgO\ (ads) \qquad (2.2)$$

$$AgO\ (ads) + H_2\ (g) \rightarrow Ag\ (s) + H_2O\ (ads) \qquad (2.3)$$

There has been some effort to explore the effect of alkali metals on the strength of oxygen adsorption using model Ag catalysts at ultra-high vacuum (UHV) conditions. Prince and Kordesch examined oxygen desorption on Ag(110) promoted with 0.25ML of Cs and observed a single peak at 300 ºC for unpromoted Ag and two desorption peaks at

320 ºC and 360 ºC for Cs-Ag [60]. Ultraviolet photoelectron spectroscopy (UPS) showed a reduction in the Cs 5p level, and it was concluded that Cs draws electrons from surface bound oxygen thereby decreasing its reactivity for combustion. In a similar study, Campbell et al examined oxygen adsorption on Ag(110) by varying the level of Cs between 0 to 0.25 ML. The quantity of O_2 adsorbed was shown to increase with Cs loading most notably below 0.1 ML Cs coverage with all oxygen desorption peaks occurring above 280 ºC [61]. Madix and Guo later investigated O_2 adsorption on Ag(110) promoted with 0.1ML Cs [49] and detected oxygen desorption as a single peak at 310 ºC for clean Ag but two peaks at 180 & 430 ºC for the Cs-Ag sample. In all cases, it is not clear whether oxygen exposed Cs exists as CsO or an Ag-Cs-O complex however what can be stated is that Cs does change the strength of the Ag-O bond.

Jingfa et al. applied temperature programmed desorption (TPD) to identify three oxygen species on unsupported Ag granules promoted with Cs_2CO_3 and NH_4ReO_4. Oxygen desorption peaks (m/e = 32) at 115, 305, and T > 500 ºC were identified as molecular, monoatomic, and subsurface oxygen using CO (m/e = 28) to selectively titrate surface bound monatomic oxygen forming CO_2 (m/e = 44). It was observed that the Ag-Re sample contained no monoatomic oxygen however upon close examination the intensity of the molecular oxygen peak at 115 ºC substantially increased implying a weakening of Ag-O interaction for Re promoted samples. UHV experiments confirmed a decrease in the Ag work function for Ag-Re and Ag-Re-Cs samples. The authors concluded that Re shifts the electron density away from Ag forming electrophilic oxygen while Cs increases the Ag charge density forming nucleophilic oxygen.

At the time of this manuscript, few have investigated promoter effects on the chemisorption of Ag samples supported on commercial α-Al_2O_3. Vannice and Badani prepared a series of catalysts from $Ag_2C_2O_4$ dissolved in ethylenediamine and impregnated on ¼" rings of 0.78 m^2/g α-Al_2O_3 [11]. Cs was added by co-impregnation with Ag using $CsNO_3$ to study the Ag-Cs interaction or CsCl to study the effect of Cl often added to the feed stream as chloroethane or vinyl chloride in an industrial reactor [32, 62]. All samples were calcined at 250 ºC in 20% O_2 Bal Ar, cooled to 200 ºC then reduced in 20% H_2 bal Ar, before oxygen adsorption followed by hydrogen titration were performed at 170 ºC using a static adsorption apparatus. With the addition of $CsNO_3$, the quantity of reversible oxygen uptake followed the trend Ag (0%) < Ag, 409ppm Cs (6%) < Ag, 1174ppm Cs (30%) and it was stated that CsO could not be reduced at the low temperature pretreatment conditions. Thus, the oxygen measurements were directly associated with a weakening of the Ag-O bond by Cs. Contrary to the Cs-Ag samples, Cl containing samples showed a significant reduction in the total quantity of adsorbed oxygen implying a geometric effect whereby chloride occupies a fraction of the Ag surface.

In the current manuscript we report a method for the selective titration of Ag-O bonds using supported Ag/α-Al_2O_3 samples containing Cs, Re, Mo, and W. Temperature programed desorption experiments on unprompted samples indicate a clean Ag surface following the removal of ethylenediamine by ex-situ calcination at 280 ºC. We further demonstrate that while 170 ºC is sufficient to titrate oxygen precovered Ag, there is insufficient thermal energy to reduce the alkali metal or high valet oxy anion promoters. Consequently, it is shown that H_2 uptake is directly related to the quantity of Ag-O bonds

and that as the surface concentration of promoter increases, the number of titration sites decreases in a manner that is only dependent on the total umol loading and not the identity of the promoter.

2.3 EXPERIMENTAL METHODS

2.3.1 Synthesis

Catalysts were prepared by co-impregnation. The $Ag_2C_2O_4$ was dissolved in ethylenediamine (EN) using a 3:1 ratio for EN: $Ag_2C_2O_4$. The impregnation solution was prepared at 5% excess pore volume of the carrier (Saint Gobain SA5562 α-Al_2O_3, 8-mm rings, BET Surface area 0.73 m^2/g by Kr BET, water accessible pore volume 0.53cm^3/g-support). Promoter salts were added using co-impregnation of NH_4ReO_4, $CsNO_3$, $(NH_4)_6[H_2W_{12}O_{40}]*2H_2O$, $(NH_4)_2MoO_4$, and $(NH_4)_2SO_4$ dissolved with $Ag_2C_2O_4$ in ethylenediamine solution. The rings were tumble dried in a 400ml round bottom flask under vacuum (10 inHg) at 70 ºC until free tumbling was observed. Following impregnation, samples were calcined in fast flowing air (5L/min) at 260 ºC for 5min. SA5562 samples containing Cs, Re, or Mo but no Ag were impregnated using a water-salt solution at 5% excess pore volume. These samples were tumbled dried in vacuum and fast calcined using the same parameters noted for Ag containing samples.

2.3.2 Catalysts Pretreatment and Hydrogen Titration

Prior to analysis, all Ag catalysts were calcined ex-situ at 280 ºC in flowing air for 4 hours to remove residual ethylenediamine and are referred to as “fresh” material. Unless specified, each experiment used 2.0g of ground sample (841-400 μm, 20/40mesh) loaded into a Micromeritics Autochem 2920 equipped with a thermal conductivity

detector (TCD) and reduced in-situ in flowing 10% H_2 bal He at 280 ºC for 2 hours. Following reduction, samples were cooled to 170 ºC in flowing 10% H_2 bal He, purged with He for 30 min, and exposed to 10% O_2 bal He for an additional 30 min to dissociate molecular oxygen [58] .The sample chamber was then flushed with He for 30 min and pulsed hydrogen titration was performed at 170 ºC and atmospheric pressure. The oxygen precoverage and hydrogen titration steps were repeated in-situ 3x and reported as an average. Good agreement was observed between all three titration experiments. Error bars reported for cumulative H_2 uptake represent select cases where 2.0g of fresh sample was loaded three separate times followed by three in-situ titration cycles (9 total cycles).

2.3.3 Temperature Programed Experiments

Temperature programed desorption (TPD) was performed using a high wattage, split-tube furnace connected to an Inficon Transpector 2 Mass Spectrometer and a series of Brooks 5850E mass flow controllers. Following fast calculation at 260 ºC, 0.5g of material was loaded into a ¼-inch quartz tube supported on a quartz plug and heated to 500 ºC at 10ºC/min in 20sccm flowing Ar while monitoring for ethylene diamine at m/e = 30 [63]. Temperature programed reduction (TPR) was performed in the same Micromeritics Autochem 2920 described above using 2.0g of "fresh" material ex-situ calcined at 280 ºC. The sample was reduced in-situ at 280 ºC for 2 hours in 20 sccm H_2, cooled to 170 ºC in 20 sccm Ar where oxygen dissociation was performed for 30 min in 20 sccm of flowing 10% O_2/He. The catalyst was then cooled to 30 ºC in 20 sccm of Ar and the feed was switched to 20 sccm 10% H_2 bal Ar before TPR was performed up to 300 ºC using a ramp rate of 20ºC/min.

2.4 RESULTS AND DISSCUSSION

2.4.1 Catalyst Pretreatment

Initial experiments were performed to confirm a clean Ag surface using unpromoted 12wt% Ag/SA5562. Figure 2.1 shows the temperature programed desorption (TPD) pattern for two samples exposed to different calcination conditions. The standard preparation notation refers to samples that were fast calcined in rapidly flowing air at 260 ºC for 5 min prior to TPD analysis. Despite fast calcination, a large ethylenediamine (EN) peak (m/e = 30) was observed with a peak center at 260 ºC demonstrating significant retention of the $Ag_2C_2O_4$ solvent. The second sample, treated ex-situ in flowing air at 260 ºC for 12 hours, had a significantly smaller EN peak intensity that was centered around 340 ºC suggesting the remaining ligand was strongly bound. From this analysis, a 4-hour pretreatment at 280 ºC in flowing air was selected for all promoted and unpromoted samples performed ex-situ to prevent fouling of the chemisorption apparatus observed as a dark brown coating on at the exit of the quartz sample holder.

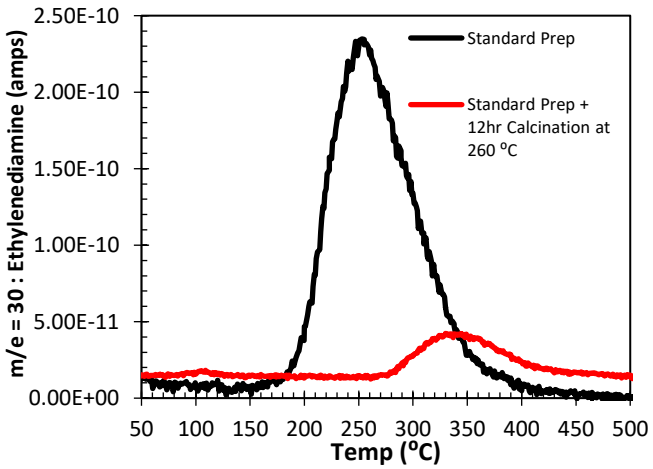

Figure 2.1: Thermal desorption of ethylenediamine (m/e = 30) in flowing Ar for two 12wt%Ag/SA5562 samples prepared from $Ag_2C_2O_4$ differing in the length of ex-situ calcination (Experimental parameters: 0.5g sample, 20sccm Ar, 10ºC/min).

Following pretreatment, the repeatability of hydrogen uptake on unprompted 12wt% Ag/SA5562 was tested using a series of pulsed titration experiments. In all cases 2.0g of fresh material supported on a bed of quartz wool were loaded into a quartz U tube. The samples were reduced in-situ at 280 ºC using 10%H_2 bal Ar, purged with Ar, then cooled to 170 ºC where oxygen dissociation and pulsed hydrogen titration were performed. The pulsed hydrogen titration is represented in Figure 2.2 for three individual 2.0g samples (9.0 g total) and has a calculated standard deviation of ± 0.004 cm^3-H_2/g-sample indicating a stable Ag surface with repeatable hydrogen consumption. The pretreatment conditions selected in this manuscript are notably different than those used in prior Ag titration studies where $AgNO_3$ was selected as an Ag^+ source [21, 64]. Vannice pretreated using hydrogen at temperatures between 170 and 300 ºC concluding a 300 ºC temperature was required to desorb carbon contaminants [21]. In earlier work, Scholten quantified the role of carbon with N_2O dissociation to from CO_2 on unsupported Ag stating that a 170 ºC in-situ calcination was sufficient to remove contamination from HCHO used to thermally reduce AgO to Ag^0 powder [64]. When $Ag_2C_2O_4$ dissolved in EN was impregnated on α-Al_2O_3 rings Vannice noted that ~3 cycles of oxygen pretreatment at 250 ºC for 2 hours were required to obtain reproducible uptake concluding that EN requires high temperatures or long exposure times to desorb [11]. This observation may also be relevant to reactor startup procedures where Ag catalysts are exposed to an oxygen rich stream at 260 ºC for up to 72hrs indicating a slow process [65-67].

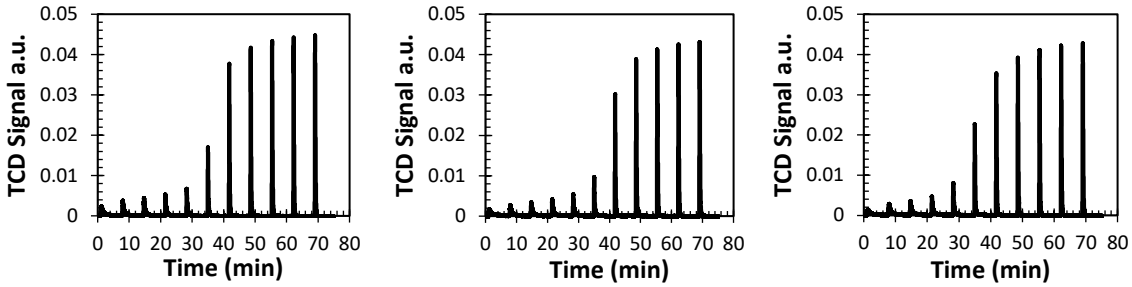

Figure 2.2: Hydrogen uptake for three separate experiments containing 2.0g of ground 841-400 μm 12wt% Ag/SA5562 particles. The results indicate reproducibility within 0.004 cm³-H_2/g-sample for unpromoted Ag pretreated ex-situ at 280 ºC in flowing air to remove residual ethylenediamine.

2.4.2 Titration Conditions

A series of experiments using α-Al_2O_3 promoted with high weight loadings of NH_4ReO_4, $CsNO_3$, or $(NH_4)_2MoO_4$ were conducted to determine if metal oxide reduction was responsible for hydrogen consumption during pulsed titration at 170 ºC. TPD was performed from 50 to 500 ºC following oxygen dissociation at 170 ºC, Figure 2.3 (left). The 3wt% Cs sample showed no hydrogen uptake below 300 ºC, minor uptake between 300 and 400 ºC, and significant uptake beyond 400 ºC. 3wt% Re followed a similar trend although uptake occurred at notably lower temperatures with minor consumption occurring between 250 and 300 ºC, rapid consumption between 300 and 400 ºC, and a plateau that continued until 500 ºC. 4wt% Mo showed no signs of hydrogen uptake until 425 ºC. To confirm the absence of hydrogen consumption at 170 ºC fresh samples of each catalyst were subjected to a series of 10%H_2 Bal/Ar pulses, Figure 2.3 (right). These experiments indicate the that the oxides of Cs, Re, and Mo do not undergo reduction at the low temperature conditions used for Ag-O titration. This finding is not unexpected and agrees with literature where it is known that the ease of oxide reduction trends with the energy required transfer electrons from lattice vacancies following oxygen removal [68, 69]. Consequently, high-valent Mo^{+6}, Re^{+7}, and other nonconductive transition metal

oxy anions are not expected to reduce at the low temperature condition used for oxygen titration.

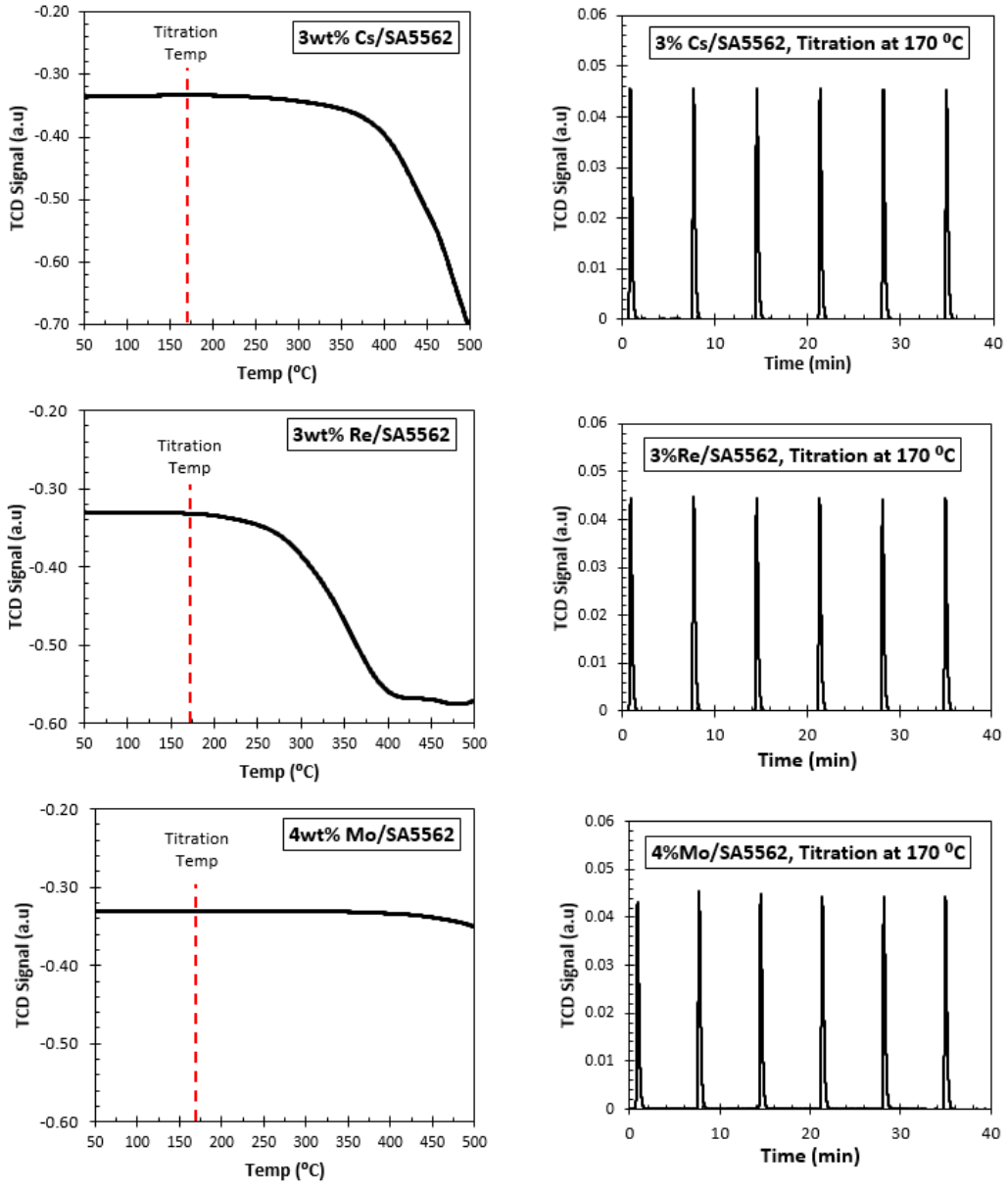

Figure 2.3: Temperature programed reduction (left) and pulsed hydrogen titration at 170 ºC (right) for, 3% Cs/SA5562 (top), 3%Re/SA5562 (middle) and 4%Mo/SA5562 (bottom). The TPR and hydrogen titrations experiments were performed following oxygen dissociation at 170 ºC (TPR parameters: 25 - 500 ºC , 20sccm 10% H_2 Bal Ar, 20ºC/min).

2.4.3 Promoter Effects on Ag-O Titration

Hydrogen consumption on oxygen precovered 12wt% Ag/SA5562 promoted with Cs, Re, and W is shown in Figure 2.4. Mono promoted Cs-Ag samples at loadings between 350 and 1000 ppm (2.6umol -7.5 umol) indicate a linear decrease in uptake with increasing Cs concentration, Figure 4 (top left). Vannice reported similar findings for static oxygen chemisorption on 12wt% Ag/SA5562 samples promoted with 400 and 1200 ppm Cs (3.0 & 9.0 umol) which had total oxygen uptakes of 3.5 and 2.7 umol O_2/g-cat [11]. However, since there unpromoted sample had an oxygen uptake of 3.0 umol O_2/g-cat the authors argued that the difference in adsorption for the Cs containing samples was not significant. What is more likely is that the variation in oxygen uptake is the result of differences in catalyst preparation as demonstrated by Bartau when analyzing the kinetics of two unpromoted Ag samples supported on α-Al_2O_3 monoliths [35]. In the current manuscript, the Cs-Re interaction was studied using a fixed Cs concentration of 350ppm (2.6 umol) and Re loadings between 150 and 500 ppm (0.8 – 2.7 umol). Like the mono promoted Cs samples the Cs-Re samples also followed the same linear decrease in hydrogen consumption as the surface concentration of promoter increased, Figure 2.4 (top right). When tungsten (W) was added using a fixed Cs and Re concentration of 2.6 and 0.8 umol respectively, hydrogen uptake was within the range expected for a sample containing 4.0 umol promoter. Consequently, these data suggest that the promoter identity has no measurable effect on hydrogen consumption and that the promoters do not co-interact to cause changes in the titration behavior. The only significant variable is the total quantity of promoter contained in the catalyst implying that the promoters are in part located on the Ag surface.

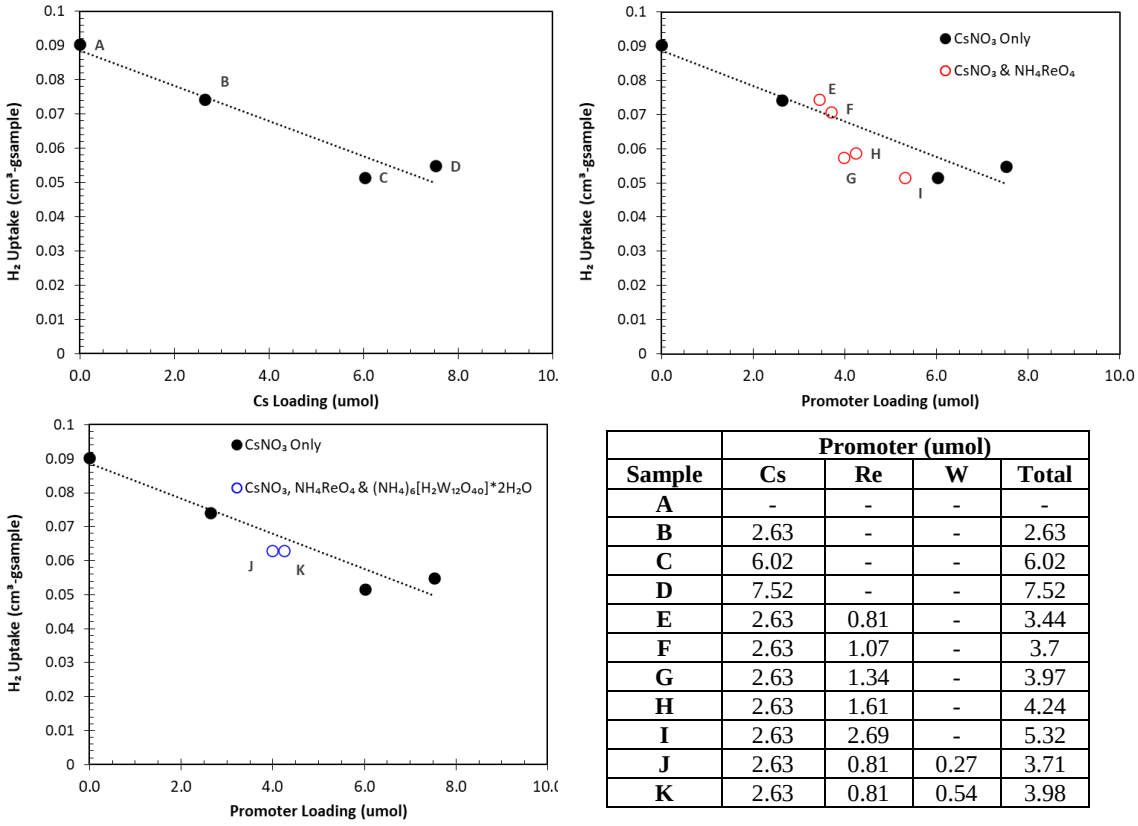

	Promoter (umol)			
Sample	**Cs**	**Re**	**W**	**Total**
A	-	-	-	-
B	2.63	-	-	2.63
C	6.02	-	-	6.02
D	7.52	-	-	7.52
E	2.63	0.81	-	3.44
F	2.63	1.07	-	3.7
G	2.63	1.34	-	3.97
H	2.63	1.61	-	4.24
I	2.63	2.69	-	5.32
J	2.63	0.81	0.27	3.71
K	2.63	0.81	0.54	3.98

Figure 2.4: Hydrogen uptake plotted against µmol promoter loading on 12wt%Ag/SA5562 samples prepared by co-imp of $Ag_2C_2O_4$ and promoter salts. The quantity of adsorbed hydrogen is independent of the promoter element and only dependent on the total promoter loading.

To determine the impact of Ag concentration on hydrogen uptake, 12 and 24wt% Ag/SA5562 catalysts were promoted using an identical loading of Cs, Re, Mo and S (total > 8.0 umol). 24 wt% Ag was obtained using a twostep impregnation of $Ag_2C_2O_4$ in which the promoters were added during the second Ag cycle. Pulsed titration results for the 12 and 24 wt% samples can be seen in Figure 2.5 where the 12wt% sample shows no hydrogen uptake following oxygen dissociation and the 24wt % sample shows considerable cumulative uptake (0.025 cm³-STP/g-sample). Control experiments comparing co-impregnation of 350 ppm Cs with 12wt% Ag with a twostep synthesis whereby the same quantity of Cs was added prior to Ag impregnation resulted in

hydrogen uptake values of 0.072 and 0.074 cm^3-STP/g-sample respectively. Consequently, these findings strongly indicate that the two-step procedure applied for the 24wt% Ag sample did not artificially increase the quantity of hydrogen consumed. Consequently, total uptake is directly related to an increasing number of Ag-O sites from an increase in Ag weight loading.

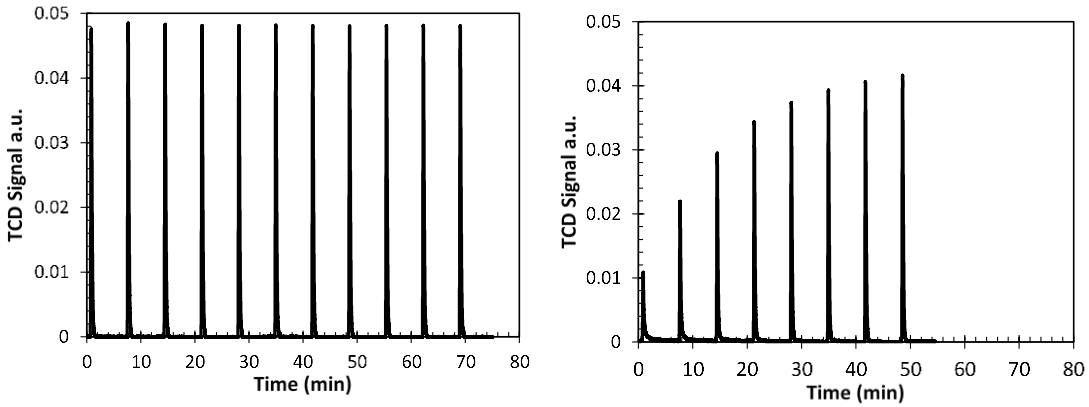

Figure 2.5: H_2 uptake for two samples containing an equal umol loading of Cs, Re, Mo, & S but 12wt % Ag (left) and 24wt % Ag (right). Hydrogen uptake in the 24wt% sample is directly associated to the number of Ag-O bonds.

There is general agreement regarding the role of Cs, Re, and co-promoters for ethylene oxide formation throughout the literature. Cesium (Cs) is by far most studied element whose effect is believed to be electronic causing a decrease in the Ag-O bond strength as a result of charge transfer from highly polarizable Cs to Ag [8, 61, 70, 71]. Re is also thought to weaken the Ag-O bond however high-valent cationic Re decreases the electron density of Ag thus forming electron deficient oxygen which can insert at the double bond of C_2H_4 [51, 72]. Monnier and coworkers proposed a similar electronic argument for fully promoted Ag/α-Al_2O_3 samples containing Re, Cs, and Mo [8]. It was shown that Re exists as Re^{+7} which increases the Ag d3 binding energy favoring the formation of electron deficient Ag sites and EO selective electrophilic oxygen. EO

selectivity for Ag/α-Al_2O_3, Re-Ag/α-Al_2O_3, Cs-Ag/α-Al_2O_3 and Re-Cs-Ag/α-Al_2O_3 samples prepared with identical promoter and Ag loadings and evaluated at 2.0 mole% EO in the product were measured at 74.5, 50, 79.7 and 82.4% respectively. Comparing the performance for mono promoted Re-Ag and the unpromoted Ag catalysts it was concluded that Re is a necessary component but requires Cs to complement its effect. Namely, that Cs and Re act at different steps in the catalytic mechanism. Re increases the electrophilicity of the Ag-O species favoring insertion at the C=C double bond and that the high polarizability factor for Cs decreases the adsorption energy of C_2H_4O prior to metal catalyzed combustion[8]. Co-Promoters such as Mo and S were shown to increase selectivity only when paired with Re thus, they must also aid the electron transfer from Ag to Re.

Figure 2.6 compares TPR results for oxygen precovered Ag on a series of 12wt% Ag/SA5562 catalysts containing Cs, Re, or a full promoter package containing Cs, Re, and co-promoters. For the unpromoted Ag sample a broad adsorption peak is observed between 100 and 300 ºC with a peak center of 180 º C. With the addition of 800ppm Cs, the consumption peak sharpens and decreases to 130 ºC. In the mono promoted 800ppm Re sample, a downshift in consumption temperature is also observed with a sharp desorption peak centered around 137 ºC. The high temperature peak occurring between 225 and 300 ºC is attributed to reduction of the rhenium oxide previously noted. The fully promoted sample containing Cs, Re, and co-promoters follows similar behavior to the Re containing sample however the low temperature peak at 130 ºC broadens and is not resolved before reduction of the high valent transition metal oxy anions. Prior results indicate that hydrogen uptake in the low temperature region can be attributed to titration

of the Ag-O bond and Figure 2.6 demonstrates that Cs, Re, and copromoters modify the interaction of monoatomic surface oxygen with gas phase adsorbates. The weakening of the Ag-O both by charge transfer from Cs to Ag and from Ag to Re with co-promoters can be explained by the heterolytic dissociation of molecular H_2 forming two monatomic hydrogen fragments [73]. One that is H fragment that is electron deficient having an affinity for Cs-Ag-O sites and a second that is electron rich strongly interacting with Re-Ag-O.

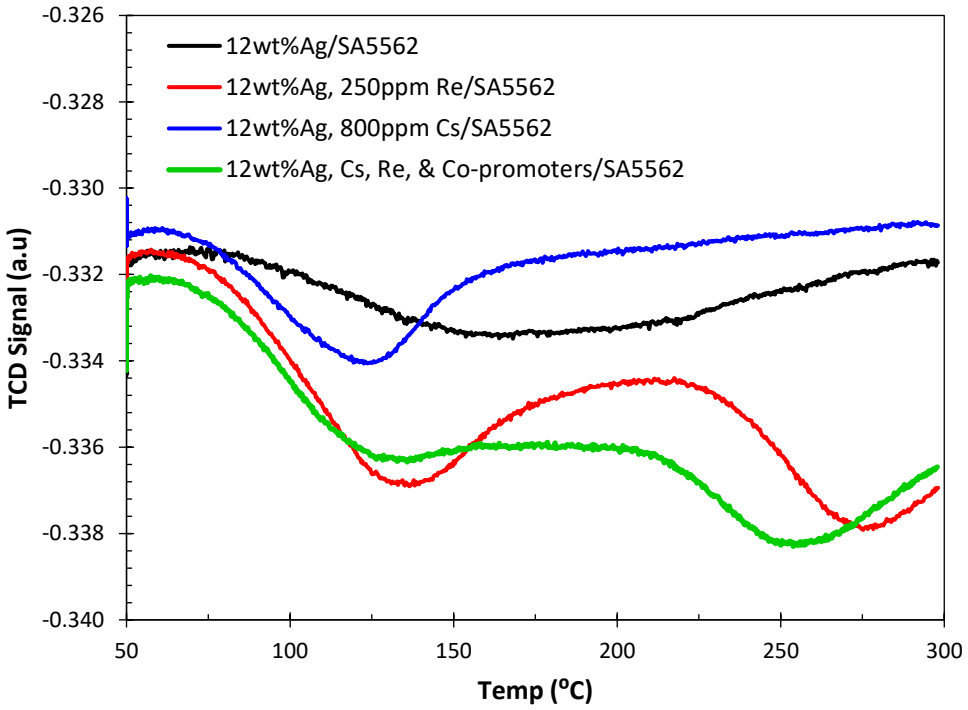

Figure 2.6: Temperature programed titration for promoted Ag samples following oxygen precoverage at 170 ºC. The addition of Cs or Re weakens the Ag-O bond decreasing the titration temperature from 175 ºC for unpromoted Ag to 135 ºC (Re-Ag), and 125 ºC (Cs-Ag). High temperature peaks beyond 225 ºC are associated with the reduction of high valet transition metal oxy anions. (TPR conditions: 20sccm 10% H_2 bal Ar, 20 ºC/min, Atmospheric pressure)

2.5 CONCLUSION

It is demonstrated that pulsed hydrogen titration of oxygen precovered Ag is a valid method for characterizing the quantity of Ag-O sites for olefin epoxidation catalysts containing common promoters and co-promoters. Using unpromoted $Ag/\alpha\text{-}Al_2O_3$ prepared by incipient wetness impregnation of $Ag_2C_2O_4$ dissolved in ethylenediamine a standard pretreatment procedure was developed whereby samples were treated ex-situ in flowing air at 280 ºC for 10 hours to remove residual organic ligand. Following oxygen dissociation at 170 ºC, pulsed hydrogen titration at 170 ºC indicated a sample-to-sample standard deviation of 0.004 cm^3-STP/g-sample. Temperature programed reduction of $\alpha\text{-}Al_2O_3$ impregnated with high weight loadings of Cs, Re, and Mo showed no reduction of the cationic salts at or below 170 ºC and pulsed hydrogen titration of the same samples following oxygen dissociation indicated no hydrogen was consumed. For supported 12wt% Ag samples, hydrogen consumption was observed to decrease with the umol loading of promoter in a manner that is independent of the promoter element on only dependent on the total surface concentration. Increasing the Ag loading from 12 to 24wt% using a fixed promoter concentration increases the detectable quantity of hydrogen consumption thus implying hydrogen uptake was directly related to an increase in the number of Ag-O bonds. Using temperature programed reduction of oxygen precovered 12wt% $Ag/\alpha\text{-}Al_2O_3$ promoted with Cs, Re, and co-promoters it is suggested that both Cs and Re shift the electron density of monatomic oxygen such that lower titration temperatures are observed due to the heterolytic dissociation of molecular hydrogen.

CHAPTER 3

MICROFIBER ENTRAPPED CATALYSTS FOR HEAT REMOVAL IN EXOTHERMIC ETHYLENE EPOXIDATION

3.1 ABSTRACT

Microfiborous entrapped catalyst (MFEC) technology was evaluated for exothermic ethylene epoxidation using lab scale ¼ and ½" outer diameter (OD) and bench scale 1" OD reactors. Control experiments in an epoxidation feed evaluating the direct combustion of ethylene on the nickel (Ni), stainless-steel (SS), and copper (Cu) mesh indicated that Cu was catalytically active for olefin combustion and formed CuO which was structurally unsound. Consequently, Ni and SS were selected for comparison with a traditional packed bed containing 350ppm Cs, 12wt % Ag/α-Al_2O_3 diluted with α-Al_2O_3 to reach the same volume and catalyst loading as the MFEC media. Evaluation studies using lab scale ½" OD reactors indicated the MFEC samples were significantly resistant to exothermic runaway and provided an isothermal intrabed temperature profile under a wide range of operating conditions. However, where SS and Ni are inert for C_2H_4 combustion a fraction of EO undergoes conversion to non-selective products at temperatures above 240 °C. Using the bench scale configuration, it was determined that the larger 1"OD reactor is externally heat transfer limited thus artificially capping performance for the MFEC. Strategies are discussed for a reactor redesign to match parameters as they pertain to commercial ethylene oxide and epoxybutane systems.

3.2 INTRODUCTION

Catalytic ethylene epoxidation occurs according to Figure 3.1 where molecular oxygen dissociates over an α-Al_2O_3 supported Ag catalyst to produce three possible products EO, CO_2 and H_2O. Where selective EO is formed via mildly exothermic partial oxidation (r1, ΔH = -105 kJ/mol), non-selective CO_2 and H_2O are formed from the highly exothermic direct combustion of C_2H_4 (r2, ΔH =-1326 kJ/mol), sequential combustion of adsorbed oxymetalic intermediates (r3', ΔH =-1222 kJ/mol) [8, 74-76], and metal catalyzed combustion of reabsorbed EO (r3, ΔH =-1222 kJ/mol) [8], Figure 3.1.

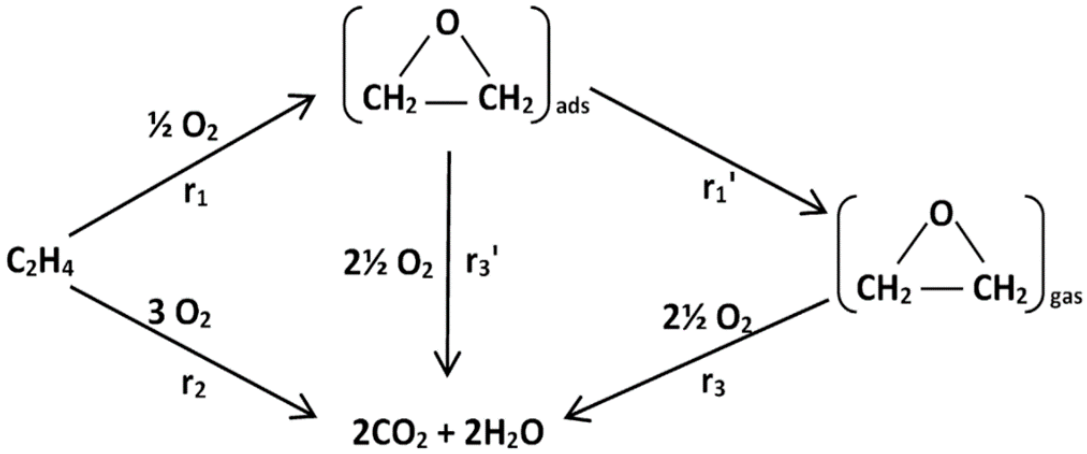

r_1	**$C_2H_4 + ½\ O_2 \rightarrow C_2H_4O$**	**ΔH = -105 kJ/mol**
r_2	**$C_2H_4 + 3\ O_2 \rightarrow 2CO_2 + 2H_2O$**	**ΔH = -1326 kJ/mol**
r_3'	**$C_2H_4O + 2½\ O_2 \rightarrow 2CO_2 + 2H_2O$**	**ΔH = -1222 kJ/mol**

Figure 3.1: Reaction network and heats of reaction for selective (r1) and non-selective (r2) oxidation of ethylene on Ag. EO intermediates may undergo direct combustion or combust following isomerization to acetaldehyde (r3'). Alternatively, gas phase EO may also reabsorb and combust (r3).

Stable operation is achieved when the heat of reaction is balanced by an equivalent quantity of heat removal according to the standard energy balance in Equation 3.1 where E_{AC} is the accumulation term, E_{in} is the energy supplied to the system, E_{out} is the energy removed from the system, E_{gen} is the heat generation term from reaction, and E_{Con} is the consumption term equivalent to zero.

$$E_{AC} = E_{In} - E_{Out} + E_{Gen} - E_{Con} \qquad (3.1)$$

If unconstrained, heat generation will lead to exothermic runaway ($E_{AC} >> 0$) whereby the rate constant for both ethylene epoxidation (k1) and combustion (k2) increase exponentially with temperature according to Arrhenius kinetics. During ignition, the selective catalyst surface is destroyed from Ag nanoparticle sintering and the volatilization of Re_2O_7 and other high valent transition metal oxy anions [70, 77, 78] at temperatures in excess of 400 °C. Reactor performance can only be recovered following a cost intensive catalyst change out requiring weeks of process downtime.

In a commercial operation, catalysts containing 12 – 30 wt% Ag supported on non-thermally conductive α-Al_2O_3 rings (30 w/m-K) are packed into bundles of 1.62" outer diameter (OD) 30' tall tubes. A typical 100kton EO reactor will contain 28000 or more tubes surrounded by a heat transfer media which supplies the thermal energy required to drive epoxidation while simultaneously removing the excess heat of reaction Figure 3.2 (top left). Since 1D thermal resistance is directly proportional to sample thickness and the net heat transfer coefficient is the sum of thermal resistance for all materials between the highest and lowest temperature [79], increasing tube diameter will significantly limit heat transfer rates (Q) since energy must move a greater distance though the thermally inert catalyst bed Figure 3.2 (bottom). Thus, it is not surprising that

commercial EO producers rely on tube side convection at high superficial gas velocity (2.2 m/s at 175 L-STP/min per tube, Table 3.1) rather than conduction to the outer tube wall, for heat removal.

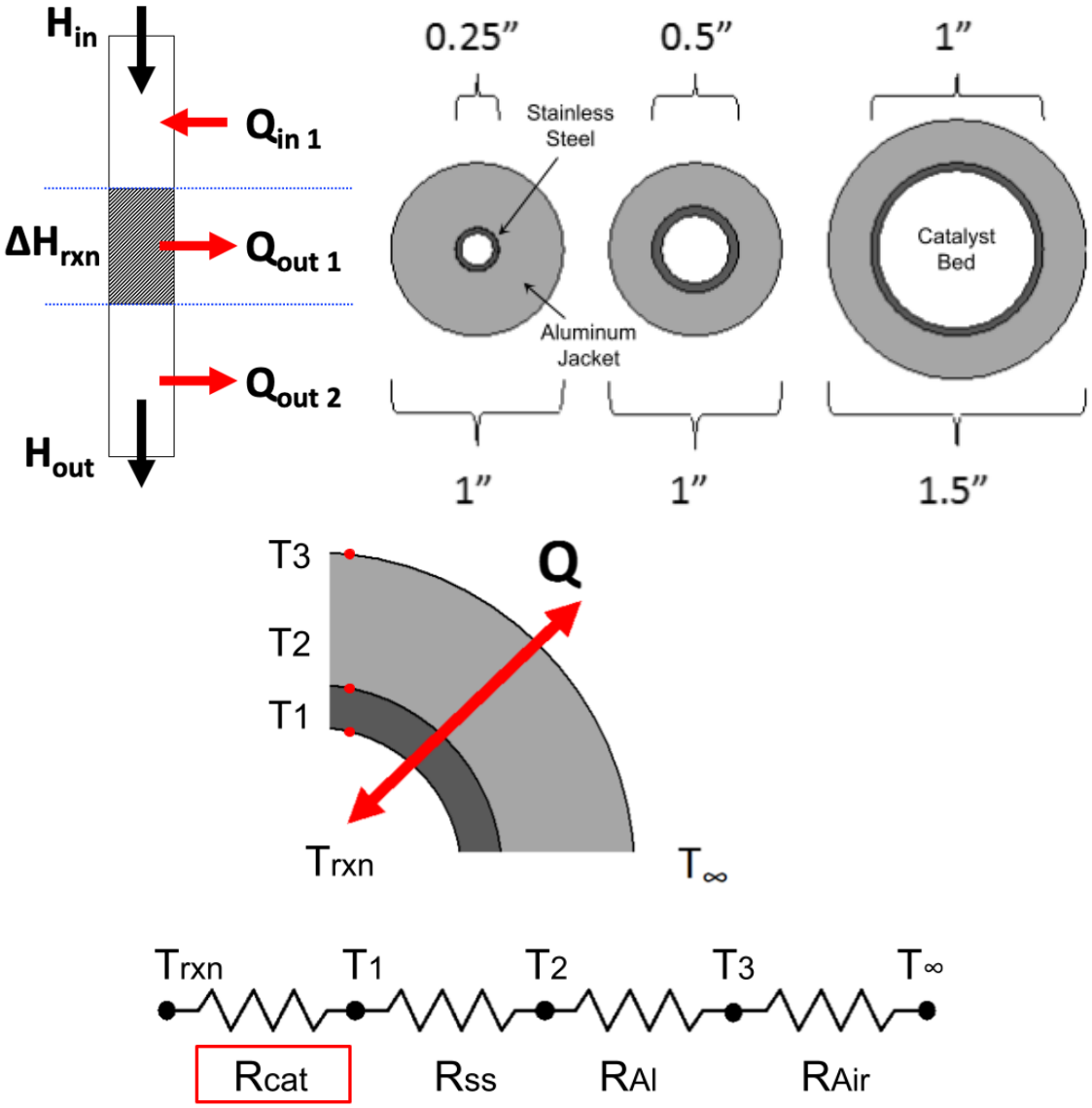

Figure 3.2: Schematic for a single tube reactor denoting heat transfer (top left). Top view of stainless-steel tubes with various outer dimensions jacketed in alumina to provide an isothermal tube temperature (top right). Schematic for overall thermal resistivity for an alumina jacketed tube containing catalysts (bottom).

Table 3.1: Operating parameters for a typical 100 kton EO reactor.

Annual production (Kiloton)	100
Feed (L-STP/(Min*Tube))	175
Feed Comp C_2H_4/ O_2/ CO_2 (%)	25 / 4-12 / 0-4
Typical C_2H_4 Conversion (%)	< 10
GHSV (1/hr)	850
Superficial velocity (m/sec)	2.2
Inner tube diameter (in)	1.62
Tube length (feet)	30
Total number of tubes	28000
Catalyst lifetime (years)	2.5
Catalyst cost ($/28000 tubes)	40,000,000
Ethylene cost ($/lb)	0.56

Convective heat removal is moderately effective strategy to counteract the heat transfer limitation however, even under ideal conditions a small fraction of tubes, typically <10%, will contain a sustained exothermic runaway. Commercially, the fraction of tubes in exothermic light off are calculated by monitoring carbon monoxide concentration in the product stream which increases as a result of direct ethylene combustion in an oxygen lean environment [80]. At 0.56 $/lb ethylene represents a significant manufacturing expense and in an ignited tube, the olefin is completely converted to non-value-added CO_2 and H_2O in stochiometric proportion with complete O_2 consumption i.e. no EO is observed in the product. Table 3.2 derived from an APSEN simulation performed by the Cremashi group at the University of Auburn accounting for feed conditioning, the EO reactor, product purification, and utilities demonstrates the cost of non-selective combustion. Here a 4% ignition of 28000 tubes will increase annual C_2H_4 consumption by 17.9 kton for a 100kton /year EO unit equivalent to approximately 22 million USD. If the simulation is repeated without varying the quantity of olefin supplied, the total EO production increases from 107 to 111 kton/year comparing 4 to 0% ignition.

Table 3.2: Economic analysis for conventional EO technology containing a fraction of tubes in exothermic runaway with MFEC technology containing no ignited tubes.

	Conventional Technology		MFEC	Results of Tube Ignition
Ignited Tubes (%)	10	4	0	Conventional technology has pore thermal transfer causing tube ignition during operation.
Operating Cost ($ Millions)	186	184	167	10% Ignition: 26.2 kton excess C_2H_4 consumption /yr 4% Ignition: 17.9 kton excess C_2H_4 consumption /yr CO_2 separation cost increases
EO Production (kton/yr)	100	107	111	Annual production decreases
EO Production Cost ($/tons)	1860	1720	1510	Cost per ton increases

Total cost per ton of EO produced reflects both feed cost and the separation of reaction products (CO_2, H_2O, & EO) that reversibly poison Ag active sites when present in the recycle [81, 82]. Where H_2O and EO can be extracted by simple condensation [83], CO_2 must be scrubbed using KOH or short chain amines including Diethanolamine (DEA), Monoethanolamine (MEA) or Methyldiethanolamine (MDEA) [84-86]. CO_2 poisoning of Ag occurs from the formation of carbonates on Ag-O sites which prevent the adsorption of ethylene and subsequent EO formation [8, 49, 61, 87]. Figure 3.3 shows the effect of feed CO_2 on catalytic activity and selectivity for an older generation 12wt% Ag/α-Al_2O_3 sample compared with the same catalysts also containing Cs and Re. In all cases the loss in catalytic activity and the increase in EO selectivity follows a Langmuir type curve where a diminishing effect is observed at higher concentrations of feed CO_2. When performance is scaled to initial values i.e. EO activity loss and EO selectivity gain are calculated according to Equations 3.2 and 3.3 where EO_I is 2.0mol% at 0% CO_2

added to the feed, EO_F is the mol % EO at a non-zero value of feed CO_2, Sel EO_I is the % selectivity to EO at 2.0 mol% at 0% CO_2 added to the feed, and Sel EO_F is the % selectivity to EO at a non-zero value of CO_2 in the feed, the activity of unpromoted Ag decreases by 30% and the activity of Re-Cs-Ag decreases by 65% with 6% CO_2 in the feed. Note at 0% CO_2 both unpromoted and promoted Ag samples were operating with a common work rate of 2.0 mol % EO obtained by adjusting reaction temperature between 200 and 260 ºC. This implies that both materials were operating with the same catalytic load before perturbation of the system.

$$EO\ Activity\ Loss = \left(\frac{EO_I - EO_F}{EO_I}\right)(100\%) \tag{3.2}$$

$$EO\ Selectivity\ Gain = \left(\frac{Sel\ EO_I - Sel\ EO_F}{Sel\ EO_I}\right)(100\%) \tag{3.3}$$

What is most important, is the precipitous drop in activity observed between 0 and 1% CO_2 for the promoted sample. This means that modern high selectivity ethylene epoxidation catalysts containing promoters and co-promoters [10] are more sensitive to carbonate formation and thus ultra-low concentrations (<1%) of CO_2 are required to obtain the same cumulative EO make as older generation high activity formulations. This finding explains why many EO producers have opted to replace KOH with ammine scrubbers which are more efficient for lowering CO_2 concentrations to ultra-low levels.

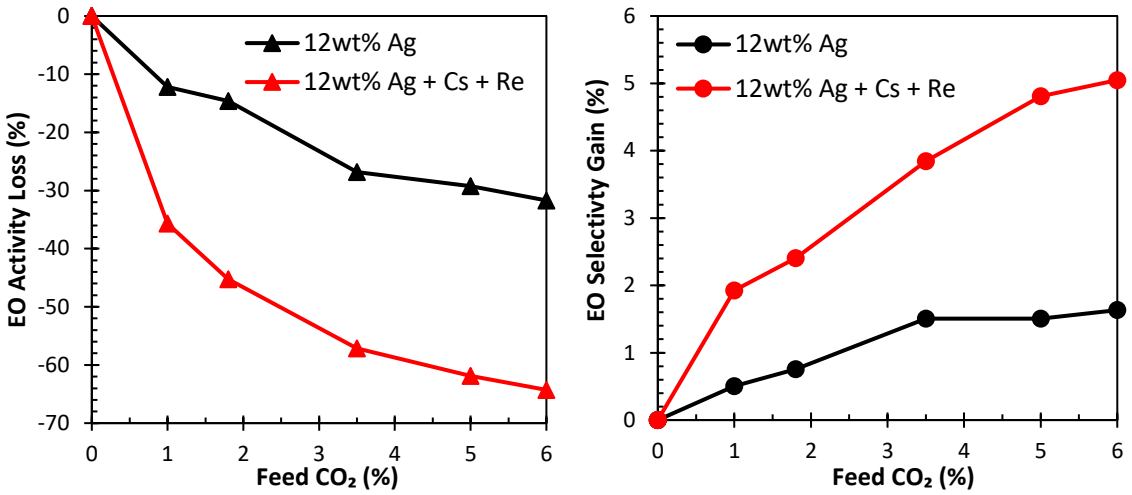

Figure 3.3: A comparison of activity (left) and selectivity (right) for 12wt% Ag/Al_2O_3 and Cs-Re promoted 12wt%Ag/ Al_2O_3 catalysts as a function of CO_2 in the feed stream. Activity decreases with increasing CO_2 concentration. Note the precipitous drop in performance between 0 and 1% CO_2 accompanied by a 2% increase in selectivity for the promoted sample.

Microfiborous entrapped catalyst (MFEC) technology represents an alternative to convective heat removal whereby the insulative properties of the inert α-Al_2O_3 carrier are negated by entrapping ground catalysts particles in a thermally conductive metallic mesh. This configuration is displayed in Figure 3.4 where ¼" OD alumina rings impregnated with catalytic metal are crushed to 177-400 μm particles then layered between precut sheets of metal fiber. This approach can be adapted to any pre-prepared, often proprietary, catalyst formulation and is independent of the synthesis method provided the final media can be ground to a size appropriate for entrapment.

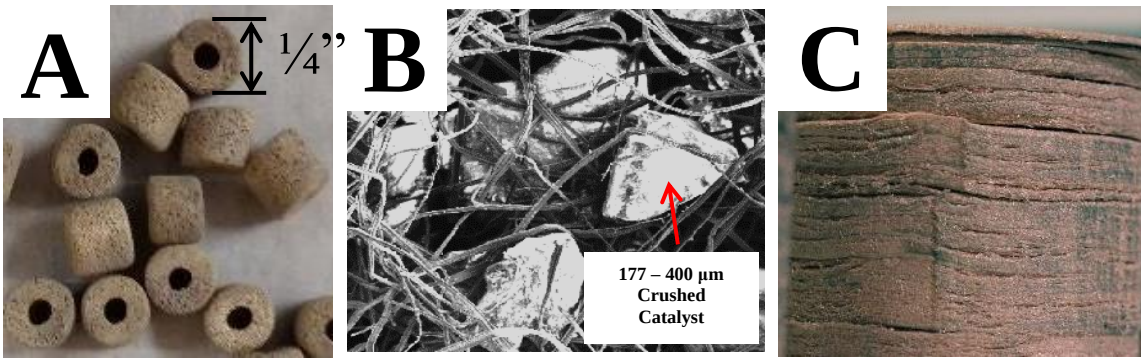

Figure 3.4: 1/4" alumina rings impregnated with catalytic metal (A). Catalyst ground to 177-400 um particles entrapped in metal mesh (B). A stack of precut Cu mesh disks loaded with catalytic media (C).

MFEC technology has been proven to increase conductive heat transfer for exothermic gas to liquid (GTL) Fischer Tropsch chemistry [88-90] where Fe-Cu-K/γ-Al_2O_3 catalyst was loaded in to a 1.33” ID stainless steel reactor and diluted with unmodified γ-Al_2O_3 to achieve the same volume loading as a Cu MFEC containing an equal quantity of catalyst. Fixed temperature measurements collected in the center of the bed normal to the vertical axis indicated an isothermal intrabed temperature profile for the MFEC and oscillations up to 20 ºC for the diluted packed bed with a radial temperature gradient of 54 ºC. The reaction was performed at 260 ºC with a H_2/CO ratio of 2/1 for 60 hours with a steady state CO conversion of 50.4 and 24.2% for the diluted packed bed and MFEC respectively. Selectivity to desired C_5-C_{20} liquid products was slightly higher for the packed bed reactor, 24.6% (PB) vs 22.8% (MFEC), although it is difficult to make direct comparisons due to the difference in CO conversion as a result of local hot spots in the diluted packed bed. What can be stated is that the Cu MFEC significantly dampens the temperature profile thus implying a wider range of safe operation.

In the current manuscript, we examine the MFEC for exothermic ethylene epoxidation using both lab scale ¼ - ½" OD and bench scale 1" OD reactors. At the ½" scale it is shown that the thermal properties of Ni and stainless steel are superior to traditional diluted bed technology however, where the MFEC is inert for direct olefin combustion, significant sequential EO combustion is observed at reaction conditions exceeding 240 °C. Evaluation at the 1" OD scale indicates that the reactor, loaded with an equal quantity of catalyst by mass and volume as the ½" OD counterpart, is externally heat transfer limited and will require redesign to effectively compared the MFEC with traditional technology.

3.3 EXPERIMENTAL METHODS

3.3.1 Fiber preparation

Nickel (Ni), stainless steel (SS), and copper (Cu) mesh were supplied from IntraMicron prepared using metal wires which are bundle drawn and formed into sheets using wet lay technology from the paper industry. These sheets referred to as "green-sheets" are sintered in an inert environment to remove residual organics deposited in the manufacturing process. A more detailed description of the fiber preparation is available in literature [88-94]. Following the sinter step, the material is cut into disks using a custom die which prevents fiber compression at the cutting interface thereby improving heat transfer to the inner tube wall. 12wt% Ag/SA5562 ¼" rings promoted with 350ppm Cs from $CsNO_3$ using the same wet impregnation procedure described in Chapters 2 are crushed to 177-400 μm particles and loaded between disks of mesh to form a stack of catalyst containing sample denoted as "loaded media" [95, 96]. The mesh fibers are 3-20 um in diameter and exist as metallic Cu, Ni, or Fe with trace amounts of FeOOH and

$Ni(OH)_2$ detected by XPS. In all cases, the exposed surface is considered to be the (111) plane (Fe, Ni, and Cu are FCC metals).

3.3.2 Catalytic Evaluation

Evaluation was conducted in a custom-built single tube bench scale reactor. The reaction mixture was prepared using two sets of four Brooks 5850E mass flow controllers sized to accommodate ¼" OD reactors or ½" and 1" diameters. Both manifolds contain individual flow controllers for CH_4, C_2H_4, O_2, and ethyl chloride (EtCl). The feed gas exists the supply manifold and is sent to a 1L expansion tank heated to 85 ºC where it is thoroughly mixed. Unless otherwise specified catalysts were evaluated with a gas composition containing 25% C_2H_4, 8%O_2, 1.5ppm EtCl, Bal CH_4, at a superficial velocity of 0.15m/s @ STP. Following expansion, the gas enters a ½" OD single pass preheater, packed with 1/8" destone beads and jacketed with a custom heating mantel fabricated by BriskHeat. With a preheater setpoint of 210 ºC gas enters at 85 ºC and exists at 156 ºC. The preheater exit temperature can be adjusted by controlling mantel temperature with a maximum jacket setpoint of 310 ºC based on equipment safety limits. After the preheater, warm gas is sent to the reactor where a second BriskHeat mantel supplies the energy required to raise the temperature to the target operating point. Control experiments in Figure 3.5 indicated that the gas temperature 7" below the reactor inlet matches the reactor set point between 180 – 270 ºC with an inlet temperature of 156 ºC (Total Flow: 3700 sccm, Pressure: 250psig, superficial velocity: 0.15 m/s @ STP).

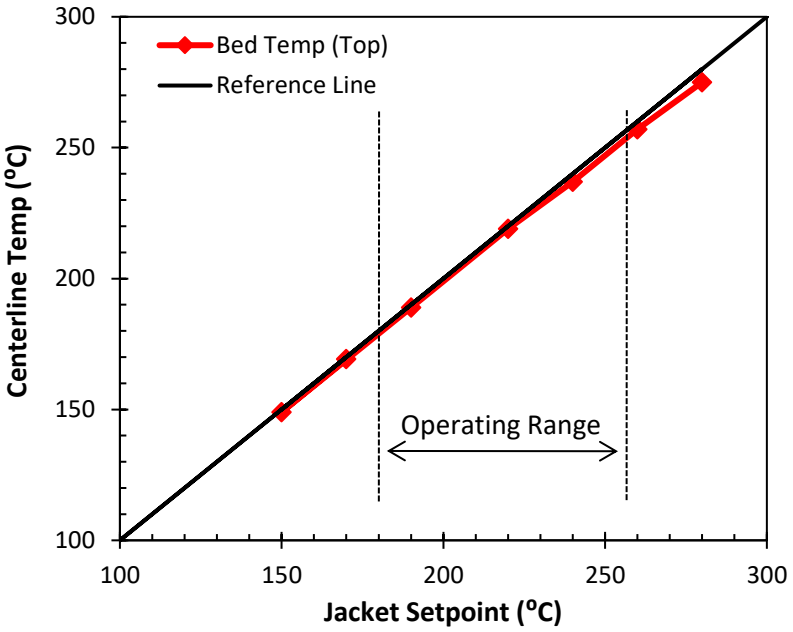

Figure 3.5: Bed temperature deviation from jacket setpoint for the 1" OD reactor using a feed flow rate of 3.6 LPM at 250 psig.

Reactor pressure, set between 20 and 500 psig but more preferably 250 psig, is controlled using a back pressure regulator (BPR) located downstream of the reactor outlet. Prior to the BPR, a 100 sccm slip stream is sent to a heated sampling system using a needle valve with 20psig of constant upstream pressure managed by a forward pressure regulator (FPR). All tubing is heated to a 110 ºC to prevent condensation of water vapor generated during operation. Gas composition is analyzed using an HP5890 gas chromatographer equipped with an FID (Plot-Q column, 30m x 0.32 ID, 19091P-QO4) and TCD (Plot-Q column, 30m x 0.32 ID, 19091P-QO4). The sampling system is custom built using three Valco two position valves. Valve one selects the reactor product or inlet, valve two selects between FID and TCD analysis, and valve three is automated to inject gas samples from a fixed 12800 nmol loop which is continuously purged with reaction gas in one position (load) and swept with GC carrier gas in the second position (inject).

The reactor is constructed from ¼” OD (0.18 ID), ½” OD (0.43” ID), or 1” OD (0.87 ID) 316 seamless stainless-steel tube and jacketed with aluminum. The aluminum jacket has an outer diameter of 1”, 1.4”, or 2” for the ¼”, ½” and 1” reactor respectively. Jacket temperature is monitored using a 0.040” OD type K thermocouple embedded in the aluminum shell where the tip touches the outer wall of SS tube and is controlled using a SOLO 4848VV PID controller. Reactors were loaded with catalyst such that the jacket thermocouple is in the same vertical location for each bed. Catalyst temperature profiles as a function of vertical position are monitored using a separate sliding 0.040” thermocouple enclosed in 0.0625” thermowell sealed with silver solder located at the axial center of each bed. A picture of the reactor assembly can be found in Figure 3.6 below.

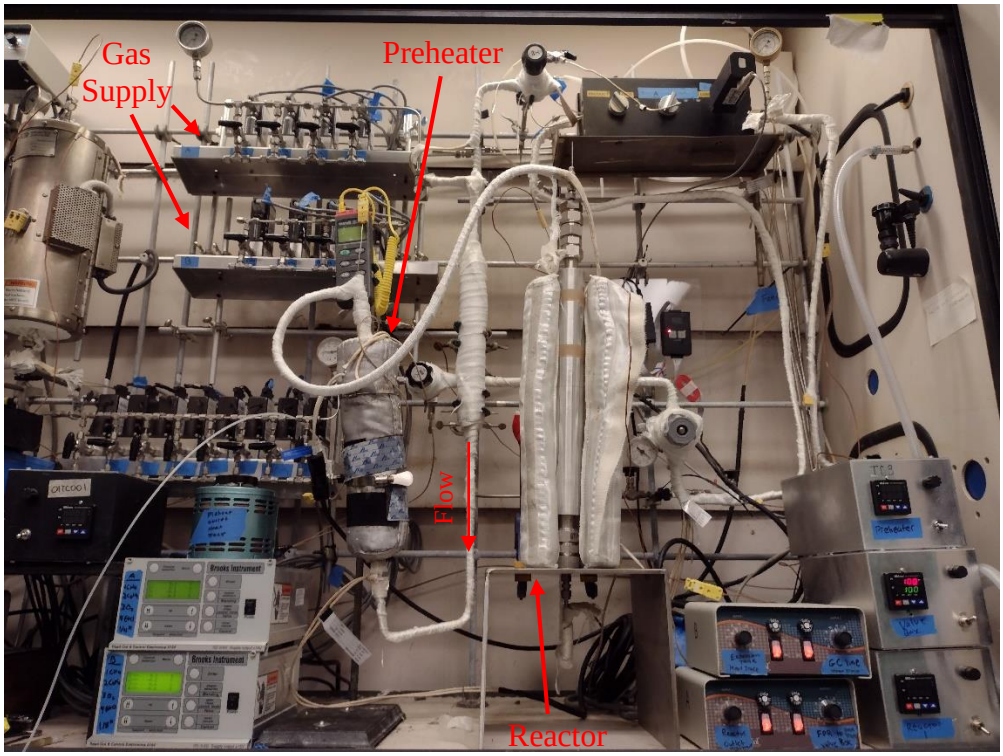

Figure 3.6: Reactor assembly used in catalytic evaluation. Gas is supplied from the two Brooks 5850E manifolds noted in the upper left.

3.4 RESULTS AND DISSCUSSION

3.4.1 MFEC Material Selection

Packed reactors containing Ni, SS, or Cu mesh were evaluated without Ag catalyst at equivalent bed volume and mesh loading by mass to provide equal contact time with the reactant stream. Figure 3.7, displays the results of CO_2 and EO production between 200 and 280 °C. Using a feed containing 25% C_2H_4, 8%O_2, 1.5ppm EtCl, Bal CH_4 with a superficial velocity of 0.15m/s @ STP, Ni and SS showed no reactivity for olefin combustion up to 280 °C however the Cu mesh showed 50 nmol and 100 nmol of CO_2 formation at 260 and 280 °C respectively. Compared to the 350ppm Cs promoted Ag/SA5562 sample at 225 °C, the quantity of CO_2 produced by the Cu mesh at 280 °C fell within the same order of magnitude suggesting a significant fraction of C_2H_4 combustion relative to EO production had the Cu MFEC been loaded with Ag catalyst. XPS analysis of the Ni sample indicated a transition from Ni and $Ni(OH)_2$ to NiO, SS changed from FeOOH to Fe_2O_3, and Cu^{+0} oxidized to CuO following reaction. Microcopy of the spent Cu mesh showed a dark black oxidation layer, Figure 3.7, and survey scans of the quartz packing located below the bed showed evidence of a Cu 2p peak indicating physical degradation. Because the lifecycle of a commercial EO catalysts is expected to be between 2 and 5 years, destruction of the Cu mesh made this material unfit for further evaluation. Microcopy and survey scans of the Ni and SS materials showed no evidence for material attrition.

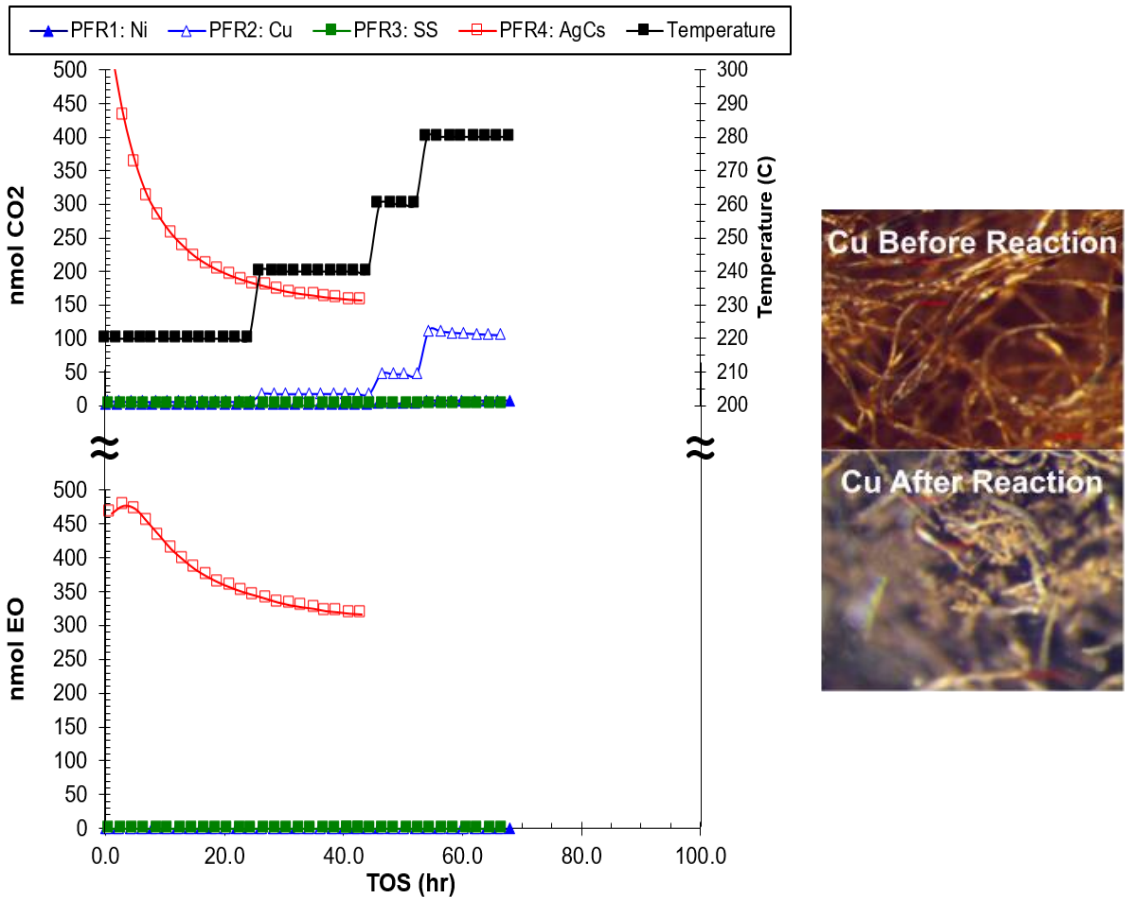

Figure 3.7: Material screening for C_2H_4 combustion compared with a 350ppm Cs, 12wt% Ag/SA5562 catalyst (left). The reactor temperature of the promoted catalyst did not exceed 245 ºC due to H_2O formation in the reactor outlet. Microscopy for the Cu mesh before and after reaction. Note the appearance of a dark black oxidation layer in the spent sample.

3.4.2 Catalytic Evaluation: ½" OD Reactor

Ni and SS mesh were selected for catalytic evaluation using ½" OD reactors loaded with 5.19g of ground and sieved 177-400 µm 350ppm Cs, 12wt% Ag/SA5562 particles. MFEC results were compared with a standard packed bed containing 5.19 g Cs-Ag catalyst diluted with α-Al_2O_3 (SA5562) to achieve equal volume loading. In the industrial literature, startup procedures are described whereby the reaction is initiated below 250 ºC more preferentially at 225 ºC using a stream containing 25% C_2H_4, 8%O_2,

1.5ppm EtCl, Bal CH_4 [12, 33]. All MFEC samples were heated to 225 ºC in flowing CH_4 before 25% C_2H_4, 8%O_2, 1.5ppm EtCl, were added to the feed with a superficial velocity of 0.15 m/s @ STP, and held at constant conditions for 30 hours at which point ignition occurred in the top 1" of the diluted catalyst bed where the highest concentration of O_2 and C_2H_4 were present. The severity of the exothermic runaway was limited by complete oxygen consumption with a maximum temperature rise of 408 ºC, Figure 3.8. Contrary to the packed bed, the Ni MFEC maintained an isothermal bed profile of 227 ºC throughout the experiment demonstrating significant conduction to the outer wall and resistance to temperature oscillations that can occur during process startup.

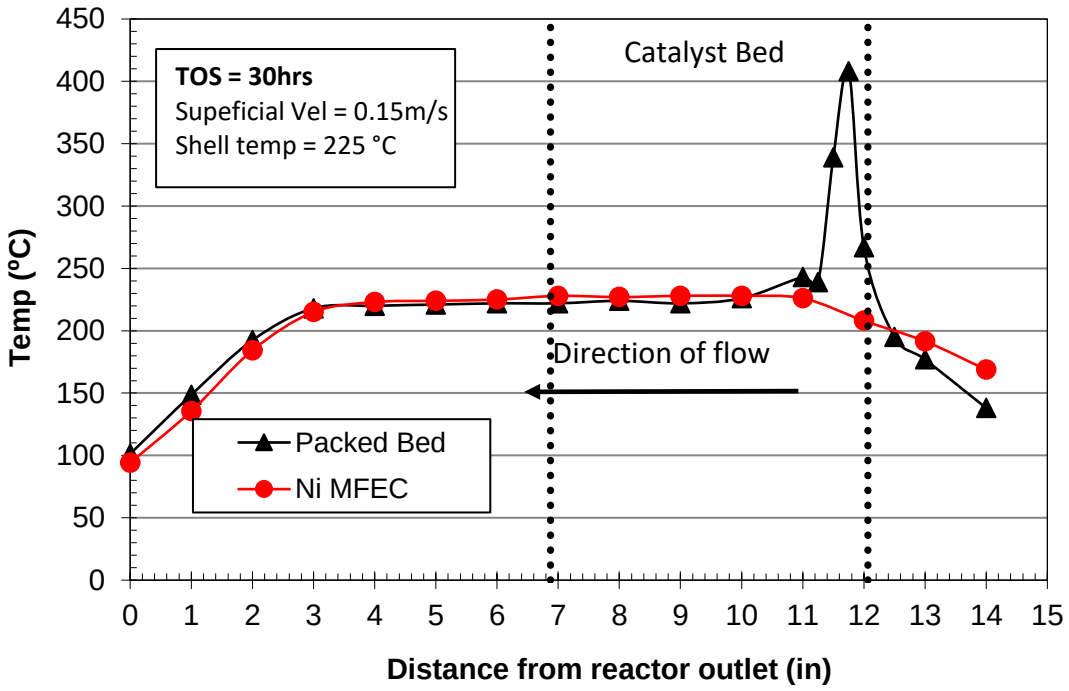

Figure 3.8: Catalyst bed profile for a ½" OD Nickel MFEC and traditional bed diluted with SA5562 α-Al_2O_3 following startup at 225 ºC. The diluted bed ignited with a max temperature of 408 ºC at complete oxygen consumption. (Feed Conditions: 25% C_2H_4, 8% O_2, 1.5ppm EtCl, Bal CH_4, superficial velocity: 0.15 m/s @ STP)

To test for the onset of exothermic runaway, a fresh ½" OD Ni, SS, and diluted packed bed containing 350ppm Cs, 12wt% Ag/α-Al_2O_3 were compared using a startup temperature of 190 ºC and an identical feed to Figure 3.8. The diluted bed was heated at 2-5 ºC every 4 hours until a hotspot was observed at a jacket temperature of 230 ºC with a temperature rise of 8 ºC located 2" above the bottom of the catalyst bed, Figure 3.9 (top left). After an additional 100 hours at constant operating conditions, the catalyst temperature profile was isothermal and the jacket temperature was increased to 250 ºC over 20 hours. Intrabed temperature oscillations up to 20 ºC have been observed in prior experiments using diluted packed beds evaluated for Fischer Tropsch synthesis. Thus the transient hot spot observed in the diluted bed for ethylene oxidation is not unexpected as the catalyst approaches steady state operation [88]. This sluggish response for heat dissipation may explain why it is common to commission EO catalysts using a 72-hour soak in an oxygen lean, reactive feed, containing C_2H_4, O_2, CO_2 and EtCl [97, 98]. This procedure may not only redistribute the surface composition of promoters, as indicated by a long conditioning time suggesting diffusion of solid [70], but may also help to stabilize bed temperature as the reactive feed generates a minor thermal load consequently lowering the risk of accidental ignition when oxygen levels are increased. In the current experiment, the temperature of the diluted bed was not increased beyond 250 ºC due to the high formation of water which will react with EO to form high boiling point condensables such as ethylene glycol.

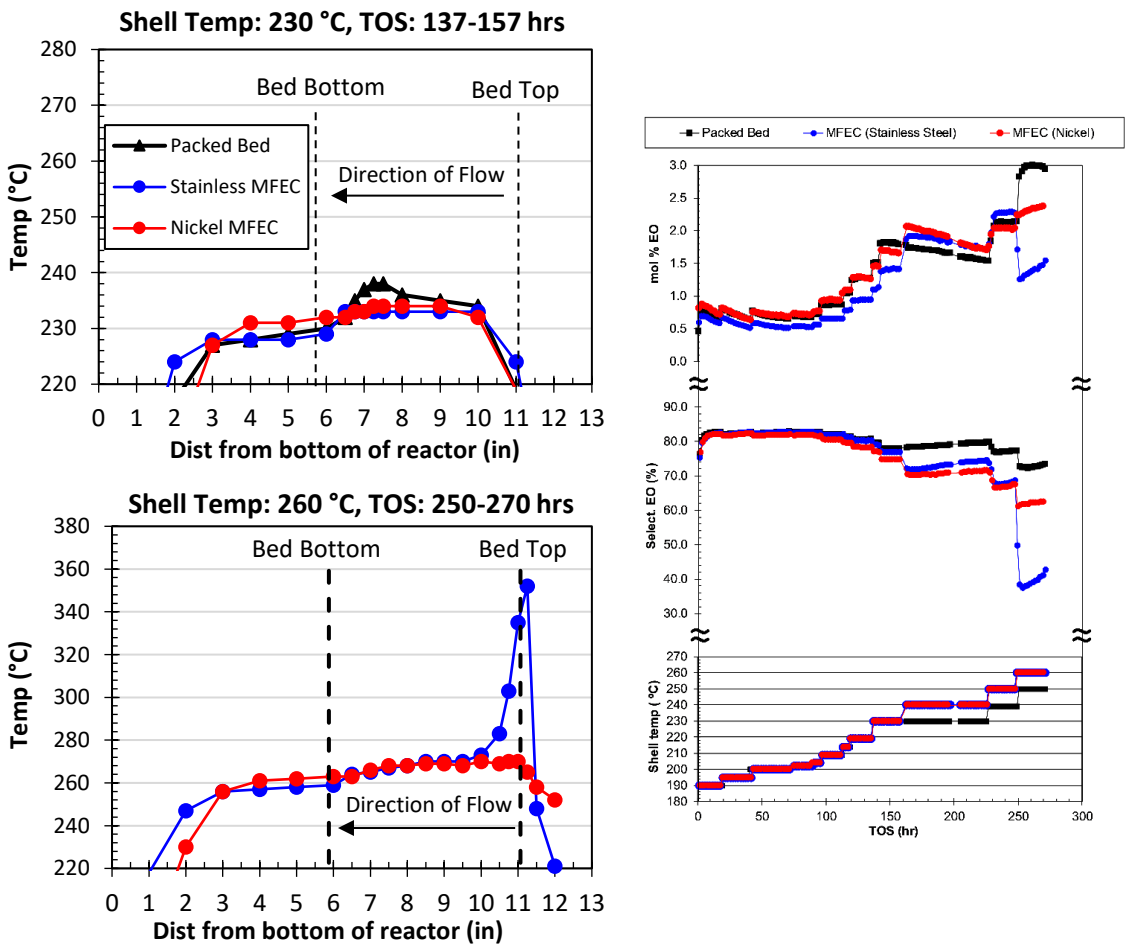

Figure 3.9: Bed profiles following low temperature startup. Catalysts were brought online in 25% C_2H_4, 8% O_2, 1.5ppm EtCl, Bal CH_4 at 190 ºC and temperature was increased to 230 ºC over 150 hours where a hotspot was observed for the 350ppm Cs, 12wt% Ag/α-Al_2O_3 catalyst diluted in SA5562 alumina. The SS and Ni MFEC temperatures were increased to 260 ºC over an additional 150 hours where the SS MFEC ignited.

Jacket temperature of the SS and Ni MFEC matched the packed bed reactor from initial startup to 160 hours online (230 ºC) at which point temperature was increased for the MFEC at 10 ºC increments every 24 – 48 hours until 260 ºC where ignition occurred for SS, Figure 3.9 (bottom left). At common conditions (TOS 160 hours, jacket 230 ºC) selectivity follows the trend: diluted bed > SS > Ni and plotting EO selectivity verses EO

production indicates nonlinearity above 240 ºC (1.7 mol% EO) for the Ni and SS samples, Figure 3.10. Ni, also present in 316 SS [99] is known to perform hydrogen abstraction in the catalytic steam reforming of light paraffins [43, 100-102]. Ethylene oxide is an inherently unstable molecule whose internal angles between the C-O-C bonds are smaller than the idealized value of approximately 109° making it highly susceptible to decomposition. Consequently, Ni catalyzed combustion may occur according to two possible pathways where 1) C_2H_4 adsorbs on Ag-O bonds forming an oxymetalic intermediate susceptible to H abstraction by an adjacent Ni atoms [75, 103] or 2) EO can reabsorb directly on the metal surface (Ni or Ag) and undergo metal catalyzed combustion [8, 104]. Due to a two carbon chain length [102] and presence of a relatively strong oxidant [105] both pathways precede within the temperature range, 200 – 260 ºC, common for ethylene oxidation.

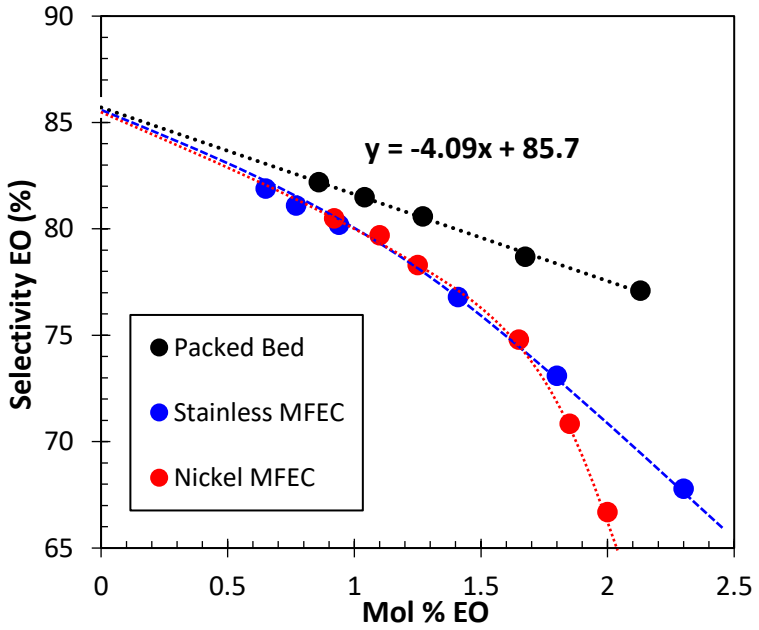

Figure 3.10: Selectivity as a function of EO production varied by increasing reaction temperature between 210 and 260 ºC. The SS and NI are catalytically active for the combustion of ethylene oxide above 240 ºC (1.7mol% EO).

Intrinsic selectivity is estimated at 86% for all reactor configurations indicated by a common point of intersection with the Y axis at 0 mole% EO in Figure 3.10. This finding agrees with prior prescreening where the MFEC was evaluated for direct olefin combustion, Figure 3.1 (r2), and further suggests that nonselective products are formed from the sequential combustion of EO. Using a feed containing 8% O_2 and 0.5% EO diluted in CH_4 from a premixed cylinder containing 2.1% EO balance He, the Ni MFEC containing no catalyst was evaluated for EO combustion. At temperatures between 200 and 245 °C less than 10% of the EO supplied was combusted to CO_2 and H_2O, Figure 3.11, with an apparent activation energy of 53kJ/mol determined from an Arrhenius plot of conversion at 200, 220 and 245 °C. Activation energies in the high temperature region were not determined due to the absence of differential conditions with a maximum EO conversion of 70% at 270 °C.

The breakage of the C-C bond has been thoroughly investigated for the hydrogenolysis of ethane, Equation 3.4 with an overall apparent activation energy of 169 kJ/mol between 177 and 219 °C for silica supported Ni catalysts [106].

$$C_2H_6 + H_2 \leftrightarrow 2\ CH_4 \qquad -\Delta H_{298} = 65\ kJ/mol \qquad (3.4)$$

In the presence of a strong oxidant such H_2O in the catalytic steam reforming of light paraffins, Equation 3.5, the apparent activation energy of light paraffins on Ni has been calculated at 76 kJ/mol for ethane and 110 kJ/mol for methane [107].

$$C_nH_m + n\ H_2O \rightarrow 2\ CO + (n + m/2)\ H_2 \qquad (3.5)$$

Therefore, considering the strained nature of the epoxide ring and the abundance of co-fed molecular oxygen the relatively low activation energy observed for EO combustion

on the Ni MFEC is not unexpected. Pacification strategies for the Ni and SS surface are being explored and will be published following submission of a provisional patent.

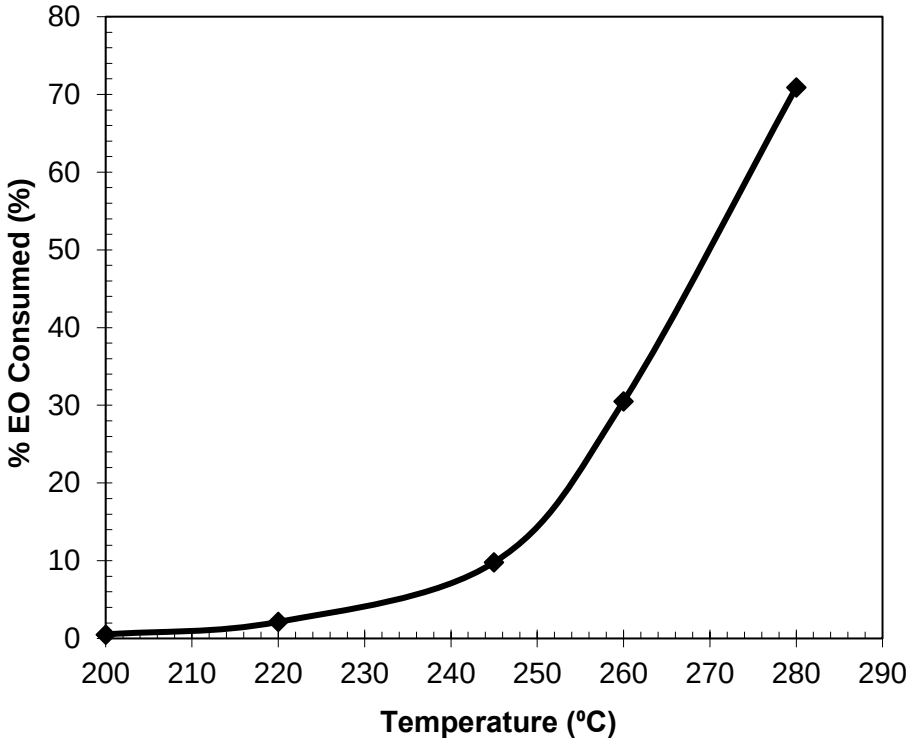

Figure 3.11: Combustion of EO as a function of nominal reactor temperature for the Ni MFEC without catalyst. Evaluation conditions, 0.5% EO, 8% O_2, Bal CH_4, superficial velocity 0.15, contact time 3.0s.

It is critical to note that despite a precipitous drop in selective epoxidation, both MFEC configurations maintain an isothermal catalyst bed below a jacket setpoint of 260 ºC. This concept is plotted in Figure 3.12 where the energy generation term in Equation 3.1 is represented as a function of catalyst selectivity. A packed bed operating with a work rate of 2.0 mol% EO at 78.5% selectivity will generate energy at a rate of ~8.0×10^5 kJ/min for a 100 kton/year EO reactor. At the same work rate, but a selectivity of 66%, the Ni MFEC has and energy generation rate of 1.25×10^6 or ~1.6x that of the diluted packed bed. This observation demonstrates that 1) the MFEC configurations were tested

using a more severe thermal load than that of the packed bed and 2) by removing the risk of exothermic ignition, producers may generate more selective product per catalyst lifecycle by operating at work rates higher than 2.0mol% EO.

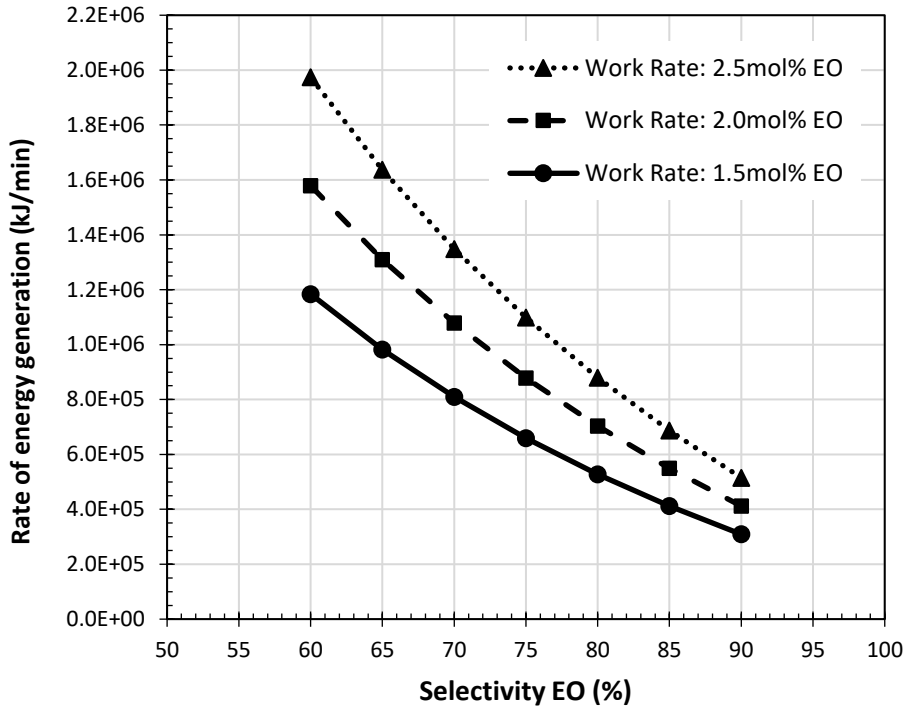

Figure 3.12: Rate of energy generation as a function of catalyst selectivity for a 100kton/year EO reactor. As selectivity decreases the heat of reaction for direct and sequential combustion dramatically increases the energy generation term. Non-linearity becomes more apparent as catalyst work rate increases.

3.4.3 Catalytic Evaluation: 1" OD Reactor

The rate of conductive heat transfer is inversely proportional to the thermal resistivity of the material which is in turn, inversely proportional to the thickness of said material [79]. Consequently, heat transfer limitation in commercial reactors using an inner diameter of 1.62" loaded with thermally inert α-Al_2O_3 is expected to increase compared with the test system using 0.43" ID (1/2" OD) tubes. To approximate MFEC thermal properties of under industrial load, it is necessary to evaluate these materials

using larger 0.87”ID (1” OD) reactors. A schematic for the 1” OD tube loaded with MFEC and 350ppm Cs, 12wt% Ag/α-Al_2O_3 catalyst is shown in Figure 3.13. Note the 7” packing of destone beads which provides sufficient contact to preaheat the feed gas from 156 ºC to a target reaction temperature up to 280 ºC prior to contact with the catalyst bed.

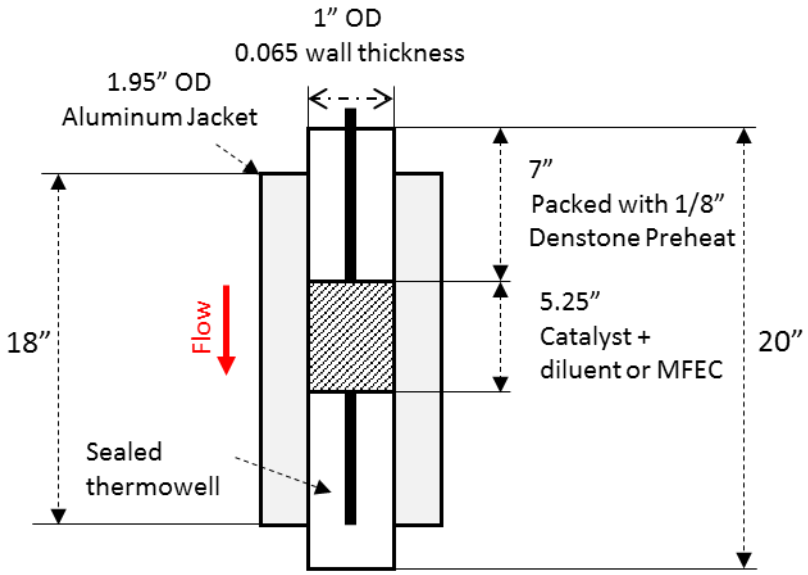

Figure 3.13: Schematic for the 1" OD reactor loaded with diluted catalyst bed or MFEC media. Note the addition of a destone preheat which mixes the feed gas and provides surface area to heat the reaction mixture to the target operating temperature.

Catalysts were brought online at 180 ºC with a gas composition of 25% C_2H_4, 8% O_2, 1.5ppm EtCl, balance CH_4. The reaction temperature was increased at 2 ºC steps every two hours until 188 ºC where the system was held at constant conditions for 13 hours then stepped to 195 ºC and held for an additional 24hrs. At 197 ºC hotspots were observed in both the SS MFEC and diluted packed bed with a temperature rise of 9 and 7 ºC respectively, Figure 3.14. When temperature was increased to 199 ºC both systems immediately ignited and were shut down by removing O_2 from the feed. Where evaluation in the ½” OD reactor implies increased heat removal in the SS MFEC, results

at the 1” OD scale show identical behavior with the traditional packed bed. This finding is not a failure of the SS mesh but is instead the result of external heat transfer limitation intrinsic to the reactor design.

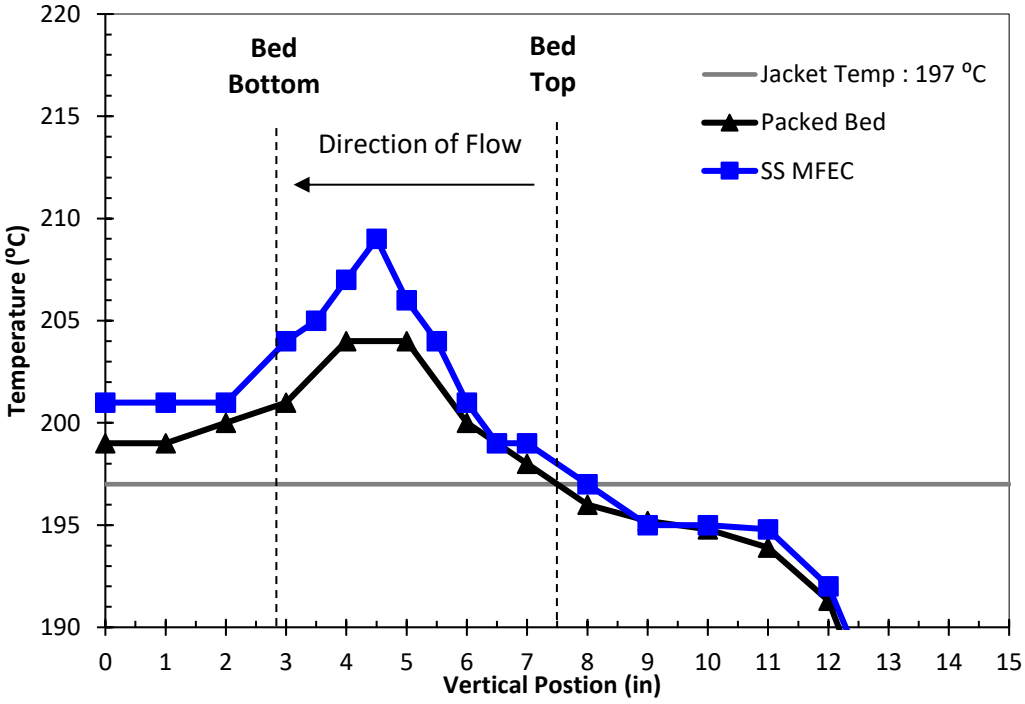

Figure 3.14: Catalyst temperature in the 1”OD reactor as a function of vertical position determined from a sliding thermocouple mounted though the center of the catalyst bed. Note both the diluted packed bed and stainless steel MFEC form hotspots at a relatively low jacket setpoint of 197 °C indicating external heat transfer limitation.

Where both the ½” and 1” OD reactor tubes are jacketed with an aluminum (Al) shell, it is the ratio between the external surface of the stainless steel tube and aluminum shell (A1/SS) that ultimately determines the rate of external heat removal. Commercially, external heat transfer limitation is overcome by the selection of a heat transfer fluid, traditionally high-pressure steam, having a heat capacity much larger than that of stagnant air. Results for the 1” and ½” OD reactors would suggest the critical Al/SS ratio lies between 4 and 7.8. An alternative strategy is to mill fins into the alumina jacket

consequently providing an air gap where a blower can be used to increase convection over the aluminum surface.

Lastly, a comparison must be made between the MFEC testing conditions and those applied industrially for EO production. The first row of Table 3.3 denotes the parameters used in our labs for catalyst screening at the ¼" scale. Note the agreement between superficial velocity for the ¼", ½" and 1" OD configuration indicating a similar internal convective heat removal term for all cases. When compared to data previously captured for a pilot tube in the epoxidation of butadiene to epoxybutane (EpB) the lab scale superficial velocity is two orders of magnitude smaller (125 cm/s vs 1.54 cm/s). Consequently, convective heat removal is significantly smaller, almost zero, compared with the industrial design. What can be stated is that previous MFEC tests performed at the ½" and 1" OD scale were done under extreme thermal load and that heat is largely removed by conduction though the MFEC. To effectively compare these materials with industrial conditions, higher gas flow rates scaled for reactor temperature and pressure are required, Table 3.3 row 5.

Table 3.3: Reactor parameters for MFEC evaluation compared with a similar pilot operation for EpB. Note the significant difference between the flow rate at STP and reaction conditions.

Reactor	Total Flow (sccm)	Temp (C)	Pressure (PSIA)	Corrected Flow (SCCM)	ID (in)	Bed Ht (in)	Cat wt (g)	Contact time (sec)	Superficial Velocity (cm/s)
1/4" EO at USC	150	225	265	15	0.18	5.25	2	5.87	1.54
1/2" MFEC	854	225	265	86	0.43	5.19	6	3.06	1.54
1" MFEC	3700	200	265	356	0.87	5.19	24	2.97	1.54
EPB Pilot Tube	175,000	190	42	104,000	1.65	252	6820	2.27	125
Commercial EO Tube	500,500 (500LPM)	225	265	50,600	0.87	5.19	24	0.02	220

3.5 CONCLUSION

Microfibourous entrapped catalyst technology can significantly improve heat transfer rates for shell and tube reactor designs by increasing conduction to the inner tube wall. This technology has been proven to provide isothermal intrabed temperature profiles for exothermic GTL Fischer-Tropsch chemistry and has been investigated for the highly exothermic epoxidation of ethylene to ethylene oxide. Following evaluation in a feed containing olefin and oxygen, SS and Ni showed no activity for direct ethylene combusted however Cu was catalytically active for non-selective product formation. Evaluation of the SS and Ni mesh loaded with 350ppm Cs, 12wt%Ag/SA5562 catalyst at the ½" OD scale indicated a significant improvement in heat transfer rates compared with a traditional diluted packed bed of the same catalyst mass and volume loading. The MFEC configurations resisted light off following an initial startup at 225°C and showed an isothermal bed profile up to 260 °C despite background activity for EO combustion on the Ni and SS mesh. Evaluation at the 1" OD scale was limited by the reactor design where overall heat transfer rates were restricted not by internal conduction but by external convention due to the presence of shell side stagnant air. Strategies are noted for eliminating background activity and parameters are proposed for a redesign of the 1"OD reactor.

REFERENCES

[1] T.E. Lefort, Process for the production of ethylene oxide, US Patent No: 1998878, (1931).

[2] N. Rizkalla, A. Rokieki, Method for making a highly selective ethylene oxide catalyst, US Patent No: 8883675, (2014).

[3] M.J.F. Maria, J.V. Westrenen, Process for the production of ethylene oxide, Us Patent No: 9067901, (2015).

[4] P. Dutia, Ethylene oxide: a techno-commercial profile, Chemical Weekly, (2010).

[5] C.A. Wurtz, Sur l'oxyde d'ethylene, (1859).

[6] R. Siegfried, M. Dieter, Ethylene Oxide, in: Ullmann's Encyclopedia of Industrial Chemistry, 2001.

[7] W.H. Orgaization, IARC monographs on the evaluation of carcinogenic risks to humans - 1,3-butadiene, ethylene oxide and vinyl halides 97 (2008).

[8] W. Diao, C.D. DiGiulio, M.T. Schaal, S. Ma, J.R. Monnier, An investigation on the role of Re as a promoter in Ag Cs Re/α-Al 2 O 3 high-selectivity, ethylene epoxidation catalysts, Journal of Catalysis, 322 (2015) 14-23.

[9] T. Pu, H. Tian, M.E. Ford, S. Rangarajan, I.E. Wachs, Overview of Selective Oxidation of Ethylene to Ethylene Oxide by Ag Catalysts, ACS Catalysis, 9 (2019) 10727-10750.

[10] H.V. Milligen, B. VanderWilp, G.J. Wells, Enhancements in the ethylene oxide/ethylene glycol manufacturing technology, in: Whitepaper, Shell Global Solutions, 2016.

[11] M.V. Badani, M.A. Vannice, Effects of cesium chloride and oxygen adsorption on promoted Ag/a-Al2O3 catalysts, Applied Catalysis A: General, 204 (1999).

[12] J.R. Lockemeyer, R.C. Yeates, D. Reinalda, Method for improving the selectivity of a catalyst and the process for the epoxidation of an olefin, US Patent No: 8148555, (2012).

[13] TechNavio, Global ehtylene oxide and ethylene gycol market 2016-2020, (2016).

[14] A. Anderson, M. Motloung, Sasol achieves beneficial operation of second Lake Charles Chemicals Project production facility, in, Sasol, 2019.

[15] A.M. Lauritzen, Ethylene oxide catalyst and process for preparing the catalyst, US Patent No: 4761394, (1988).

[16] A.M. Lauritzen, Ethylene oxide catalyst process and preparing the catalyst, US Patent No: 4766105, (1988).

[17] K. Punyawudho, D.A. Blom, J.W.V. Zee, J.R. Monnier, Comparison of different methods for determinination of Pt surface site concentrations for supported Pt electrocatalysts, Electrochimica Acta, 55 (2010).

[18] W. Medlin, J.R. Monnier, Particle size distribution of 13.4wt% Ag supported on alpha alumina, Unpublished work, (1997).

[19] J.R. Anderson, Structure of metallic catalysts, Academic Press, 1975.

[20] D.E. Strohmayer, G.L. Geoffroy, M.A. Vannice, Measurment of silver surface area by H2 titration of chemisorbed oxygen, Applied Catalysis, 7 (1983) 189-198.

[21] S.R. Seyedmonir, D.E. Strohmayer, G.L. Geoffroy, M.A. Vannice, Characterization of supported silver catalysts I. Adsorption of O2, N2, N2O and the H2-Titration of adsorbed oxygen on well dispersed Ag on TiO2 Journal of Catalysis, 87 (1984) 424-436.

[22] B. Egelske, M. Rahman, J.R. Monnier, Hydrogen titration of oxygen precovered Ag for ethylene oxide catalysts containing common promoters and co-promoters, In preparation, (2021).

[23] X.E. Verykios, F.P. Stein, R.W. Coughlin, Influence of metal crystallite size and mophology on selectivity and activity of ethylene oxidation catalyzed by supported silver, Journal of Catalysis, 66 (1980) 368-382.

[24] J.K. Lee, X.E. Verykios, R. Pitchai, Support and crystallite size effects in ethylene oxidation catalysis, Applied Catalysis, 50 (1989).

[25] V.Y. Gavrilov, R.A. Byanov, N.N. Bobrov, Standardization of methods apparatusses and devices for the control over commercial catalysts quality, Proc. USSR Symp (in Russian), (1991).

[26] J.E.v.d. Reijen, S. Kanungo, T.A.J. Welling, M. Versluijs-Helder, T.A. Nijhuis, K.P.d. Jong, P.E.d. Jongh, Preparation and particle size effects of Ag/a-Al2O3 catalysts for ethylene epoxidation, Journal of Catalysis, 356 (2017) 65-74.

[27] A.J.F.v. Hoof, E.A.R. Hermans, A.P.v. Bavel, H. Friedrich, E.J.M. Hensen, Structure sensitivity of silver-catalyzed ethylene epoxidation, ACS Catalysis, 9 (2019) 9829-9839.

[28] W. Diao, J.M. Tengco, A.M. Gaffney, J.R. Regalbuto, J.R. Monnier, Rational synthesis of bimetalic catalysts using electroless deposition methods, in: J. Spivey, Y.F. Han, D. Shekhawat (Eds.) Catalysis, Royal Society of Chemistry, 2020.

[29] T.H. James, The therory of the photographic process, Eastman Kodak Co, Rochester, NY, 1977.

[30] S.N. Goncharov, B.S. Bal'zhinimaev, S.V. Tsybulya, V.I. Zaikovskii, A.F. Danilyuk, Synthesis of silver supported catalysts with narrow particle size distribution Preparation of catalysis, VI (1995).

[31] H.J. Ploehn, J.R. Monnier, X. Chen, Systems and methods for measurement of gas permeation through polymer films, US Patent No: 8424367, (2009).

[32] J.R. Monnier, J.L. Stavinoha, G.W. Hartley, Effects of chlorine and chlorine dynamics during silver-catalyzed epoxidation of butadiene, Journal of Catalysis, 226 (2004) 321-333.

[33] J.R. Lockemeyer, R.C. Yeates, D. Reinalda, Method for improving the selectivity of a catalyst and process for the epoxidation of an olefin, US Patent No: 7485597, (2009).

[34] W.E. Evans, J.R. Lockemeyer, D.M. Rekers, A.J.T. Raa, T. Wermink, Method for the start-up of an epoxidation process and a process for the epoxidation of an olefin, US Patent No: 7102022, (2006).

[35] J.T. Jankowiak, M.A. Barteau, Ethylene epoxidation over silver and copper-silver bimetallic catalysts: I. Kinetics and selectivity, Journal of Catalysis, 236 (2005) 366-378.

[36] K.E. Hayes, The role of reaction products in the silver-catalyzed oxidation of ethylene, Canadian Journal of Chemisty, 38 (1960).

[37] P. Sykes, A guidbook to the mechanism in organic chemistry, 1985.

[38] R.B. Grant, R.M. Lambert, A single crystal study of the silver-catalysed selective oxidation and total oxidation of ethylene, Journal of Catalysis, 92 (1984) 365-375.

[39] M. Schaal, A. Pickerell, C. Williams, J. Monnier, Characterization and evaluation of Ag–Pt/SiO2 catalysts prepared by electroless deposition, Journal of Catalysis, 254 (2008) 131-143.

[40] S.S. Djokic, P.L. Cavallotti, Electroless depostion: Theory and applications, in: S. Science (Ed.) Modern Aspecs of Electrochemistry, 2010.

[41] I. Ohno, Electrochemistry of electroless plating, Materials Science and Engineering, 146 (1991) 33-49.

[42] G. Tate, A. Kenvin, W. Diao, J.R. Monnier, Preparation of Pt-containing bimetallic and trimetallic catalysts using continuous electroless deposition methods, Catalysis Today, 334 (2019) 113-121.

[43] B.T. Egelske, J.M. Keels, J.R. Monnier, J.R. Regalbuto, An analysis of electroless deposition derived Ni-Pt catalysts for the dry reforming of methane, Journal of Catalysis, 381 (2020) 364-384.

[44] S. PAK, Silver impregnation method for producing ethylene oxide catalyst with enhanced catalytic ability, US Patent No: 0201595, (2018).

[45] S. Eskandari, Y. Li, F.F. Tao, J.R. Regalbuto, The use of salts to control silica supported Pt particle size in charge enhanced dry impregnation syntheses, Catalysis Today, 334 (2019) 187-192.

[46] A.K. Datye, Q. Xu, K.C. Kharas, J.M. McCarty, Particle size distributions in heterogeneous catalysts: What do they tell us about the sintering mechanism?, Catalysis Today, 111 (2006) 59-67.

[47] A.J.F.v. Hoof, R.C.J.v.d. Poll, H. Friedrich, E.J.M. Hensen, Dynamics of silver particles durring ethylene epoxidation, Applied Catalysis B: Environmental, 272 (2020).

[48] J.R. Monnier, The selective epoxidation of non-allylic olefins over supported silver catalysts, 3rd World Congress on Oxidation Catalysis, (1997).

[49] X.C. Guo, R.J. Madix, Adsorption of oxygen and carbon dioxide on cesium-reconstructed Ag(110) surface, Surface Science, 550 (2004) 81-92.

[50] C. Guckel, Ethylene oxide catalyst with optimized cesium content, US Patent No: 9115104, (2015).

[51] Y. Jun, D. Jingfa, Rhenium as a promoter for ethylene epoxidation Applied Catalysis, 92 (1992).

[52] H. Pines, W.O. Haag, Alumina: Catalyst and support. I. Alumina, its intrinsic acidity and catalytic activity, JACS, 82 (1959).

[53] K. Tanabe, Solid acids and bases their catalytic properties, Tokyo, 1970.

[54] R.W. Mcnamee, C.M. Blair, Process for making olefin oxides, US Patent No: 2238474, (1941).

[55] G.W.S. Jr, Process and catalyst for producing ethylene oxide, US Patent No: 2615900, (1952).

[56] D.K. Sacken, Promoted supported silver surface catalyst and process for prepairing same, US Patent No: 2671764, (1954).

[57] R.P. Nielsen, J.H.L. Rochelle, Catalyst for production of ethylene oxide, US Patent No: 3962136, (1976).

[58] A.W. Czanderna, The adsorption of oxygen on silver, The Journal of physical Chemistry 68 (1964).

[59] B.T. Egelske, W. Xiong, J.R. Monnier, An investigation of structure sensitivity for Ag/Al2O3 olefin expoxidation catalysts In preparation, (2021).

[60] K.C. Prince, M.E. Kordesch, Coadsorption of oxygen and caesium on silver (110), Applications of Surface Science, 22 (1985).

[61] J.M. Cambell, S. Reiff, J.H. Block, Coadsorbate induced adsorption of CO2 on Ag(110): CO2 intercations with Cs/Ag(110) and with O/Cs/Ag(110), Langmuir, 10 (1994).

[62] J.W. Harris, A. Bhan, Moderation of chlorine coverage and ethylene epoxidation kinetics via ethane oxychlorination over promoted Ag/α-Al2O3, Journal of Catalysis, 367 (2018) 62-71.

[63] NIST, Ethylenediamine, in: NIST Chemistry WebBook, SRD 69, U.S. Department of Commerce, 2021.

[64] J.J.F. Scholten, J.A. Konvalinka, F.W. Beekman, Reaction of nitrous oxide and oxygen with silver surfaces, and application to the determination of free-silver surface areas of catalysts, Journal of Catalysis, 28 (1973).

[65] W.E. Evans, J.M. Kobe, M. Matusz, Process for improving the selectivity of an EO catalyst, US patent No: 0277447, (2012).

[66] A.C. Liu, L. Zhang, Methods for enhancing the efficiency of rhenium-promoted epoxidation catalysts and epoxidation methods utilizing these, US Patent No: 0267973, (2010).

[67] W.E. Evans, A method for the start-up of an epoxidation process, a catalyst and a process for the epoxidation of an olefin, European Patent No: 1532125, (2003).

[68] A.R. Puigdollers, P. Schlexer, S. Tosoni, G. Pacchioni, Increasing oxide reducibility: The role of metal/oxide interfaces in the formation of oxygen vacancies, ACS Catalysis, 7 (2017) 6493-6513.

[69] S. Bourgeois, B. Domenichini, J. Jupille, Excess electrons at oxide surfaces, in: Defects at Oxide Surfaces, 2015, pp. 123-147.

[70] J. Monnier, J. Stavinohajr, R. Minga, Stability and distribution of cesium in Cs-promoted silver catalysts used for butadiene epoxidation, Journal of Catalysis, 226 (2004) 401-409.

[71] R.B. Grant, R.M. Lambert, Alkali-metal promoters and catalysis: A single-crystal investigation of ethylene epoxidation on Cs-doped Ag(11 1), Langmuir, 1 (1985).

[72] D. Jingfa, Y. Jun, Z. Shi, Y. Xiaohong, Promoting effects of Re and Cs on silver catalyst in ethylene epoxidation, Applied Catalysis, 244 (1992).

[73] Chapter 6 Reduction of Oxides, in: H.H. Kung (Ed.) Transition Metal Oxides - Surface Chemistry and Catalysis, 1989, pp. 91-109.

[74] S. Linic, M. Barteau, Formation of stable surface oxametallacycle that produces ethylene oxide, Journal of American Chemical Society, 124 (2002).

[75] K.C. Waugh, M. Hague, The detailed kinetics and mechanism of ethylene epoxidation on an oxidised Ag/α-Al2O3 catalyst, Catalysis Today, 157 (2010) 44-48.

[76] H.T. Spath, K.D. Handel, Kinetics and mechanism of the oxidation of ethylene over silver catalysts, in: A.C. Societry (Ed.) Chemical Reaction Engineering, Washington DC, 1974.

[77] S.B. Ziemecki, G.A. Jones, J.B. Michel, Surface mobility of Re2O7 in the system Re7+Pd0/gamma-Al2O3, Journal of Catalysis, 99 (1986).

[78] Y. Jia, L. Duan, D. Zhang, J. Qiao, G. Dong, L. Wang, Y. Qiu, Low-temperature evaporable Re2O7: An efficient p-dopant for OLEDs, The Journal of Physical Chemistry C, 117 (2013) 13763-13769.

[79] T.L. Bergman, A.S. Lavine, F.P. Incropera, D.P. Dewitt, Introduction to heat transfer, 6 ed., John Wiley & Sons, Inc, 2012.

[80] I. Glassman, R.A. Yetter, N.G. Glumac, Combustion, Elsevier, 2014.

[81] E.P.S. Schouten, P.C. Borman, K.R. Westerterp, Influence of reaction products on the selective oxidation of ethylene, Chemical Engineering and Processing, 35 (1995).

[82] P.L. Metcalf, P. Harriott, Kinetics of silver-catalyzed ethylene oxidation, Industrial and Engineering Chemistry Research, 11 (1972).

[83] G. Cocuzza, B. Calcagno, G. Torreggiani, Process for the simultaneous separation of ethylene oxide and cabon dioxide from the gaseous mixtures obtained in the direct oxidation of ethylene with oxygen, US Patent No: 3948621, (1976).

[84] U. Tsao, Process for producing an olefinic oxide, US Patent No: 3523957, (1970).

[85] Pentair, Entrainment of aerosolized heavy lube oils from compressors, Whitepaper, (2012).

[86] Pentair, Lean amine filtration in natural gas processing plant, Whitepaper, (2019).

[87] C. Backx, C.P.M.D. Groot, P. Biloen, W.M.H. Sachtler, Interaction of O2, CO2, CO, and C2H4 with Ag(110), Surface Science, 128 (1983).

[88] X. Cheng, H. Yang, B.J. Tatarchuk, Microfibrous entrapped hybrid iron-based catalysts for Fischer–Tropsch synthesis, Catalysis Today, 273 (2016) 62-71.

[89] H.A. Choudhury, X. Cheng, S. Afzal, A.V. Prakash, B.J. Tatarchuk, N.O. Elbashir, Understanding the deactivation process of a microfibrous entrapped cobalt catalyst in supercritical fluid Fischer-Tropsch Synthesis, Catalysis Today, 343 (2020) 112-124.

[90] M. Sheng, H. Yang, D.R. Cahela, W.R. Yantz, C.F. Gonzalez, B.J. Tatarchuk, High conductivity catalyst structures for applications in exothermic reactions, Applied Catalysis A: General, 445-446 (2012) 143-152.

[91] R.R. Kalluri, D.R. Cahela, B.J. Tatarchuk, Comparative heterogeneous contacting efficiency in fixed bed reactors: Opportunities for new microstructured systems, Applied Catalysis B: Environmental, 90 (2009) 507-515.

[92] B.J. Tatarchuk, M.F. Rose, Mixed fiber composite structures, US Patent No: 5102745, (1992).

[93] B.J. Tatarchuck, M.F. Rose, G.A. Krishnagopalan, J.N. Zabasajja, D.A. Kohler, Preparation of mized fiber composite structures, US Patent No: 5304330, (1994).

[94] R.A. Overbeek, A.M. Khonasari, Y.F. Chang, L.L. Murrell, B.J. Tatarchuk, M.W. Meffert, Production of composite structures, US Patent No: 6231792, (2001).

[95] B.J. Tatarchuck, H. Yang, R. Kalluri, D. Cahela, Microfibrous media and packing method for optimizing and controlling highly exothermic and highly endothermic reactions/processes, US Patent No: 8420023, (2013).

[96] H. Yang, S. Dimick, T.J. Barron, B.J. Tatarchuk, Methods for preparing highly porous microfibrous media with functional particles immobilized inside, US Patent No: 9964355, (2018).

[97] C. Verrier, W.L. Suchanek, Epoxidation Process, US Patent No: 10040055, (2018).

[98] W.E. Evans, J.M. Kobe, M. Matusz, Process for improving the selectivity of an EO catalyst, US Patent No: 9174928, (2015).

[99] Specification sheet: Alloy 316/316L, in: S.S. Company (Ed.), Philadelphia, PA.

[100] J.H. Jacobsen, C.V. Ovesen, C. Daugaard, Steam refroming catalyst and method oc makeing therof, US Patent No: 9789470, (2017).

[101] J.R. Rostrup-Nielsen, J.-H.B. Hansen, CO2-Reforming of methane over transition metals, Journal of Catalysis, 144 (1993) 38-49.

[102] J.R. Rostrup-Nielsen, Catalytic steam reforming, 1984.

[103] S. Linic, M.A. Barteau, On the mechnanism of Cs promotion in ethylene epoxidation on Ag, JACS Communications, (2004).

[104] L. Yanxia, L. Chaoming, L. Zhongliang, L. Feng, Experimental study on catalytic combustion of methane in a microcombustor with metal foam monolithic catalyst, Catalysts, 8 (2018).

[105] P. Minh, D. Pham, X.-H. Siang, T. Ji, N.V. Dai-Viet, Review on the catalytic tri-reforming of methane - Part I: Impact of operating conditions, catalyst deactivation and regeneration, Applied Catalysis A: General, 621 (2021).

[106] J.H. Sinfelt, Catalytic hydrogenolysis over supported metals, Catalysis Reviews, 3 (1970) 175-205.

[107] J.R. Rostrup-Nielsen, Activity of nickel catalysts for steam reforming of hydrocarbons, Journal of Catalysis, 31 (1973).

APPENDIX A

CHAPTER 1 SUPPLEMENTAL INFORMATION

0.1wt% Ag Fresh

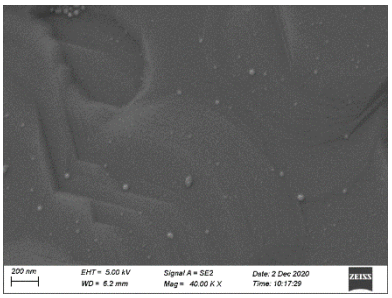

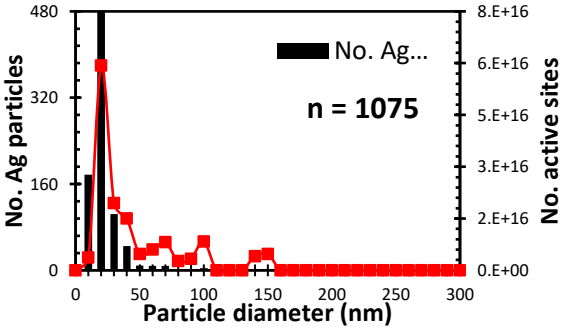

0.1wt% Ag Spent

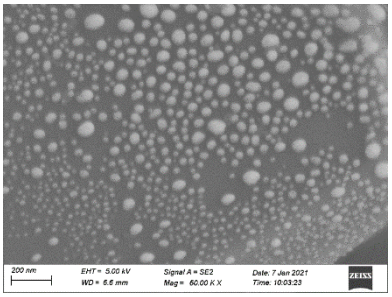

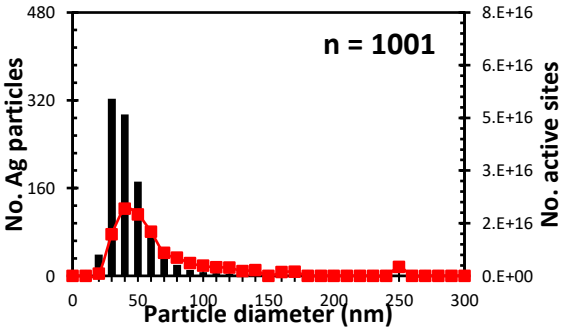

0.3wt% Ag Fresh

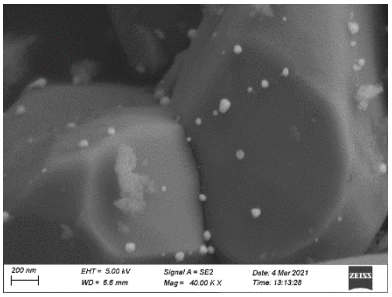

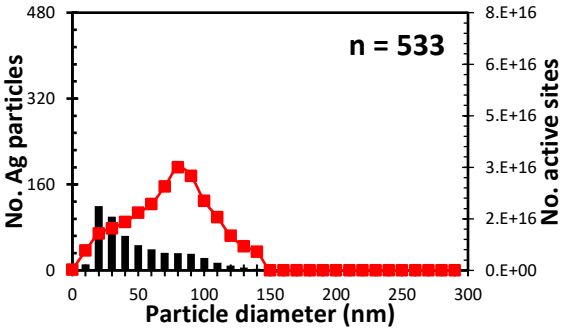

0.3wt% Ag Spent

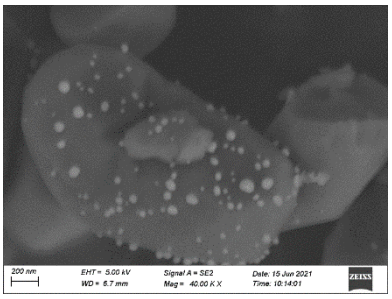

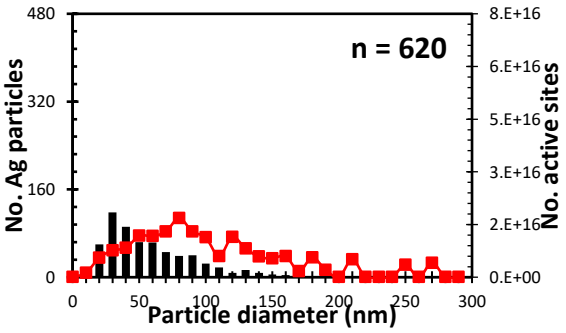

0.5wt% Ag Fresh

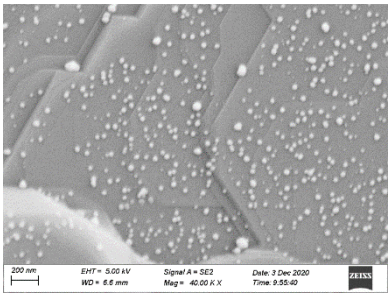

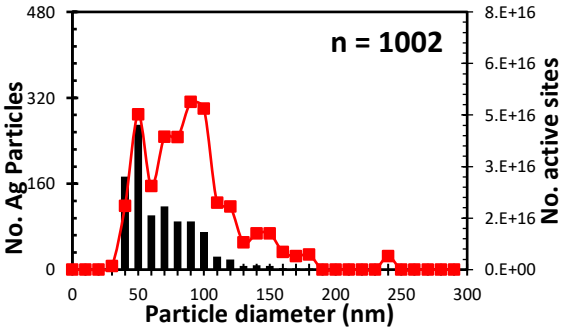

0.5wt% Ag Spent

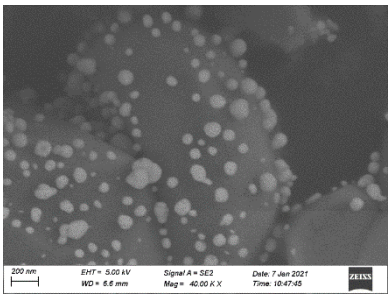

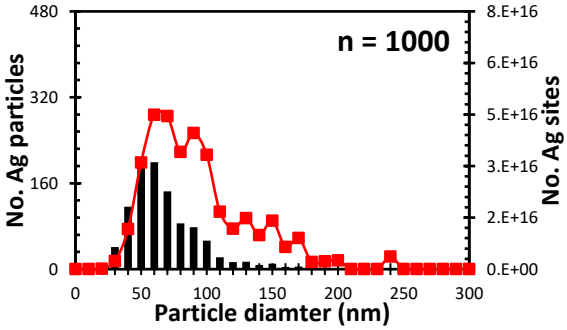

0.9wt% Ag Fresh

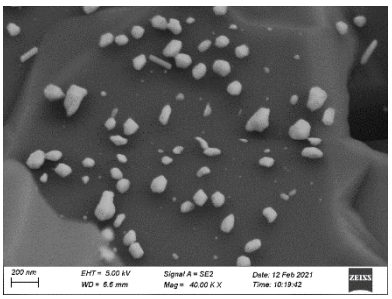

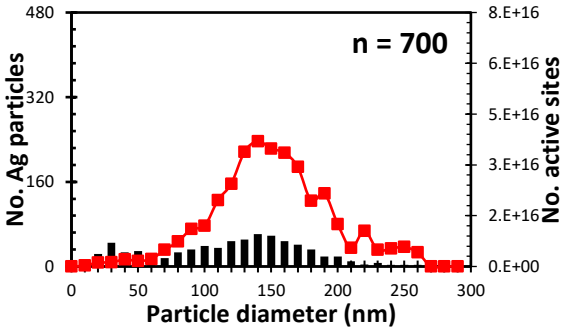

0.9wt% Ag Spent

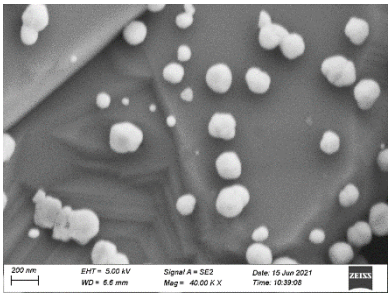

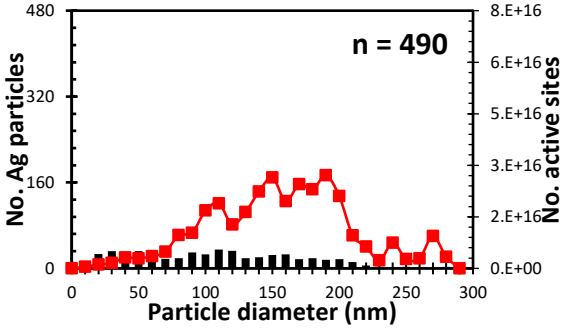

1.5wt% Ag Fresh

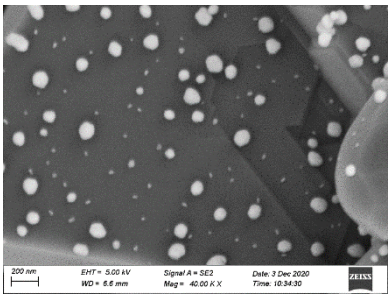

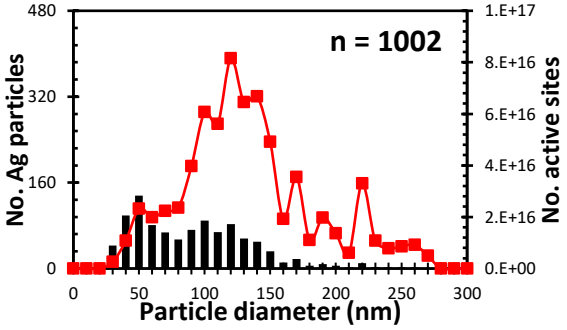

1.5wt% Ag Spent

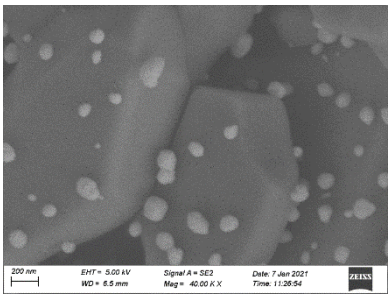

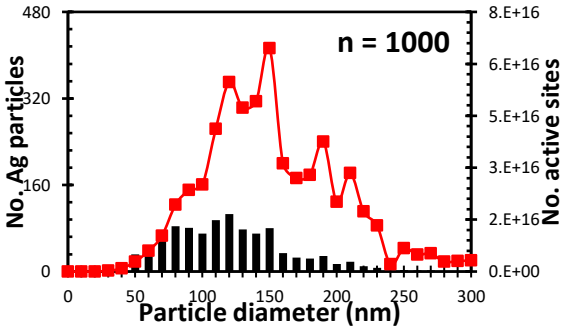

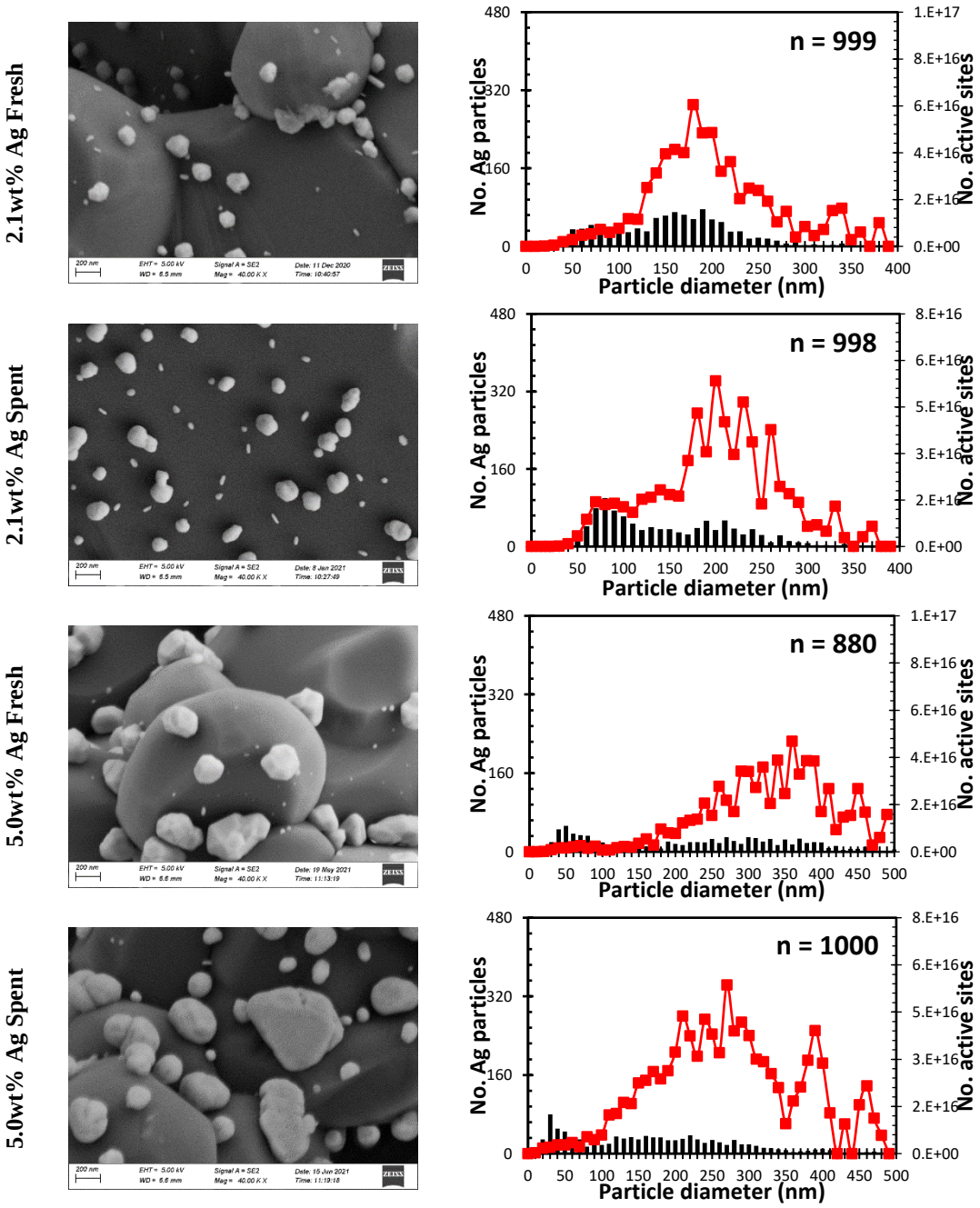

Figure A. 1 Particle size distribution and active site concentrations derived from SEM for all electroless deposition samples.